sustainability

MDPI

Review

A Comprehensive Review on Atrazine Adsorption: From Environmental Contamination to Efficient Removal Technologies

Yamil L. Salomón [1], Jordana Georgin [2,3,*], Daniel Gustavo Piccilli Allasia [1], Matias Schadeck Netto [4], Chukwunonso O. Aniagor [5], Joshua O. Ighalo [5] and Dison S. P. Franco [3,*]

[1] Graduate Program in Environmental Engineering, Federal University of Santa Maria, Santa Maria 97105–900, Brazil
[2] Graduate Program in Civil Engineering, Federal University of Santa Maria, Santa Maria 97105–900, Brazil
[3] Department of Civil and Environmental, Universidad de la Costa, CUC, Calle 58 # 55–66, Barranquilla 080002, Colombia
[4] Department of Chemical Engineering, Integrated Regional University, Santo Angelo 98802–470, Brazil
[5] Department of Chemical Engineering, Nnamdi Azikiwe University, Awka PMB 5025, Nigeria
* Correspondence: jordanageorgin89@gmail.com (J.G.); francodison@gmail.com (D.S.P.F.)

Abstract

The expansion of global agriculture has intensified the use of herbicides such as atrazine (ATZ), resulting in widespread environmental contamination. Given its documented harmful effects, the development of effective treatment strategies is crucial. This review synthesizes the fundamental mechanisms behind ATZ adsorption, identifying it as a spontaneous and energetically favorable process, predominantly governed by specific physicochemical interactions. The analysis reveals that adsorption efficiency is critically influenced by the pH of the medium, since this parameter determines the charge state of the adsorbent surface and the ATZ molecule itself, thus modulating the attractive forces. The high adsorption capacity observed in various materials is intrinsically linked to their porous architecture and surface area, which facilitate the capture and retention of molecules. The desorption process, in turn, demonstrates the reversible nature of certain interactions, allowing for the regeneration and reuse of materials. The unique contribution of this analysis lies in its mechanistic approach, which transcends the mere presentation of data to offer guiding principles for the design of adsorbents. By connecting operational parameters to molecular phenomena, the review establishes a critical basis for translating promising laboratory results into real-world applications, providing a roadmap for developing practical and sustainable solutions against ATZ contamination.

Keywords: atrazine; adsorption; contamination; toxicology; environment

check for updates

Academic Editor: Yawei Shi

Received: 26 October 2025
Revised: 13 November 2025
Accepted: 18 November 2025
Published: 21 November 2025

Citation: Salomón, Y.L.; Georgin, J.; Allasia, D.G.P.; Netto, M.S.; Aniagor, C.O.; Ighalo, J.O.; Franco, D.S.P. A Comprehensive Review on Atrazine Adsorption: From Environmental Contamination to Efficient Removal Technologies. *Sustainability* **2025**, *17*, 10455. https://doi.org/10.3390/su172310455

Copyright: © 2025 by the authors. Licensee MDPI, Basel, Switzerland. This article is an open access article distributed under the terms and conditions of the Creative Commons Attribution (CC BY) license (https://creativecommons.org/licenses/by/4.0/).

1. Introduction

The increasing global demand for food production has led to intensified use of pesticides and herbicides, contributing significantly to soil contamination. This, in turn, adversely affects both human health and environmental quality [1,2]. Conventional wastewater treatment plants (WWTPs) struggle to effectively remove many of these contaminants, particularly the herbicide atrazine (ATZ), resulting in their discharge into aquatic ecosystems [3,4]. In the environment, ATZ undergoes transformation via chemical, photochemical, and biological pathways, yielding a range of metabolites [5]. With the molecular formula $C_8H_{14}ClN_5$ (Table 1), atrazine (2-chloro-4-ethylamino-6-isopropylamino-1,3,5-triazine) is

widely applied to crops such as maize, sugarcane, citrus fruits, sorghum, and pineapple [6,7]. This white, crystalline triazine compound exhibits moderate water solubility (33 mg L^{-1} at 20 °C) and high solubility in organic solvents, with a melting point of 173 to 175 °C [7]. Due to its environmental persistence (30–100 days), ATZ remain frequently detectable in surface and groundwater [8]. Its presence disrupts aquatic ecosystems, for instance, by impairing fish reproduction and inhibiting photosynthesis in aquatic plants, and poses serious human health risks, as it is classified as potential teratogen, carcinogen, and endocrine disruptor [9]. Consequently, the effective removal of triazine herbicides from water sources is essential to safeguard both ecological integrity and public health [10].

Table 1. Physicochemical properties of the herbicide atrazine.

Chemical Name	**Atrazine (ATZ)**
Molecular formula	$C_8H_{14}ClN_5$
Molecular size (nm)	0.80–0.85
Solubility (mg L^{-1}, 25 °C)	33
Molar mass (g mol^{-1})	215.68
Log K_{ow}	2.67
pK_a	1.85
Chemical Family	Organochlorine
Pesticide type	Insecticide
Chemical structure	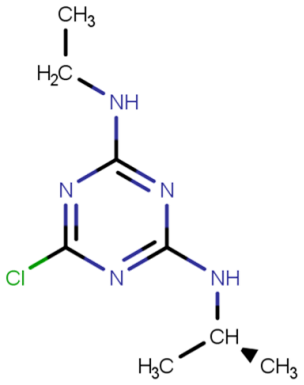

The application of herbicides for weed control is a globally adopted agricultural practice that enhances both crop yield and quality [4,11]. However, excessive or repeated use can lead to herbicide accumulation in soil, promoting surface runoff, particularly under rainfall or irrigation, and facilitating the transport of contaminants into aquatic systems [12,13]. Owing to its recalcitrance to conventional degradation pathways, ATZ poses significant environmental challenges, necessitating advanced decontamination strategies [14]. A range of treatment technologies, physical, chemical, and biological, has been extensively investigated in the literature [15,16], including photocatalysis [4], photolytic degradation [17], biodegradation [18], Fenton-based oxidation [19], advanced oxidation processes (AOPs) [20], and adsorption [21]. Among these, adsorption stands out for its operational simplicity, cost effectiveness, and versatility across a wider spectrum of adsorbents (activated carbons, biochar, clay, and engineered nanomaterials) [22–24]. Moreover, compared to energy or reagent intensive alternatives, adsorption is relatively straightforward to implement at both laboratory and pilot scales [25].

Adsorption, as a wastewater treatment technology, relies on the capacity of solid materials to accumulate target contaminants from the aqueous phase onto their surfaces

through interfacial interactions [26]. Several adsorbents have been investigated for the removal of ATZ from water, including organo-modified zeolites [27], carbon nanotubes [28], jack fruit peel carbon [29], biochar [30], nanocomposite materials [31], graphene oxide nanosheets [32], hydrochar synthesized from *Prunus serrulata* bark [33], activated carbon prepared from araçá (*Psidium cattleyanum*) fruit husks [34], and iron oxide-functilonalized graphitic porous carbon [35], among others. Notably, activated carbons derived from agricultural residues, such as nut shells, wheat straw, rice husks, and fruit peels, have gained increasing attention as sustainable, low-cost alternatives. Their utilization not only enhances ATZ remediation efficiency but also contributes to the valorization of agro-industrial waste, aligning waste management with circular economy principles [36].

The well-documented adverse effects of atrazine (ATZ) on human health, wildlife, and aquatic ecosystems, including its suspected carcinogenicity in humans, induction of hermaphroditism in amphibians, and inhibition of photosynthesis in aquatic plants, underscore the urgency of mitigating its environmental release [9,37–39]. Far from supporting its continued use, this body of evidence highlights the need for stringent regulatory measures and safer alternatives. Given ATZ's widespread environmental occurrence and considerable toxicity, the present review aims to critically evaluate strategies for minimizing its ecological and public health impacts. Specifically, global monitoring data on ATZ concentrations in environmental matrices are synthesized; toxicity endpoints across trophic levels are examined; key physicochemical and operational parameters influencing adsorptive removal (e.g., pH, temperature, adsorbent porosity, surface functionality, and coexisting ions) are analyzed; and the feasibility of adsorbent regeneration, desorption kinetics, and scalability is assessed through fixed-bed column studies, critical considerations for industrial, scale implementation. Particular emphasis is placed on low-cost, biomass-derived adsorbents, in alignment with sustainable remediation goals. To ensure comprehensiveness and scientific rigor, the review draws on 272 peer-reviewed publications (1999–2025) retrieved from PubMed, Scopus, Web of Science, and Google Scholar. While only a subset report direct experimental data on ATZ, the full corpus spans fundamental adsorption theory, material characterization, ecotoxicological endpoints, and engineering-scale implementation, providing a holistic foundation for evaluating ATZ removal strategies.

2. The Presence of ATZ in the Environment Around the World

ATZ is a selective triazine herbicide widely applied to maze and sugarcane crops for the control of broadleaf weeds [37]. Despite its high toxicity, ATZ has remained among the most extensively used herbicides since its introduction in the 1950s, with annual consumption estimated at 70,000 to 90,000 metric tons [38–40]. Uncontrolled agricultural application, coupled with industrial discharge of effluents containing ATZ and co-pollutants (both organic and inorganic) pose significant risks to human and ecological health [4,41,42]. As a result, surface water is frequently contaminated by complex mixtures of emerging contaminants, primarily originating from primarily originating from non-point agricultural runoff and point-source industrial discharges [43,44]. ATZs have also been detected in groundwater, drinking water sources, and other aquatic systems [45,46], with contamination occurring via leaching, a process facilitated by the compound's moderate water solubility, environmental resistance, and mobility [47,48]. Indeed, ATZ exhibits a prolonged half-life, ranging from 13 to 261 days in soil and exceeding 200 days in aquatic environments under certain conditions [49]. Its persistence is such that residues have been identified in soils mora than two decades after the last application [50]. A further analytical challenge arises from the wide concentration range of ATZ in environmental matrices (ng L^{-1} to mg L^{-1}), compounded by limited access to, and high operational costs of, advanced instrumentation (e.g., LC–MS/MS) required for reliable quantification at trace

levels [51]. Although individual concentrations may be fall below acute toxicity, additive or synergistic effects from multiple diffuse sources (e.g., agricultural runoff and urban drainage) can increase the ATZ concentrations [52].

Table 2 summarizes reported ATZ concentrations in environmental and drinking water samples across selected countries. Although banned in the European Union since 2004 due to groundwater contamination concerns, ATZ remains widely used in agriculture across the Americas, particularly in maize production in the United States, Brazil, and Mexico, and is registered for use in over 70 countries worldwide [53,54]. Regulatory limits for ATZ in drinking water reflect regional risk assessments: the U.S. Environmental Protection Agency (EPA) has established a maximum contaminant level (MCL) of 3 $\mu g \cdot L^{-1}$ (annual average) and a maximum contaminant level goal (MCLG) of zero, based on potential carcinogenic and endocrine effects [55]. Environmental monitoring data reveal variable exposure levels: in the San Joaquin River Basin (California, USA), ATZ concentrations reached up to 39.1 $\mu g \cdot L^{-1}$ during peak application seasons [56]; in the Bayou Lamoque (Mississippi River Basin, Louisiana, USA), a mean concentration of 33.3 $\mu g \cdot L^{-1}$ was reported, with authors noting no acute risk to non-target organisms under those conditions [52]. Notably, groundwater samples in the USA and Mexico have shown levels exceeding regulatory thresholds, up to 88 $\mu g \cdot L^{-1}$ and 21.26 $\mu g \cdot L^{-1}$, respectively [57]. In contrast, treated drinking water in Montreal, Quebec (Canada), exhibited ATZ concentrations ranging from 30 to 195 $ng \cdot L^{-1}$ (i.e., 0.030–0.195 $\mu g \cdot L^{-1}$), well below both Canadian and WHO guidelines [58].

Table 2. Reported atrazine concentrations in environmental and drinking water samples from matrices at various locations around the world.

Location	Water Type	Concentration ($\mu g\ L^{-1}$)	Refer
USA (San Joaquin River)	Surface water	0.039	[56]
USA (Lake Erie and Sandusky River)	Surface water	0.0005–0.0113	[59]
USA (Bayou Lamoque River)	Surface water	0.0333	[52]
USA	Subterranean water	88	[57]
Canadian	Surface water	0.030–0.195	[58]
Mexico	Subterranean water	21.26	[57]
Italy	Subterranean water	8.2	[57]
Italy (Volturno river)	Surface water	0.0045–0.1055	[60]
France	Natural mineral water and spring water	2.4–4.5	[61]
Czech republic	Surface and underground water	0.3–1.0	[62]
Slovenia (Drava river)	Subterranean water	0.229	[63]
France (Chalk aquifer)	Subterranean water	0.255–1.9	[64]
France, Belgium, and the Netherlands (Meuse River)	Surface water	1.0	[65]
Belgium and Holland	Surface water	0.01–0.736	[66]

Table 2. *Cont.*

Location	Water Type	Concentration (μg L^{-1})	Refer
Türkiye	Surface water	0.031–0.041	[67]
Spain	Surface water	0.0016	[67]
Germany	Surface water	0.0021	[67]
Greece	Subterranean water	0.22	[68]
Argentina	Água pluvial	0.22–26.9	[69]
Argentina	Surface water	1.4	[70]
Brazil	Subterranean water	18.9	[71]
Brazil	Surface water	0.25–9.3	[71]
Brazil	Surface water	0.0007–0.0031	[72]
Brazil	Surface water	0.13–0.82	[73]
Brazil	Subterranean water	0.19–0.0.69	[73]
Brazil	Surface water	0.002–0.018	[74]
Brazil	Surface water	0.16–0.32	[75]
Brazil	Surface water	10.4	[76]
Brazil	Surface water	7.0–15.0	[77]
Brazil	Surface water	0.066–4.95	[78]
China	Subterranean water	3.29	[57]
China (Liao-He river)	Surface water	0.18–1.6	[79]
India	Well water	0.0022	[80]
India (Yamuna river)	Surface water	0.1	[81]
South Korea (Han river)	Surface water	0.00034	[82]
Iran	Surface water	0–2175.8	[83]
South Africa (Crocodile river)	Surface water	0.13	[84]
Australia	Surface water	1.0–7.6	[85]

In the European Union, ATZ was withdrawn from the market in 2004 following the European Commission's decision not to renew its approval, primarily due to persistent groundwater contamination exceeding the parametric value of 0.1 μg·L^{-1} for individual pesticides in drinking water, as established under Directive 98/83/EC (later reinforced by Directive (EU) 2020/2184) [38,86,87]. Despite this ban, ATZ and its transformation products remain widely detected in European environmental compartments, including groundwater, surface waters, and sediments, reflecting its historical use and high environmental persistence (half-life up to 261 days in soil) [88,89]. For instance, residual concentrations in the Czech Republic range from 0.3 to 1.0 μg·L^{-1} in groundwater and surface waters [62], while elevated levels have been reported in Belgium and the Netherlands [66]. ATZ has also been identified in drinking water supplies and groundwater across multiple countries: in the Chalk aquifer (France) [64], the Llobregat River basin (Catalonia, Spain) [90], Maribor (Slovenia) [63], Italy [57], and wells in Greece [68]. Marine monitoring further confirms its widespread dispersion, with ATZ detected in coastal waters of the North Aegean Sea, the Dardanelles (Turkey), the Baltic Sea (Germany), the North Adriatic Sea (Italy), and near Barcelona (Spain) [67]; Notably, the first comprehensive survey of ATZ and its metabolites in the Central Mediterranean revealed concentrations ranging from 4.5 to 105.5 ng·L^{-1}

in surface waters from the Volturno River (Italy) to offshore stations, values reported in ng·L^{-1}, not ng·g^{-1} (a likely unit error in the original source) [60]. Furthermore, ATZ is among the most frequently detected micropollutants in the Danube River, the largest river in Central and Southeastern Europe, underscoring its regional-scale transport and long-term environmental legacy [91].

ATZ has also been widely detected across South America. In Argentina, it has been identified in rainwater samples at concentration ranging from 0.22 to 26.9 μg L^{-1} (median to maximum), as well as agricultural soils [69]. Furthermore, ATZ concentration up to 1.4 μg L^{-1} has been found in Argentinian subbasins [70]. In Brazil, an ATZ concentration in Mato Grosso state of 18.9 μg L^{-1} was found [71,92], which is 945% higher than the limit of 2 μg L^{-1}, according to the Brazilian national regulation [74]. Additional detections include low-level occurrences in Alagoas state [72]; widespread presence across 19 municipalities in Rio Grande do Sul state [78]; and measurable concentrations in the Agudo, Arvorezinha, and Cristal Basins river basins [73], as well as in surface waters of Ceará state [77]. In Oceania, ATZ is extensively used in Australian agriculture, particularly in western Australia [6]. Residues have been identified in soils and groundwater in the Toolara Forest (Queensland, Australia) [93], while surface water monitoring in other regions has reported concentrations between 1.0 to 7.6 μg L^{-1} [85].

On the Asian continent, ATZ is also used on a large scale, such as in China [88] and India [94]. Thus, ATZ can also be detected in China, such as in groundwater at concentrations greater than permitted limits (3.29 μg L^{-1}) [57] and in the Liao-He River (Liaoning Province) [79]. In India, these compounds are present at high concentrations in well water [80] and in the Yamuna River (Delhi) [95]. In South Korea, the occurrence of ATZ was also observed in the Han River [82]. Qu et al. [96] investigated the presence of sediments with a high capacity to accumulate ATZ from six lakes in Hubei Province (China) and reported that almost all lakes contain this herbicide in their sediments, highlighting the ability of lake sediments to adsorb ATZ six times faster than soils. Furthermore, Iran also uses ATZ on a large scale [88], in which high concentrations of ATZ residues were observed in the soil of Fars Province due to the leaching and dissipation of the herbicide [97] and concentrations above the standard in water (0.1 and 2175.8 μg L^{-1}) [83]. On the African continent, ATZ is restricted in countries such as South Africa but prohibited in some countries such as Angola [98]. Therefore, it was also possible to identify concentrations of ATZ in the Crocodile River of South Africa [84]. Based on the vast number of reports of ATZ detection in the ecosystem, especially in the aquatic environment, the application of effective technologies to solve problems related to the contamination of this pollutant has become evident and urgent. Furthermore, the legislation of countries, with regard to the acceptable limit of ATZ, must be more stringent or must be revised to reduce or eliminate the concentrations still found in water resources.

3. Atrazine Ecotoxicology and Risks to the Environment

The indiscriminate use of pesticides causes contamination of soils, surfaces, and groundwater and is a global concern, resulting in impacts on human health and aquatic ecosystems [99–101]. ATZ has compounds called s-triazine, which are recalcitrant; that is, they have the characteristic of slow biodegradation in the environment [102]. There is serious worry about the possible harm that these compounds could cause to aquatic flora and animals [70]. Nevertheless, the degree of concentration and the length of time that the pollutants endure determine the true environmental risk [103]. Some herbicides, such as ATZ, are stable in the environment and thus can cause bioaccumulation along trophic chains, resulting in toxic effects on insects, fish, and other aquatic organisms, birds,

mammals, and even humans [104]. Figure 1 illustrates the toxicological effects that ATZ can have on humans, vertebrates, plants, and aquatic animals.

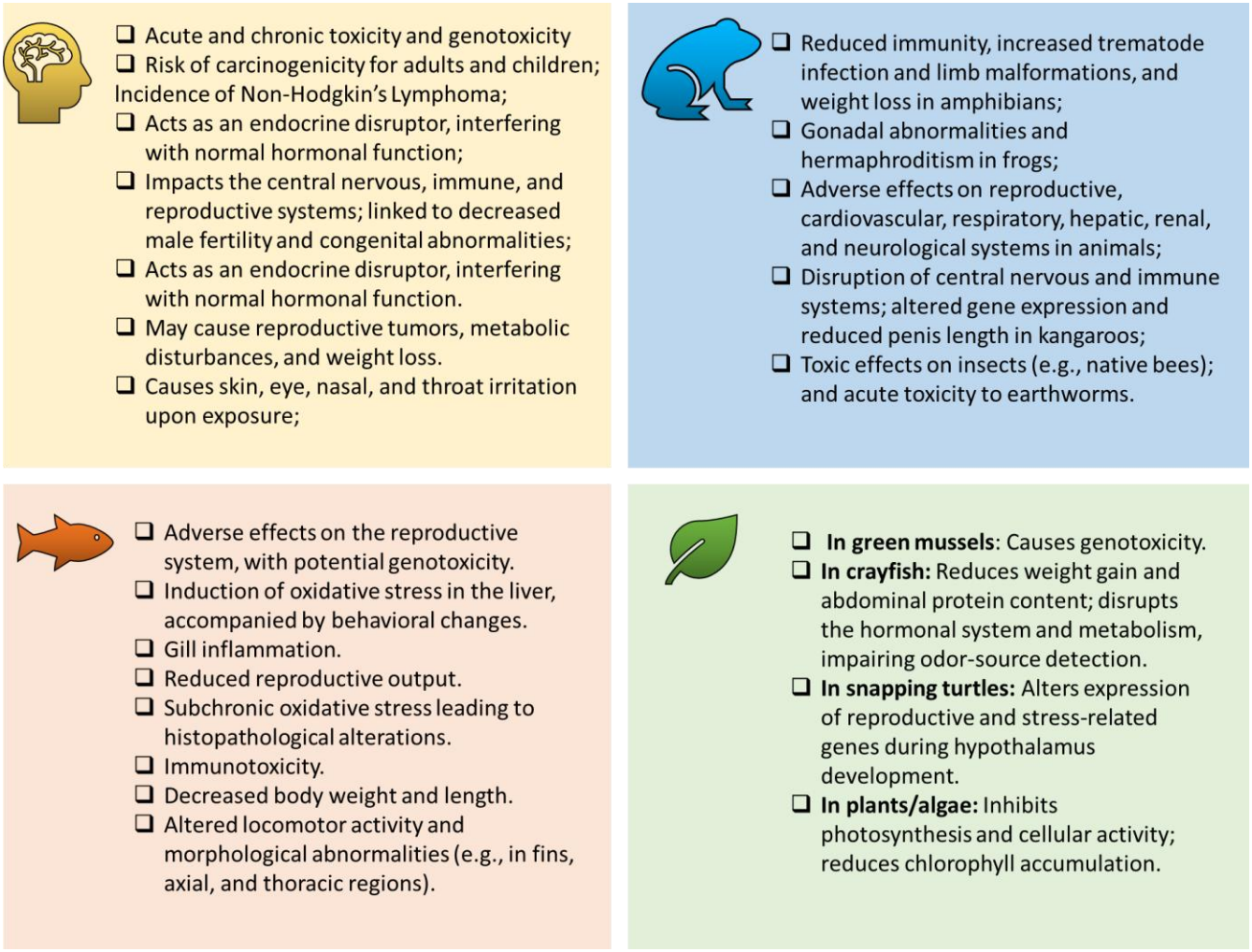

Figure 1. Some of the main ecotoxicological effects caused by the herbicide atrazine on humans, animals, fish, plants, and aquatic environments.

In humans, ATZ exposure occurs primarily via contaminated water and food, leading to documented acute and chronic health effects, including genotoxicity, endocrine disruption, and reproductive toxicity [60,105]. Although its moderate log K_{ow} (2.67) limits bioaccumulation, chronic low-dose exposure remains a concern due to its endocrine-disrupting potential. ATZ is classified in Group III as a possible carcinogen for humans [21,60,106,107]. In a study by [83], results indicated the risk of carcinogenicity of ATZ for adults and children due to exposure to water and not food. In work by Wirbisky et al. [108], it was found that embryonic exposure to ATZ alters human miRNAs associated with angiogenesis, cancer, and neurodevelopment. Continuous exposure to ATZ in water can cause mammary gland tumors and promote estrogen-like activity in ovarian cancer cells [21,109]. Kettles et al. [110] reported an important statistical relationship between exposure to triazine herbicides and increased risk of breast cancer in Kentucky (USA). An increase in the incidence of non-Hodgkin's lymphoma after exposure to ATZ drinking water from Nebraska (USA) has also been reported [111]. The central neurological, immunological, and reproductive systems are among the many systems that are harmed by ATZ, which may result in reduced male fertility and congenital abnormalities [51,112]. Because ATZ is classified as an endocrine disruptor [21], it can disrupt normal hormonal processes, which

may lead to weight loss and reproductive cancers in humans [113]. Furthermore, ATZ can irritate the skin, eyes, nose, and throat [114], and potential biomarkers that may provide new information about its toxicity include changes in the plasma metabolome and effects on the metabolism of alpha-linolenate [115].

Regarding animals, some studies have reported that although ATZ is administered at lower doses, it may still pose a danger to the environment [114]. This is corroborated by the study by [116], where they found that at herbicide levels as low as 0.1 ppb, sexual deformities were caused in frogs, and at high levels, other health problems developed. At ATZ concentrations above 0.1 mg L^{-1}, problems such as delayed gonadal development and hermaphroditism were observed in frogs [117]. Additionally, at doses above the standard, in animal studies, negative effects have been demonstrated on the reproductive system, heart, and lungs, in addition to changes in liver, kidney, and brain functions [114]. Furthermore, it can cause reproductive abnormalities in a wide variety of vertebrates, as it is an endocrine disruptor [118]. Among the animals whose reproductive systems are affected are rats, pigs, amphibians, and other wild animals [119,120]. Other serious damage to frogs and wild animals has been observed, affecting the central nervous and immune systems [48]. Additionally, in rats, ATZ can induce a response to oxidative stress in the rat ovary [121]. Chronic exposure to ATZ at low concentrations has been reported to induce obesity and insulin resistance in rats [122]. Exposure to ATZ is also associated with reduced amphibian immunity, increased trematode infections, and limb malformations caused by these infections [123], in addition to the weight loss that has been reported [113]. The results also showed that ATZ affects the reproductive and immune systems by interfering with related gene expression changes during male development in *Xenopus laevis* [124], in addition to the toxic effects of chronic exposure to ATZ on the intestinal microbiota, metabolism, and transcriptome of *Pelophylax nigromaculatus* larvae [125]. New evidence of neurotoxicity in quail was provided in a study by Xia et al. [126]. In a study by [118], adult female kangaroos (*Macropus eugenii*) were exposed to drinking water containing ATZ (450 ppm) during pregnancy, birth, and lactation, and it was observed that the gene expression necessary for testicular function was altered, in addition to a reduction in the length of the penis. The results of Podda et al. [127] indicated that ATZ has toxic effects on the central nervous system, and these effects on the cerebellar somatosensory cortex may be related to the motor disorders commonly observed in animals intoxicated with ATZ. In the first report on ATZ residues in bovine milk in Argentina, the moderate capacity of dairy cows to incorporate ATZ was highlighted, and monitoring is suggested in areas that indicate contamination by the herbicide [128]. There is concern regarding the co-exposure of pollinators to herbicides, including ATZ, given that herbicides have already been detected in pollen and beehive wax, which may result in increased mortality of individual bees [129,130]. The results indicate toxicological effects and environmental impacts on insects, such as the native bee *Partamona helleri* [131]. Finally, acute toxicity in *Eisenia fetida* earthworms was verified [132].

In aquatic animals, ATZ is also toxic [110]. In fish, it can affect the reproductive system [133], in addition to having genotoxic potential by causing ruptures in the erythrocytes of *Carrasius auratus* [134]. It is important to highlight the study by Araújo et al. [135], in which it was demonstrated that the presence of ATZ affected the spatial distribution of fish in freshwater, forming a chemical barrier that isolates fish populations. Additionally, in freshwater fish (*Channa punctatus*), signs of stress in the form of behavioral changes were observed, as well as the induction of oxidative stress in the liver, as proven through increased levels of lipid peroxidation [136]. In common carp (*Cyprinus carpio* L.), ATZ causes harm, such as necroptosis through the P450/reactive oxygen species (ROS) pathway, inflammation in the gills [137], subchronic oxidative stress and histopathological effects,

and dysregulation of the expression of pro-/anti-inflammatory cytokines in immune organs [138]. Among other negative effects of ATZ on fish are the occurrence of different gills and histopathological changes in the liver; increased acetylcholinesterase activity in the brain in *Piaractus mesopotamicus* [76]; reduced reproduction in Japanese medaka (*Oryzias latipes*) [139]; alteration of hepatic metabolism; the induction of estrogenic effects and oxidative stress, in addition to immunotoxicity, in rainbow trout (*Oncorhynchus mykiss*) [140,141]; and a reduction in weight and body length in brook trout (*Salvelinus fontinalis*). In zebrafish, ATZ influences markers of oxidative stress and detoxifying enzymes [62]; it was also found that embryonic exposure to ATZ altered miRNAs associated with angiogenesis, cancer, and neurodevelopment [108], in addition to causing immunotoxicity in zebrafish larvae [142]. Furthermore, ATZ and its metabolites altered the locomotor activity of zebrafish (*Danio rerio*) larvae, in addition to influencing development, such as heartbeat, hatchability, and morphological abnormalities [143]. Bordin [144] aimed to evaluate the effects of environmentally relevant concentrations of ATZ on embryos of South American catfish (*Rhamdia quelen*), which exhibit the most frequent deformities: damage to the fins and axial and thoracic fins. Overall, the data suggest that ATZ and some of the degradation products have minimal effects on the cortisol-mediated stress response in zebrafish [145]. In green mussels (*Perna viridis*), exposure to different concentrations of ATZ caused genotoxicity, in addition to the inhibition of acetylcholinesterase (AChE) and 7-ethoxyresorufin (EROD) [146]. The effect of ATZ on weight gain and abdominal protein content was evaluated in the young crayfish *Cherax quadricarinatus*, which significantly decreased, in addition to endocrine disruption in the hormonal system responsible for sexual differentiation of the species under study [147]. Additionally, in crayfish (*Faxonius virilis*), ATZ can cause metabolic changes that decrease the ability of crayfish to locate an odor source, making it difficult to locate food and find a mate, in addition to affecting the expression and activity of detoxification enzymes. cytochrome P450 and glutathione-S-transferase [148]. Finally, in the snapping turtle (*Chelydra serpentina*), changes in the expression of reproductive and stress genes during the development of the hypothalamus were also observed [149].

Furthermore, there is concern regarding aquatic plants that are nontarget organisms, given that ATZ can inhibit photosynthesis [52]. Kabra et al. [150] evaluated the toxicity of the herbicide ATZ on the green microalga *Chlamydomonas mexicana* at low (10 μg L^{-1}) and high (25, 50, and 100 μg L^{-1}) concentrations; no profound effect was observed on the microalgae (low concentrations), but inhibition of cellular activity and chlorophyll accumulation was observed at high concentrations. For gibbous duckweed (*Lemna gibba*), a 50% reduction in growth was observed, even at low exposure (37 ppb) [52]. However, some countries, such as the USA and China, have increased the use of ATZ annually [151]. Therefore, it is necessary to adopt legal sanitary measures, such as legislation and stricter standards, regarding the use and control of ATZ herbicide, including inspection, in addition to prioritizing an efficient removal strategy in the treatment of effluents containing ATZ.

4. Adsorbents Used and the Main Parameters That Influence Atrazine Adsorption

In view of the problems surrounding ATZ, it is understood that adequate treatment and disposal are necessary to protect the aquatic environment and human health. There are a variety of techniques that can be used to treat effluents because of their advantages and disadvantages. However, only the adsorption technique is discussed in this review. Among the advantages of adsorption are easy operation, simple design, low energy consumption, and cost–benefit compensation [6,152,153]. Adsorbates, which are liquid, gaseous, or dissolved solid molecules, adhere to the surface of an adsorbent material during the adsorption process [154]. Therefore, this process's efficacy depends on the adsorbent's potential

to display substantial adsorption [155]. In the literature, a series of materials that were used for experimental tests with ATZ are presented in this section, and the fundamental parameters that act on adsorption are discussed. Table 3 presents the main factors that influence adsorption, such as pH, dosage, temperature, and initial concentration, in addition to the characteristics found in adsorbents, such as textural properties. Another important piece of information is the adsorption equilibrium, as this approach provides a greater understanding of the adsorption process [156]. Therefore, in this section, the isothermal models that best fit will also be analyzed, in addition to kinetic and thermodynamic studies. Finally, this section will also cover the analysis of adsorption in different aqueous matrices to evaluate the real applicability of adsorbents for the treatment of effluents containing ATZ. This review addresses the efforts of scientists to solve the problems caused by ATZ through adsorption studies and the production of new and efficient adsorbents that are alternatives for removing ATZ.

Table 3. Characteristics and adsorption capacities of various adsorbents investigated for atrazine removal. Data includes adsorbent type, pH, dosage (g L^{-1}), kinetic parameters (T, K), initial concentration (C_0, mg L^{-1}), specific surface area (S_{BET}, m^2 g^{-1}), pore volume (Vp, cm^3 g^{-1}), and particle diameter (Dp, nm), alongside maximum adsorption capacity (q_{max}, mg g^{-1}) and adsorption model utilized (Langmuir or Freundlich).

Adsorbent	pH	Dosage (g L^{-1})	T (K)	C_0 (mg L^{-1})	S_{bet} (m^2 g^{-1})	V_p (cm^3 g^{-1})	D_p (nm)	q_{max} (mg g^{-1})	Model	Reference
Natural sepiolite	–	–	298	20×10^{-4} [a]	–	–	–	0.86	Langmuir	[157]
Wood charcoal		–	300	0.5–7.5	–	–	–	0.80	Freundlich	[99]
Diatomaceous earth	2	–	277–313	10	–	–	–	1.1	Freundlich	[158]
Heat-treated kerolite samples (K–600)	–	–	298	15	224	0.026–0.64	5000–10,000	2.291	Freundlich	[159]
Organovermiculite	7.5	–	298	0.05–1.00	31.4	0.014	–	0.015	–	[160]
Heat-treated kerolite (K–600)	7.5	–	283	–	224	0.026–0.64	–	11.1	Langmuir	[161]
Conventional activated carbon (F400)	5	0.01	298	–	–	–	–	39.37	Freundlich	[162]
Annealed carbon sample (F400AN)	5	0.01	298	–	–	–	–	40.32	Freundlich	[162]
Aminated carbon sample ($F400NH_2$)	5	0.01	298	–	–	–	–	34.60	Freundlich	[162]
Heat-treated diatomaceous earth	2	–	–	–	–	–	–	0.8	–	[163]
Organo-zeolites	–	–	–	1.1–164.5 [b]	–	–	–	2.01 [c]	Langmuir–Freundlich	[27]
Carbon nanotubes r–MWNT	7.8	–	298	13.3	299.63	0.7934	20–40	100.43	Polanyi–Manes	[28]

Table 3. *Cont.*

Adsorbent	pH	Dosage (g L^{-1})	T (K)	C_0 (mg L^{-1})	S_{bet} (m^2 g^{-1})	V_p (cm^3 g^{-1})	D_p (nm)	q_{max} (mg g^{-1})	Model	Reference
Dairy manure-derived biochar (BC 200)	6.99	–	–	0–20	2.62	–	–	641 [c]	Langmuir	[164]
Modified cellulose fibers	–	–	298	130 [d]	–	–	–	28 [d]	–	[165]
Multiwalled carbon nanotubes MWCNTs–O (0.85%)	6.5	–	298	4.5	167	0.619	–	61.10	Polanyi–Manes	[166]
Multiwalled carbon nanotubes MWCNTs–O (2.16%)	6.5	–	298	4.5	178	0.629	–	36.62	Polanyi–Manes	[166]
Multiwalled carbon nanotubes MWCNTs–O (7.07%)	6.5	–	298	4.5	185	0.756	–	25.62	Polanyi–Manes	[166]
Coal fly ash	6.75	–	–	10	285	–	–	0.38	Freundlich	[167]
Jack fruit peel carbon	–	–	–	–	45	–	–	20.12	Freundlich	[29]
Activated carbon/iron oxide composites (5/1)	–	–	–	–	568	0.239	<2	≅ 22	–	[168]
Acid-activated zeolite-rich tuff (T–CPL)	–	–	298	15–25	105	–	–	1.10	–	[14]
Greenwaste biochar		–	–	10	–	–	–	435 [e]	Freundlich	[169]
Waste rubber tire	2	0.10	298	12	–	–	–	104.9	Langmuir	[170]
Granular activated carbon	–	–	296	1–30	925	–	2–3	178.1	BET	[171]
Carbon nanotubes	–	–	–	1–30	189	–	12–14	63.9	PMM	[171]
Organobentonite	5	–	298	–	–	–		0.77	–	[172]
Lipoid adsorption material (LAM)	–	–	303	19.01	20.27	–	47.18	55.924	–	[173]
Powdered activated carbon (PAC)	–	–	303	19.01	–	–	–	78.86	–	[173]
Zeolite–A	7.5	0.5	298	2–10	333	–	–	0.65	Langmuir	[174]
Zeolite–X	6.8	0.5	298	2–10	688	–	–	11.86	Langmuir	[174]
Treated banana peels	7–8.2	15	298	1–150	–	–	–	14	Langmuir	[175]

Table 3. *Cont.*

Adsorbent	pH	Dosage (g L^{-1})	T (K)	C_0 (mg L^{-1})	S_{bet} (m^2 g^{-1})	V_p (cm^3 g^{-1})	D_p (nm)	q_{max} (mg g^{-1})	Model	Reference
Magnetic multiwalled carbon nanotube	6	0.2	298	5	138.66	–	–	40.16	Freundlich	[176]
Granular activated carbon	6.9–7.5	–	298	0.159–0.940	950	0.23	2.80	7.5	Freundlich	[177]
Granular Carbon	6.85	–	–	–	561.2	–	–	5	Freundlich	[49]
CS450 biochar	7	0.2	298	5	44.966	0.0345	–	7.84	Redlich–Peterson	[178]
ADPCS450 biochar	7	0.2	298	5	356.010	0.142	–	53.85	Redlich–Peterson	
N-biochar	10.5	–	293	–	–	0.31–0.64	–	<30	Freundlich	[179]
O-biochar	10.5	–	293	–	–	0.31–0.32	–	<30	Freundlich	[179]
Polymeric Adsorbent	–	–	–	–	737	–	6.96	32.6	Freundlich	[13]
Fe_3O_4/sepiolite magnetic composite (MSEP)	6.5	2	298	2–28	112.44	0.2437	2–50	15.9 [f]	Langmuir	[112]
Coconut shell-based PAC	7	0–20	293	–	–	–	–	<20	Freundlich	[180]
Nylon6/polypyrole composite	7		298	200	32.5	–	220	14.8	Freundlich	[181]
Activated carbon F400	–	–	298	40	1234	0.615	0.7–2	212.26	Langmuir	[182]
Activated carbon NPK	–	–	298	40	782	0.489	<0.7	119.45	Freundlich	[182]
Activated carbon SBC	–	–	298	40	260	0.161	–	45.49	Langmuir	[182]
Biochars produced from soybeans (SBB)	9.21	–	300	15	17.5	0.19	–	1.376 [e]	Freundlich	[30]
Biochars produced from corn stalks (CSB)	8.91	–	300	15	19.6	0.09	–	0.73 [e]	Freundlich	[30]
Biochars produced from rice stalks (RSB)	9.46	–	300	15	25.8	0.08	–	1.116 [e]	Freundlich	[30]
Biochars produced from poultry manure (PMB)	8.1	–	300	15	15.4	0.05	–	0.6 [e]	Freundlich	[30]
Biochars produced from cattle manure (CMB)	8.93	–	300	15	13.5	0.08	–	0.936 [e]	Freundlich	[30]

Table 3. *Cont.*

Adsorbent	pH	Dosage ($g\ L^{-1}$)	T (K)	C_0 ($mg\ L^{-1}$)	S_{bet} ($m^2\ g^{-1}$)	V_p ($cm^3\ g^{-1}$)	D_p (nm)	q_{max} ($mg\ g^{-1}$)	Model	Reference
Biochars produced from pig manure (PgMB)	8.88	–	300	15	13.4	0.05	–	0.581 [e]	Freundlich	[30]
Silver nanoparticles	6	2	298	5–30	–	–	6.28–6.70	1.569	Freundlich	[183]
Magnetic molecularly imprinted polymer	6.5	0.4	298	0.1–50	52.313	0.1791	13.696	69.53	Langmuir	[184]
Organo-beidellites (1.0 CEC–OBd)	7	–	298	10	4.3	0.032	–	0.30	–	[185]
Moringa oleifera pods (MOPT)	6.7	2	298	5	70.54	0.151	2.94	7.47	Langmuir	[186]
Single-walled CNTs (SWCNTs).	4	–	298	–	–	–	–	100 [g]	Langmuir	[187]
Activated carbon (AC)	–	2	293	30	–	–	–	53.7	Liu	[88]
composite of AC/MgO/ZnO	–	2	303	30	–	–	–	32.33	Liu	[88]
Wheat straw-derived biochar	–	10	293	2.80–8.70	–	–	–	12	Langmuir	[132]
Nanocomposite material	7	2.5	293	0.03	–	–	–	0.011	Freundlich	[31]
Activated Peanut Husk	6	0.5	–	0.5–25	–	–	–	4.12	Freundlich	[188]
Corn straw biochar	6	0.02	298	0.5–30	32.85	0.0148	5.01	1.94	Langmuir	[48]
Na_2S modified biochar	6	0.02	298	0.5–30	53.58	0.0209	5.84	2.69	Langmuir	[48]
KOH modified biochar	6	0.02	298	0.5–30	59.23	0.0231	7.63	2.84	Langmuir	[48]
Fe_3O_4/reduced graphene oxide nanocomposite	5	0.5	298	2–54	–	–	–	54.8	Langmuir	[189]
C_B–HDTMA material	7	–	298	10–20	–	–	–	3.9121	Langmuir	[190]
C_B–BODA material	7	–	298	10–20	–	–	–	4.2448	Langmuir	[190]
Activated carbon modified with sodium dodecylbenzene sulfonate	2	–	308	70–110	992.98	0.405	0.582	222.22	Langmuir	[191]
Activated biochar from *Calligonum Comosum*	7	0.4	313	100–400	1473	0.81	2.19	714.3	Langmuir	[192]
Hydrous iron oxide (HIOD301)	4	–	298	2–12	–	–	–	133.039	Freundlich	[193]

Table 3. *Cont.*

Adsorbent	pH	Dosage ($g\ L^{-1}$)	T (K)	C_0 ($mg\ L^{-1}$)	S_{bet} ($m^2\ g^{-1}$)	V_p ($cm^3\ g^{-1}$)	D_p (nm)	q_{max} ($mg\ g^{-1}$)	Model	Reference
Hydrous aluminum oxide (HAOD301)	4	–	298	2–12	–	–	–	53.893	Langmuir	[193]
Magnetic porous carbon-based sorbent	7	–	298	5–100	104	0.24	9.14	21.753	Dubinin–Ashtakhov	[194]
Sucrose-porous carbon (S–PCS–1)	–	–	298	25	457.6434	0.064	1.93	239.51	Freundlich	[195]
Activated carbons from apricot shells (ASAC)	3	0.2	293	80	276.15	0.21	3.69	46.30	Freundlich	[196]
Activated carbons wood (WAC)	3	0.2	293	80	553.33	0.41	3.41	303	Freundlich	
Activated carbons walnut shells (WSAC)	3	0.2	293	80	614.21	0.46	3.40	294.12	Freundlich	
Biochar–graphene oxide composite	6	0.25	298	10	15.0869	0.09874	6.2415	72.179	Langmuir	[197]
Biochar (BC)	6	0.25	298	10	7.8232	0.02363	12.0837	58.273	Langmuir	
Pyro-hydrochar from corn straw (PHC–CS_{500})	–	–	–	20	86.83	0.1023	4.713	3.2	–	[198]
Metal−organic framework materials (UiO–67)	–	–	298	25	2345	1.249	–	26	Freundlich	[199]
Metal−organic framework materials (ZIF–8)	–	–	298	25	1875	0.714	–	14.77	Langmuir–Freundlich	[199]
Commercial activated carbon (F400)	–	–	298	25	1135	0.584	–	26.7	Langmuir	[199]
Modified *Moring Oleifera* Lam. seed husks	5	1.6	298	2–30	5.77	0.0409	–	10.32	Langmuir	[200]
Cyclodextrin-based polymers (α–EPI)	7	0.075	298	2–8	–	–	–	0.122	Freundlich	[11]
Cyclodextrin-based polymers (β–EPI)	7	0.075	298	2–8	–	–	–	0.232	Freundlich	[11]
Cyclodextrin-based polymers (γ –EPI)	7	0.075	298	2–8	–	–	–	0.163	Freundlich	[11]
Biochar from corn straw (CSWP)	7	0.05	298	1–120	638.1	–	3.18	79.55	Freundlich	[201]
Biochar (BC800B)	7	–	298	15–55	277.126	0.217	5.058	48.6	Langmuir	[202]

Table 3. *Cont.*

Adsorbent	pH	Dosage ($g\ L^{-1}$)	T (K)	C_0 ($mg\ L^{-1}$)	S_{bet} ($m^2\ g^{-1}$)	V_p ($cm^3\ g^{-1}$)	D_p (nm)	q_{max} ($mg\ g^{-1}$)	Model	Reference
Rice Husk Ash	6.8	–	298	25–100	147.6	34	–	7.33	Langmuir	[203]
Nanoporous carbons (APM–8)	–	1	298	1–50	1080	0.459	–	51	Langmuir	[42]
Nanohydrogel chitin-cl-polyl	7	0.02	298	5–30	–	–	–	204.08	Langmuir	[204]
Water-treated biochars (WBC600)	–	–	–	0.5–50	359.6197	0.122445	3.3891	1.254	Dual–mode	[151]
Acid-treated biochars (ABC600)	–	–	–	0.5–50	381.2811	0.129245	2.9975	1.223	Dual–mode	[151]
Laser-induced graphitic material (LIG)	9	0.2	298	5	133.6	–	38	15	Langmuir	[205]
B-cyclodextrin functionalized rice husk-based cellulose (β–CD@RH–C)	5.5	–	283	–	–	–	–	162.21	Langmuir	[109]
GO/nZVI composites	–	1	–	25	–	–	–	21.0	–	[206]
Byproducts of Wood industry (BM350)	–	–	–	2–10	1.467	0.006	–	0.424	Freundlich	[207]
Graphene oxide nanosheets	5.37	0.121	318	27.03	187	0.12	17.3	138.19	Langmuir	[32]
Modified carbon dots with amine supported onto cellulose sponge	2	0.002–0.010	283	15–35	–	–	–	32.06	Freundlich	[208]
Biochar from fallen leaf modified with MgO nanoparticles	4	–	298	30	4.134	–	38.709	22.4	Langmuir	[209]
PAN nanofibers	10	0.035–0.336	298	10	–	–	748.6	10.080	Freundlich	[211]
PAN–CD nanofibers crosslinked with citric acid	8	0.035–0.336	298	10	–	–	1325.71	23.529	Freundlich	[211]
Biochar from bamboo culm (BE450)	9.5	2	295	2–10	4.9	0.009	31.4	2.68	Langmuir	[22]
Framework of nano metal oxides N–NiO@N–Fe_3O_4@N–ZnO	5	–	298	40	–	–	30–50	25.38	Langmuir	[212]
Polyacrylate-divinylbenzene microspheres	6.5	–	298	10	–	–	–	119.60	Langmuir	[213]
Thermally active adsorbent (MCM–41)	6	0.1	313	10–40	25.9	–	500	89.99	Langmuir	[210]

Table 3. *Cont.*

Adsorbent	pH	Dosage ($g\ L^{-1}$)	T (K)	C_0 ($mg\ L^{-1}$)	S_{bet} ($m^2\ g^{-1}$)	V_p ($cm^3\ g^{-1}$)	D_p (nm)	q_{max} ($mg\ g^{-1}$)	Model	Reference
Biochars from cedar bark sawdust (BCC)	7	1.5	298	5	47.31	0.0095	3.66	3.44	Koble–Corrigan	[214]
Biochars from cedar bark sawdust (BACB)	7	1.5	298	5	98.12	0.0099	3.66	2.70	Koble–Corrigan	[214]
Cob biowaste sorbents	2	0.25–8	–	1–25	~350.22	0.133	–	11.31–19–58	–	[23]
Low-cost adsorbent coal FA (Kosovo A)	–	–	–	2–10	–	–	–	0.45	Freundlich	[6]
Biochar from *Cedrella fissilis*	4	1.5	328	5–15	27.96	0.018	1.13	7.68	Langmuir	[214]
Novel multifunction sulfonated polyacrylate-divinylbenzene (PADVB–S3)	6.5	–	298	1–50	361.30	0.339	3–50	280.08	Langmuir	[215]
Graphene oxide (rGO)	–	–	–	6.25–150	357.56	0.35	3.94	1083.94	Sips	[216]
Graphene oxide (GO)	–	–	–	6.25–150	246.31	1.60	26	1011.94	Sips	[216]
Graphene nanoplatelets (GNP)	–	–	–	6.25–150	26.52	0.18	26.70	1005.77	Sips	[216]
Ionic liquid-functionalized porous m-aminophenol formaldehyde polymer	–	–	–	0.5–20	17.60–247.9	0.06–1.50	7.76–73.1	5.21	Freundlich	[10]
Chemically activated biochar produced from corn straw	6.5	0.015–0.11	298	30	573	0.3054	–	26.9	Langmuir	[217]
Activated carbon obtained from the araçá husks	7	1	298	5–40	431	0.280	–	55.85	Liu	[34]
Novel hydrochar derived from *Prunus serrulata* bark	3	0.8	328	50	9.85	0.030	12.17	63.35	Langmuir	[33]
Hovenia dulcis activated carbon	6	0.5	328	10–60	898.4	0.296	1.24	58.65	Freundlich	[34]
Diospyros kaki fruit waste activated carbon	7	0.43	328	0–150	1067	0.530	1.84	211.5	Freundlich	[218]
Hovenia dulcis biochar	6	1	328	50	–	–	–	73.20	M1:1	[219]
KOH-activated N-doped hydrochar	7	1	308	5–20	1205.82	–	<2 and >50	216.50	Langmuir	[220]

Table 3. *Cont.*

Adsorbent	pH	Dosage (g L^{-1})	T (K)	C_0 (mg L^{-1})	S_{bet} (m^2 g^{-1})	V_p (cm^3 g^{-1})	D_p (nm)	q_{max} (mg g^{-1})	Model	Reference
Biochar prepared from apricot shells (XH–240)	–	–	308	–	9.4761	0.0391	1.0669	18.931	Freundlich	[221]
Aged polystyrene	–	–	308	1–15	2.689	–	–	0.940	Langmuir	[222]
Aged polypropylene	–	–	308	1–15	2.964	–	–	0.677	Langmuir	[222]
Aged polystyrene	–	–	308	1–15	2.184	–	–	0.663	Langmuir	[222]
Polystyrene (PS)	–	–	308	1–15	1.556	–	–	0.565	Langmuir	[222]
Polyethylene (PE)	–	–	308	1–15	1.729	–	–	0.535	Langmuir	[222]
Polypropylene (PP)	–	–	308	1–15	1.504	–	–	0.410	Langmuir	[222]
Rice husk hydrochar (10 KHC)	–	–	–	2–30	5.16	0.016	12.66	4.06	Freundlich	[1]
LDH dispersed on bamboo biochar (LDHBC)	7	–	328	5–30	257	0.23	–	87.05	Freundlich	[223]
Cu–Zn–Fe Layered double hydroxides (LDH)	7	–	328	5–30	168	0.20	–	37.91	Langmuir	[223]
Novel nitrogen (N)–doped cellulose biochar (NC 1000–10)	7	–	293	–	192	–	0.628–0.733	103.59	Langmuir	[224]
Fallen leaf biochar (700 LBC)	7	30	298	30	5.664	0.018	–	91.69	Freundlich	[225]
Graphitic porous carbon modified with iron oxides	5.46	0.50	323	0.5–250	358	0.248	–	275.4	Langmuir	[35]

[a] = unit in cmol dm^{-3}; [b] = unit in μmol dm^{-3}; [c] = unit in μmol kg^{-1}; [d] = unit in μmol g^{-1}; [e] = unit in (mg kg^{-1})/(mg $L^{-1})^{1/n}$; [f]: unit in μg m^{-2} (amount of atrazine adsorbed per unit surface area of sepiolite); [g] = unit in mg C g^{-1}. "–" stands for not given.

The maximum adsorption capacity (q_{max}) and specific surface area (S_{BET}) of the primary material classes studied for atrazine removal from aqueous systems are contrasted in Figure 2. To account for the large range of reported values, both axes are shown on a logarithmic scale. The linear regression indicates a correlation of 0.72 between the surface of the adsorbent and the ATZ adsorption capacity. This indicates that, adsorption capacity is dependent on the adsorbent surface. However, it should be noted that other factors, such as functional groups and pH conditions, both control the adsorbent mechanisms. There is a wide range of data showing that the adsorption capacity of ATZ is not only controlled by surface area but also heavily impacted by the surface chemistry and physicochemical properties of each adsorbent.

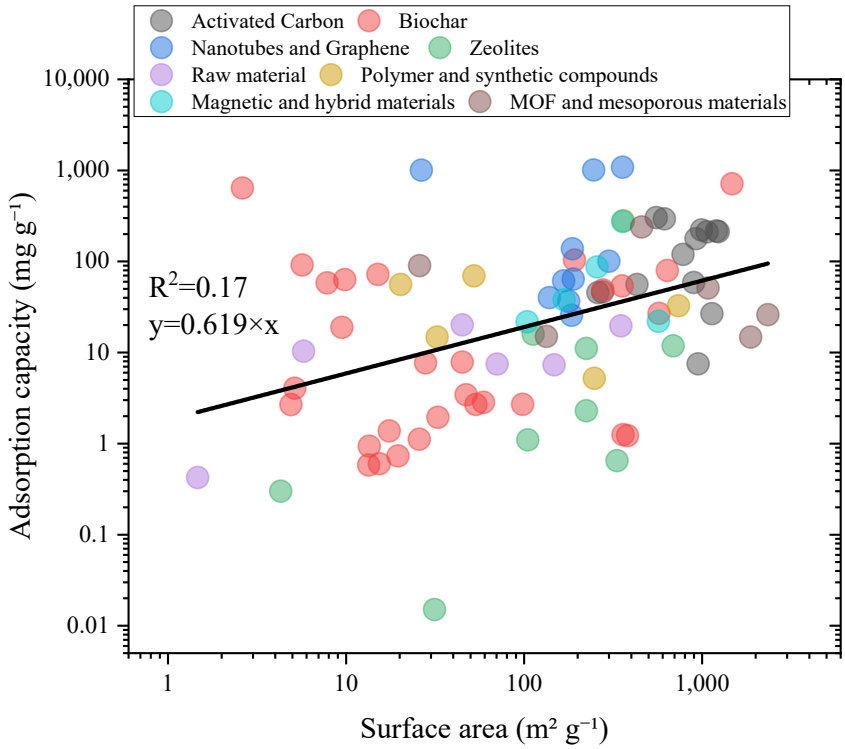

Figure 2. Relationship between surface area of adsorbent and atrazine adsorption capacity according to material; scales are presented on a logarithmic scale.

Surface area and adsorption capacity appear to be generally increasing; however, the relationship is not linear. The significance of well-developed porosity and π–π interactions between the aromatic rings of ATZ and the carbon surface is reflected in the fact that carbon-based materials, including graphitic structures and activated carbons, cluster primarily in the intermediate-to-high surface area range (100–1000 m^2 g^{-1}), with adsorption capacities usually above 10 mg g^{-1}. Because of their many functional groups and delocalized π-electron systems, nanotubes and graphene derivatives have some of the highest capacities (>1000 mg g^{-1}), demonstrating their tremendous affinity for organic micropollutants. On the other hand, biochars exhibit a greater dispersion, and although having moderate surface areas, their capacities range from less than 1 mg g^{-1} to several hundred mg g^{-1}. Surface charge, pore formation, and oxygenated functional groups are all directly impacted by variations in precursor materials, pyrolysis conditions, and surface modification, which are reflected in this heterogeneity. An intermediate area of the plot is occupied by magnetic and hybrid materials, which combine the practical benefit of simple magnetic recovery with a satisfactory adsorption efficiency (10–300 mg g^{-1}).

At higher surface areas (>1000 m^2 g^{-1}), MOFs and mesoporous materials also exhibit comparatively high adsorption, underscoring the significance of consistent pore networks and adjustable surface chemistry. In contrast, zeolites and raw minerals have lower adsorption capacities (<10 mg g^{-1}), highlighting the fact that microporosity by itself does not ensure efficient ATZ absorption, especially when molecular diffusion and interaction are limited by surface charge or hydrophilicity. Synthetic and polymeric substances perform moderately, usually between 1 and 100 mg g^{-1}; this can be improved by functionalizing them with carboxyl, hydroxyl, or amine groups. All things considered, Figure 2 emphasizes that adsorption efficacy results from a mix of chemical and textural elements rather than just surface area. The intricate relationship between surface functionality, pore architecture, and electrostatic or π–π interactions is depicted by the data dispersion. The need to create customized adsorbents that combine high specific area with appropriate surface

chemistry in order to improve atrazine removal effectiveness is further supported by this comparative visualization.

4.1. Effect of pH

Solution pH critically influences the surface charge of adsorbents and the speciation of ATZ, thereby governing adsorption mechanisms. For adsorbent bearing oxygen-containing functional groups (e.g., carboxyl, COOH), protonation occurs under acidic conditions occurs under acidic conditions (pH < pK_a ≈ 4–5) yielding a net positive surface charge; conversely, deprotonation at alkaline pH (pH > pK_a) results in a negatively charged surface. The point of zero charge (pH_{PZC}), defined as the pH at which the net surface charge is zero, is thus a key parameter for predicting electrostatic interactions. ATZ (pK_a ≈ 1.7) is a weak base: below this pH, it exists predominantly in its protonated, cationic form (ATZ–H^+); above pH 1.7, the neutral species dominates across the environmentally relevant pH range (pH 3–9) [14,199,226]. Given its neutrality under near-neutral conditions, ATZ adsorption is generally governed by non-electrostatic forces (e.g., hydrogen bonding, van der Waals, π–π interactions, hydrophobic effects) rather than Coulombic attraction. This explains why weak adsorption has been observed at pH ≈ 7 on certain materials [176], and why optimal removal often occurs at pH values where complementary interactions are maximized, not necessarily at pH_{PZC}.

For instance, Nagarajan et al. [208] reported enhanced ATZ uptake at pH 2 using amine-functionalized carbon dot cellulose sponges, attributed to electrostatic attraction between protonated ATZ (ATZ–H^+) and deprotonated amine groups. ATZ may also interact with ionic surface groups and persist on the adsorbent via specific affinity, even in the absence of strong electrostatic driving forces [158]. Conversely, on nylon 6/polypyrrole (PPy) composites, an inherently basic adsorbent, adsorption capacity decreased at high pH due to diminished favorable interactions between neutral ATZ and the increasingly negatively charged surface (pH > pH_{PZC}. ≈ 10). Notably, when pH exceeded the adsorbent's pH_{PZC}., any improvement in uptake likely stems from specific mechanisms such as hydrogen bonding with deprotonated functional groups, rather than electrostatic attraction to the neutral ATZ molecule. Therefore, accurate prediction of ATZ adsorption requires integrated consideration of: (i) ATZ speciation (pK_a ≈ 1.7), (ii) adsorbent surface chemistry (functional groups, pH_{PZC}), and (iii) dominant interaction mechanisms under prevailing pH conditions [181].

Activated carbon and biochar were selected as representative carbon-based adsorbents due to the extensive availability of experimental data. As illustrated in Figure 3a, the maximum adsorption capacity (q_{max}, mg g^{-1}) of atrazine (ATZ) on both materials exhibits a pronounced pH dependence, with peak performance typically observed under near-neutral conditions (pH 6–8). This trend is consistent with the speciation profile of ATZ, as revealed by microspecies distribution modeling (Figure 3). The molecule exists predominantly in its neutral form, above pH~2.0, but a critical transition occurs around pH 5.7: below this value, the cationic species (protonated at one amino group) remains significant (~10–60%), while above pH 5.7, the neutral form dominates (>95%). At near-neutral pH (6–8), electrostatic repulsion between the neutral ATZ and negatively charged adsorbent surfaces (e.g., carboxylate groups) is minimized, while non-electrostatic interactions, such as hydrogen bonding with protonated amine or hydroxyl groups, π–π stacking, and hydrophobic effects, are maximized. Moreover, the decline in cationic species concentration beyond pH 5.7 reduces potential competition for anionic sites on the adsorbent, further favoring adsorption via affinity-driven mechanisms. Thus, the observed pH optimum reflects not only the dominance of the neutral ATZ species but also the synergistic optimization of surface–molecule compatibility across multiple interaction pathways.

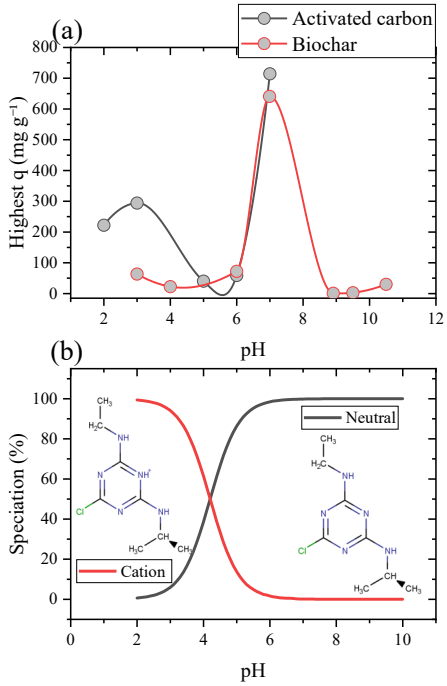

Figure 3. (**a**) Peak atrazine adsorption on carbon materials occurs at near-neutral pH (6–8), coinciding with dominance of neutral species. (**b**) Atrazine speciation shifts from cationic (<pH 5.7) to neutral (>pH 6.0), according to simulations done in Marvinsketh from Chemdraw.

The adsorption capacity is decreased at acidic pH (<4) due to competition protonation, wherein excess H^+ ions compete with ATZ for binding, particularly on biochar surface rich in oxygenated functional groups (–COOH, –OH). As the pH increases, these groups progressively deprotonate, enhancing the availability of electron-rich sites capable of interacting with ATZ's aromatic triazine ring via π–π or n–π interactions. Conversely, under alkaline conditions (pH > 8), these groups will acquire negative charges, while the ATZ is found in neutral form, this renders the interaction between the ATZ and the surface, thus diminishing the overall adsorption capacity. Despite these general trends, biochar and activated carbon exhibit distinct pH sensitivities. Activated carbon displays a broader adsorption plateau across a wider pH range, suggesting greater surface stability and dominance of hydrophobic interactions. In contrast, biochar shows a narrower, more pronounced adsorption maximum near neutrality (pH 6–7), reflecting its heterogeneous surface chemistry and stronger dependence on the protonation state of surface functional groups. Collectively, the results in Figure 3 demonstrate that optimal ATZ removal occurs within a narrow near-neutral pH window, where favorable surface interactions are maximized and electrostatic repulsion is minimized.

4.2. Time of Adsorption Equilibrium

A critical factor influencing adsorption capacity within these experiments was the quantity of adsorbent utilized. Specifically, ATZ concentration, temperature, and pH were maintained as constant variables throughout the study [170]. As shown in Table 3, the influence of the dosage on ATZ adsorption changed from 0.002 to 30 g L^{-1} in the 97 studies. For this analysis, several authors created a graph in which the intersection between the adsorption capacity and removal indicated the ideal dosage, which was fixed in subsequent experiments. However, it is worth noting that not all studies presented experiments related to dosage. According to previous studies, the adsorption capacity of ATZ improved with increasing dosage [88,169,210–212]. This effect is attributed to the expanded surface area and the generation of additional active sites resulting from higher adsorbent concentrations,

which subsequently led to a greater percentage of ATZ adsorbed [11,211]. However, further increases in the amount of adsorbent can result in saturation of the material, promoting a reduction in removal efficiency [210]. That is, the opposite behavior related to the increase in dosage stands out, with the initial occurrence of an increase in the percentage of removal and a gradual decrease in the removal capacity [208,218,227]. Finally, it is important to understand that increasing the dosage of the material will increase the cost of treatment. Therefore, it is essential to define the appropriate dose so that there is a balance between removal efficiency and treatment cost [228].

4.3. Examining the Influence of Contact Time and the Most Appropriate Kinetic Model

Adsorption kinetics describes the rate at which solutes are adsorbed onto a solid surface, with time being a critical parameter in this process. For the design of industrial-scale systems, determining the conditions (including equilibrium time) required to achieve contaminant removal levels mandated by regulatory standards is essential. Adsorption kinetic models are widely employed assess adsorbent performance and elucidate mass transfer mechanisms [151,229,230]. Initially, the adsorption rate is typically rapid due of vacant surface sites and high concentration gradient, the primary driving force for adsorption. As the adsorption proceeds, the rate gradually decreases as activate sites become occupied and the concentration gradient diminishes, leading to convergence between the adsorbate concentrations in fluid phase and within the adsorbent [231]. Ultimately, the system approaches dynamic equilibrium, at which point the amount of adsorbed solute stabilizes. The time required to reach equilibrium depends on the system specific factors, such as the affinity between the solute and the adsorbent surface, the initial concentration of the solute, and the temperature [229]. Conventional kinetics models, such as the pseudo-first-order and pseudo-second-order, are typically formulated based on the overall adsorption process, treating it analogously to a chemical reaction while often neglecting individual diffusion steps [232]. In contrast, diffusion-based models explicitly account for the three sequential stages of mass transfer: (i) external (film) diffusion, where the adsorbate migrates from the bulk solution to the external surface of the adsorbent particle; (ii) intra-particle diffusion, involving transport through the pore network into the particle interior; and (iii) surface adsorption, where the adsorbate binds to active sites via specific physicochemical interactions [233].

Table 4 indicates a preference for utilizing the pseudo-second-order model to characterize adsorption kinetics. This model posits that adsorption involves valence forces and electron exchange between groups, alongside the principle that the rate of adsorption is directly proportional to the square of the available active sites [234]. Additionally, the pseudo-second-order model operates under the assumption of constant adsorbate concentration over time and relates the total number of binding sites to the amount of adsorbate adsorbed at equilibrium. A key benefit of employing this equation is its capacity to minimize the impact of random experimental errors, thereby improving the accuracy of theoretical adsorption capacity estimations [227].

Table 4. Contact time and best kinetic adjustment models obtained for adsorbents used to remove atrazine.

Adsorbent	Contact Time (min)	Kinetic Model	R^2	Reference
Wood charcoal	45	–	–	[99]
Rubber granules	100	–	–	[99]
Bottom ash	210	–	–	[99]

Table 4. *Cont.*

Adsorbent	Contact Time (min)	Kinetic Model	R^2	Reference
Sajor caju	240	–	–	[99]
Florida	240	–	–	[99]
Carbon cloth	125	First-order	0.999	[235]
Rubber granules	120	Pseudo-second-order	–	[236]
Conventional activated carbon (F400)	–	Pseudo-second-order	0.998	[162]
Annealed carbon sample (F400AN)	–	Pseudo-second-order	0.999	[162]
Multiwalled carbon nanotubes MWCNTs–O (0.85%)	180	Pseudo-second-order	1	[166]
Coal fly ash	120	–	–	[167]
Acid-activated zeolite-rich tuffs	–	Pseudo-second-order	–	[14]
Activated carbon prepared from waste rubber tire	60	Pseudo-first-order	0.994	[170]
Granulated activated carbon and carbon nanotubes	–	Pseudo-second-order	>0.93	[171]
Lipoid adsorption material (LAM)	120	–	–	[173]
Nanoscale zero-valent iron supported on organobentonite	120	Langmuir–Hinshelwood	0.998	[172]
Silica gel	–	Elovich	0.969	[237]
Humic acid	–	Elovich	0.996	[237]
Magnetic multiwalled carbon nanotube (MMWCNT)	360	Pseudo-second-order	0.999	[176]
Biochar produced under oxygenated (O-Biochar) conditions	–	Pseudo-second-order	1.000	[179]
Biochar produced oxygen-free (N-biochar)	–	Pseudo-second-order	1.000	[179]
Specific polymeric (G1)	210	Pseudo-second-order	0.992	[13]
Specific polymeric (P2)	210	Pseudo-second-order	0.993	[13]

Table 4. *Cont.*

Adsorbent	Contact Time (min)	Kinetic Model	R^2	Reference
Magnetic hypercrosslinked microsphere (Q150)	100	Pseudo-second-order	0.996	[228]
Organo-beidellites (1.0 CEC–OBd)	60	Pseudo-second-order	1.000	[185]
Carbons SBC	35	Intraparticle	–	[182]
Sludge-derived biochars (SDBCs)	2160	Pseudo-second-order	0.999	[238]
Silver nanoparticles (AgNPs)	840	Pseudo-first-order	0.983	[183]
Carbon sponge	120	Pseudo-second-order	0.914	[181]
Magnetic mesoporous imprinted adsorbent based on Fe_3O_4–modified sepiolite	–	Pseudo-second-order	0.995	[184]
Biochar	10,080	Pseudo-first-order	>0.916	[48]
Composite of AC/MgO/ZnO	150	General order	0.994	[88]
Carbon nanotubes (CNTs)	–	Pseudo-second-order	–	[187]
Activated peanut husk	180	Pseudo-second-order	0.997	[188]
Wheat straw-derived biochar (WS750)	3600	Pseudo-second-order	0.998	[132]
Iron nanocomposite material	–	Pseudo-second-order	0.924	[31]
Moringa oleifera pods	60	Pseudo-second-order	>0.879	[186]
Magnetically recoverable Fe_3O_4/graphene nanocomposite	70	Pseudo-second-order	0.994	[189]
Activated biochar (CAB) from *Calligonum comosum* biomass	30	Pseudo-second-order	0.994	[192]
Hydrous iron oxide (HIOD301)	–	Pseudo-second-order	0.999	[193]
Hydrous aluminum oxide (HAOD301)	–	Pseudo-second-order	0.999	[193]
Zeolite (Z_1–HDTMA)	720	Pseudo-second-order	0.989	[190]
Clay (C_B–BODA)	600	Pseudo-second-order	0.905	[190]

Table 4. *Cont.*

Adsorbent	Contact Time (min)	Kinetic Model	R^2	Reference
SDBS-modified coal-based activated carbon (SCACs)	720	Pseudo-second-order	0.999	[196]
Metal−organic framework (UiO–67)	2	Pseudo-second-order	1.000	[199]
Metal−organic framework (ZIF–8)	40	Pseudo-second-order	0.987	[199]
RGO–BC	150	Pseudo-second-order	0.995	[197]
RGO	300	Pseudo-second-order	0.998	[197]
BC	150	Pseudo-second-order	0.993	[197]
Pyro-hydrochar (PHC–CS_{500})	–	Pseudo-second-order	0.999	[198]
Pyro-hydrochar (BC–CS_{500})	–	Pseudo-second-order	0.991	[198]
Wood activated carbons (WAC)	300	Pseudo-second-order	0.99	[196]
Walnut shells activated carbons (WSAC)	360	Pseudo-second-order	0.99	[196]
Apricot shells activated carbons (ASAC)	120	Pseudo-second-order	0.99	[196]
Porous carbon sponge obtained from sucrose	120	Pseudo-second-order	0.914	[195]
P-doped biochar from corn straw (CSWP)	20	Pseudo-second-order	0.997	[201]
Rice husk ash (RHA)	40	Pseudo-second-order	0.999	[203]
Biochar (BC_{800B})	600	Pseudo-second-order	0.988	[202]
Modified *Moringa oleifera* Lam. seed husks	1200	Pseudo-second-order	0.981	[200]
Laser-induced graphitic material (LIG)	2880	Pseudo-second-order	0.999	[205]
Nanoporous carbons (AMP–7)	480	Avrami	0.99	[42]
Nanoporous carbons (AMP–8)	240	Avrami	0.99	[42]
Nanoporous carbons (AMP–9)	240	Avrami	0.98	[42]

Table 4. *Cont.*

Adsorbent	Contact Time (min)	Kinetic Model	R^2	Reference
Nanohydrogel chitin–cl–polyl	180	Pseudo-second-order	0.975	[204]
β-cyclodextrin-functionalized rice husk-based cellulose (β–CD@RH–C)	180	Pseudo-first-order	0.991	[109]
Peanut shell biochar	4320	Elovich	>0.977	[151]
Graphene oxide-supported nano zero-valent iron (GO/nZVI) composites	–	Pseudo-second-order	>0.999	[206]
Byproducts of wood industry	–	Pseudo-first-order	0.969	[207]
Modified carbon dots with amine supported onto cellulose sponge	30	Pseudo-first-order	0.990	[208]
Graphene oxide nanosheets	–	Avrami	0.984	[32]
Activated carbon from macauba endocarp (*Acrocomia aculeate*)	30	Pseudo-second-order	0.989	[239]
Thermally activated (MCM–41)	–	Intraparticle diffusion	0.994	[210]
Polyacrylate-divinylbenzene microspheres	–	Pseudo-second-order	0.962	[213]
Nanofiber membranes (PAN)	–	Pseudo-second-order	0.999	[211]
Nanofiber membranes (PAN–CD)	–	Pseudo-second-order	0.999	[211]
Nano-MgO modified fallen leaf biochar (MgO–LBC)	100	Pseudo-second-order	0.985	[209]
Framework of nano metal oxides N–NiO@N–Fe_3O_4@N–ZnO	80	Pseudo-second-order	0.998	[212]
Biochar from bamboo	14,400	Internal diffusion	>0.940	[22]
Cellulose doped with nitrogen	30	Pseudo-second-order	>0.983	[224]
Biochar rom cedar bark sawdust (BCC)	–	LDF	0.9724	[214]

Table 4. *Cont.*

Adsorbent	Contact Time (min)	Kinetic Model	R^2	Reference
Biochar from cedar bark sawdust (BACB)	–	LDF	0.9753	[214]
Activated biochar produced from corn straw	600	Intraparticle Diffusion	0.9778	[217]
Graphene oxide (GO)	540	Elovich	0.985	[216]
Reduced graphene oxide (rGO)	540	Elovich	0.998	[216]
Graphene nanoplatelets (GNP)	540	Elovich	0.993	[216]
Multifunction sulfonated polyacrylate-divinylbenzene (PADVB) microspheres	–	Intraparticle diffusion	0.977/0.983	[215]
Residual husks of the edible fruits of *Psidium cattleianum*	>105	General order	0.999	[34]
Cedrella fissilis	25	LDF	0.983	[214]
Apricot kernel shell biochar	2880	Pseudo-second-order	0.998	[221]
Cu–Zn–Fe layered double hydroxides (LDH)	180	Pseudo-second-order	0.976	[223]
Cu–Zn–Fe layered double hydroxides dispersed on bamboo biochar (LDHBC)	180	Pseudo-second-order	0.993	[223]
Rice husk hydrochar	1440	Pseudo-second-order	0.99	[1]
Diospyros kaki fruit waste activated carbon	240	LDF	0.910	[218]
Novel hydrochar derived from *Prunus serrulata* bark	240	Elovich	0.979	[33]
Ionic liquid-functionalized porous m-aminophenol formaldehyde polymer	60	Pseudo-second-order	0.999	[10]
Hovenia dulcis activated carbon (Hd–AC)	180	LDF	$\geq$0.965	[34]

Table 4. *Cont.*

Adsorbent	Contact Time (min)	Kinetic Model	R^2	Reference
Microplastics (PS)	900	Pseudo-second-order	0.934	[222]
Microplastics (PE)	900	Pseudo-second-order	0.976	[222]
Microplastics (PP)	900	Pseudo-second-order	0.967	[222]
Microplastics (Aged–PS)	900	Pseudo-second-order	0.977	[222]
Microplastics (Aged–PE)	900	Pseudo-second-order	0.971	[222]
Microplastics (Aged–PS)	900	Pseudo-second-order	0.942	[222]
KOH-activated N-doped hydrochar (KHCN)	720	Avrami	0.990	[220]
Fallen leaf biochar (LBC)	150	Pseudo-second-order	>0.92	[225]
Graphitic porous carbon (GPC)-based material	60	Elovich	0.998	[35]

"–" stands for not given.

4.4. Effects of Equilibrium, Temperature, and Thermodynamic Parameters

The isotherm can provide information about the adsorbent–adsorbate interaction relationship, as well as obtain the maximum adsorption capacity, which is indicative of the performance of the adsorbent [155,156,240]. Furthermore, isothermal parameters are used to estimate thermodynamic equilibrium [241,242]. Various isotherm models are utilized to determine the maximum adsorbent capacity, guiding the selection of optimal dosages for achieving desired efficiencies. Analyzing statistical coefficients is crucial for identifying the most appropriate model. Commonly employed isotherms include the Langmuir, Freundlich, Langmuir–Freundlich, Sips, Redlich–Peterson, Toth, and Dubinin–Radushkevich models [243]. Of the 137 adsorbents examined in the literature, the Langmuir (52 adsorbents) and Freundlich (49 adsorbents) models demonstrated the best fit to the data [205]. The Langmuir isotherm is primarily applicable to monolayer adsorption on uniform surfaces, while the Freundlich model is better suited for heterogeneous surfaces, accommodating both monolayer and multilayer adsorption processes [244]. Several models, including the Liu, Sips, Langmuir, and Freundlich models, have been previously identified as effective for describing adsorption kinetics. Notably, some studies omitted isothermal models altogether. The Langmuir and Freundlich models were deemed most suitable for adapting to varying temperatures, with capacities observed between 277 and 328 K. Consequently, employing these models at room temperature would represent the most efficient and practical approach for real-world applications, minimizing energy consumption [245,246].

Most studies have reported that increasing temperature results in greater adsorption of ATZ molecules, revealing endothermic behavior [30,32,175,192]. This can be explained by the agitation of the molecules as the temperature increases, which consequently allows easier adsorption of contaminants in the pores [247]. Alahabadi and Moussavi [192] studied

the effect of temperature between 282 and 313 K on two different materials, standard activated carbon (SAC) and powdered carbonate-activated biochar (CAB). The results showed that for CAB, adsorption improved with increasing temperature, but for SAC, the efficiency decreased with increasing temperature [32]. The authors also reported the influence of temperature (288–318 K) on the adsorption of ATZ by graphene oxide (GO) nanosheets. However, at lower temperatures, the removal efficiency increased with increasing temperature up to 648 K but decreased when the temperature increased to 648 K. This exothermic process was also reported in studies by Kovaios, Paraskeva, and Koutsoukos [237], Liu et al. [112], and Sharma et al. [204] using humic acid and silica, an Fe_3O_4/sepiolite magnetic composite (MSEP), and a nanohydrogel chitin–cl–polyl as materials, respectively. On the other hand, in an investigation by Ureña-Amate, Socías-Viciana, González-Pradas, and Saifi [161] using heat-treated kerolite, it was shown that adsorption was more effective at low temperatures. The experiment suggested that kerolite does not have much affinity for ATZ, and therefore there is no competition from the solvent for adsorption sites. In a study by Nam et al. [180], using activated carbon, it was highlighted that a low temperature (278 K) of water reduced the removal of hydrophobic compounds, such as ATZ. Therefore, this study highlights the importance of hydrophobic interactions in the adsorption process, considering that the diffusion of sorbates in sorbents positively influences intermolecular interactions. Finally, the studies by Agdi et al. [158] and Jamil, Gad-Allah, Ibrahim, and Saleh [174] with different materials reported that temperature did not affect the removal efficiency of the pesticide atrazine. However, the adsorption capacity can vary according to the nature of the sorbent and sorbate [174].

Thermodynamic evaluation, based on parameter calculations, contributes to the analysis of ATZ adsorption efficiency and assists in the effective design of water treatment systems [175]. In thermodynamic work for ATZ removal, studies have varied the temperature between 277 and 348 K, in which most studies used three different temperatures for the tests. Therefore, Table 5 presents data on the thermodynamic parameters obtained for the adsorption of ATZ on different adsorbents found in the literature, in addition to the different temperatures measured and used in the studies. The parameters included the free standard of Gibbs free energy variation (ΔG^0, kJ mol^{-1}), enthalpy variation (ΔH^0, kJ mol^{-1}), and entropy variation (ΔS^0, J mol^{-1} K^{-1}). However, it is worth noting that not all studies have presented experiments related to thermodynamic parameters. Of the 35 studies that proposed evaluating the thermodynamic parameters with different materials for the adsorption of atrazine, practically all presented a negative value for the Gibbs free energy (ΔG^0), except for the study by Liu and Chen [184], which observed a positive value. A negative value ($\Delta G^0 < 0$) indicates that the adsorption of the herbicide was spontaneous and favorable [35,248]. As mentioned, the study by Liu and Chen [184] presented positive values for Gibbs free energy at all temperatures, which indicates that the adsorption reaction was not spontaneous and that the system obtained energy from an external source.

Positive values of ΔH^0, confirms the endothermic nature of the adsorption process. This behavior has been reported for ATZ adsorption on *Hovenia dulcis* derived activated carbon [248] and on various biochars [30]. Consistent with this Goyal et al. [210] observed an increase in ATZ removal efficiency, from 88.6 to 94.5%, as the temperature rose from 293 to 313 K, further supporting an endothermic process ($\Delta H^0 > 0$). In contrast, Chen et al., reported exothermic ATZ adsorption ($\Delta H^0 < 0$) on multiwalled carbon nanotubes (MWCNTs), highlighting the dependence of thermodynamic behavior on adsorbent surface properties. Additionally, the standard enthalpy change serves as key indicator for distinguishing between physisorption ($\Delta H^0 < 40$ kJ·mol^{-1}) and chemisorption ($\Delta H^0 > 80$ kJ·mol^{-1}) mechanisms [189].

Table 5. Thermodynamic parameters for adsorption of atrazine on different adsorbents found in literature.

Adsorbent	T (K)	ΔG^0 (kJ mol^{-1})	ΔH^0 (kJ mol^{-1})	ΔS^0 (J mol^{-1} K^{-1})	Reference
Rubber granules	–	–14.448 –17.346	–12.885	5.166	[236]
Conventional activated carbon (F400)	298	−14.618	–	–	[162]
	308	−14.340	–	–	
	318	−15.334	–	–	
Annealed carbon sample (F400AN)	298	−15.609	–	–	
	308	−14.852	–	–	
	318	−15.599	–	–	
Carbon nanotubes (SMWNT20)	291	–35.60	–87.36	–195.9	[28]
	298	–35.00		–197.8	
	303	–33.45		–203.1	
	291	–38.12		87.0	
Carbon nanotubes (r–MWNT)	298	–38.87	–12.75	87.6	
	308	–39.56		87.0	
Multiwalled carbon nanotubes MWCNTs–O (0.85%)	288	–13.1	–36.87	–82.56	[166]
	298	–12.14		–85.88	
	308	–11.45		–88.29	
Multiwalled carbon nanotubes MWCNTs–O (2.16%)	288	–12.14	–28.39	–56.44	
	298	–11.47		–58.76	
	308	–11.01		–60.35	
Multiwalled carbon nanotubes MWCNTs–O (7.07%)	288	–9	–37.24	–98.06	
	298	–7.68		–102.65	
	308	–7.04		–104.86	
Activated carbon prepared from waste rubber tire	298	–17.15	–138.27	–406.44	[170]
	308	–13.09			
	318	–9.02			
Carbon nanotubes	288	–27.11	–32.29	–11.89	[171]
	296	–26.97	–30.54	–12.05	
	304	–26.92	–28.69	–11.89	
Banana peel	298	–5.7	67.8	0.25	[175]
Biochar CS450	283.15	–25.61	136	12.376	[178]
	298.15	–29.25			
	313.15	–29.69			
Biochar ADPCS450	283.15	–25.06	35.6	–15.247	
	298.15	–26.40			
	313.15	–26.13			
Granular carbon	–	–23.38	–	–	[49]
Magnetic molecularly imprinted polymer (MSEP@MIP)	278	2.747	–2.988	–8.257	[30]
	288	3.196			
	298	3.886			
	308	4.352			

Table 5. *Cont.*

Adsorbent	T (K)	ΔG^0 (kJ mol^{-1})	ΔH^0 (kJ mol^{-1})	ΔS^0 (J mol^{-1} K^{-1})	Reference
Functionalized nylon6/polypyrrole core–shell nanofibers mat (PA6/PPy NFM)	293	–0.177	12.7	0.044	[181]
	303	–0.653			
	323	–1.606			
	343	–2.356			
Iron nanocomposite material	293	–6.05	–6.68	-2.45×10^{-3}	[31]
	298	–6.11			
	303	–6.15			
Chemically treated *Moringa oleifera* pods (MOPC)	298	–1.93	12.3	0.048	[186]
	308	–2.40			
	318	–2.88			
Thermally treated *Moringa oleifera* pods (MOPT)	298	–10.49	16.14	0.089	
	308	–11.32			
	318	–12.28			
Activated biochar from *Calligonum comosum* biomass	283	–0.7	157.1	283.8	[192]
	293	–1.3			
	303	–3.1			
	313	–5.2			
Magnetically recoverable Fe_3O_4/graphene nanocomposite	293	–1.298	2.48	0.035	[189]
	298	–1.370			
	303	–1.443			
	308	–1.570			
Activated carbons onto wood (WAC)	293	–4.11	22.27	0.09	[196]
	308	–5.46			
	323	–6.81			
Activated carbons onto walnut shells (WSAC)	293	–8.045	13.57	0.07	
	308	–9.16			
	323	–10.26			
Activated carbons onto apricot shells (ASAC)	293	–0.40	41.57	0.14	
	308	–2.55			
	323	–4.70			
Cyclodextrin based polymers α–EPI	298	–7.878	–7.159	2.246	[11]
	323	–7.767			
	348	–8.009			
Cyclodextrin based polymers β–EPI	298	–7.507	–4.585	9.820	
	323	–7.767			
	348	–7.996			
Cyclodextrin based polymers γ–EPI	298	–6.621	–4.906	5.748	
	323	–6.760			
	348	–6.908			

Table 5. *Cont.*

Adsorbent	T (K)	ΔG^0 (kJ mol^{-1})	ΔH^0 (kJ mol^{-1})	ΔS^0 (J mol^{-1} K^{-1})	Reference
P-doped biochar (Corn straw)	298	–4.8363	–27.9616	–77.4640	[201]
	308	–4.1891			
	318	–3.2814			
Moringa oleifera Lam. seed husks	298	–23.449	14.775	0.128	[200]
	308	–24.441			
	318	–26.075			
β-cyclodextrin functionalized rice husk-based celulose (β–CD@RH–C)	283	–23.66	–13.00	–38.48	[109]
	303	–25.11			
	323	–25.20			
Modified carbon dots with amine supported onto cellulose sponge	283	–6.38	–4.324	0.0073	[208]
	293	–6.46			
	303	–6.53			
Thermally activated MCM– 41	293	–86.8	9.409	–6.14	[210]
	298	–88.7			
	303	–91.3			
	308	–95.5			
	313	–98.3			
Novel hydrochar derived from Prunus serrulata bark	298	–22.19	5.33	0.0922	[33]
	308	–23.06			
	318	–24.05			
	328	–24.93			
Diospyros kaki fruit waste activated carbon	298.15	–18.00	8.89	0.09	[218]
	308.15	–18.80			
	318.15	–19.62			
	328.15	–20.74			
Apricot kernel shell biochar XH–190	288	–21.99	10.88	0.11	[221]
	298	–22.38			
	308	–24.26			
Apricot kernel shell biochar XH–210	288	–21.56	8.35	0.10	
	298	–22.90			
	308	–23.65			
Apricot kernel shell biochar XH–240	288	–22.65	2.01	0.09	
	298	–23.30			
	308	–24.05			
Novel nitrogen (N)-doped cellulose biochar (NC1000–5)	277	–32.59	14.31	0.17	[224]
	285	–33.95			
	293	–35.38			
	301	–36.64			
	309	–38.02			

Table 5. *Cont.*

Adsorbent	T (K)	ΔG^0 (kJ mol^{-1})	ΔH^0 (kJ mol^{-1})	ΔS^0 (J mol^{-1} K^{-1})	Reference
Cellulose doped with nitrogen	277	–34.34	15.93	0.18	[224]
	285	–35.76			
	293	–37.11			
	301	–38.71			
	309	–40.12			
Novel nitrogen (N)-doped cellulose biochar (NC1000–20)	277	–33.30	15.12	0.18	
	285	–34.75			
	293	–36.37			
	301	–37.47			
	309	–38.93			
Novel nitrogen (N)-doped cellulose biochar (NC1000–30)	277	–32.91	14.36	0.17	
	285	–34.23			
	293	–35.59			
	301	–37.06			
	309	–38.32			
Corn cob bio-waste (CBS, 600 °C–4 h)	288	–0.070	32.972	0.125	[23]
	298	–0.346			
	308	–1.838			
Ionic liquid (IL)-functionalized porous m-aminophenol formaldehyde polymer (IL–PMAPFP)	298	–13.64	13.96	92.61	[10]
	308	–14.56			
	318	–15.49			
Biochar from *Cedrella fissilis*	298.15	–28.899	15.721	0.142920	[214]
	308.15	–30.029			
	318.15	–31.845			
	328.15	–33.271			
Activated carbon of *Hovenia dulcis*	298	–38.59	8.21	0.1571	[248]
	308	–40.28			
	318	–41.79			
	328	–43.31			
Activated carbon of araçá fruit husks (*Psidium cattleianum*)	298.15	–14.29	129.5	0.5000	[34]
	308.15	–24.63			
	318.15	–29.49			
	328.15	–34.50			
Porous N-doped hydrochar (KHC)	288	–30.05	20.23	32.04	[220]
	298	–28.5			
	308	–30.78			
Porous N-doped hydrochar (KHCN)	288	–24.7	–7.13	110.45	
	298	–25.72			
	308	–26.91			

Table 5. *Cont.*

Adsorbent	T (K)	ΔG^0 (kJ mol^{-1})	ΔH^0 (kJ mol^{-1})	ΔS^0 (J mol^{-1} K^{-1})	Reference
Microplastics PS	288.15	–3.06	22.28	87.93	[222]
	298.15	–3.94			
	308.15	–4.81			
Microplastics PE	288.15	–11.49	25.22	127.39	
	298.15	–12.76			
	308.15	–14.04			
Microplastics PP	288.15	–6.96	22.09	100.83	
	298.15	–7.97			
	308.15	–8.98			
Microplastics Aged–PS	288.15	–5.07	21.28	91.48	
	298.15	–5.99			
	308.15	–6.91			
Microplastics Aged–PE	288.15	–12.78	22.92	123.91	
	298.15	–14.02			
	308.15	–15.26			
Microplastics Aged–PP	288.15	–9.33	20.17	76.8	
	298.15	–10.10			
	308.15	–10.86			
Cu/Zn/Fe LDH composites	303	–24.397	30.474	86.619	[223]
	318	–25.605			
	328	–26.410			
Cu/Zn/Fe LDHBC composites	303	–16.968	24.253	56.081	
	318	–17.808			
	328	–18.368			
Graphitic porous carbon modified with iron oxides	303	–24.3	–	–	[35]
	313	–26.6			
	323	–26.4			

Physisorption typically involves ΔG^0 in the range of −20 to −40 kJ·mol^{-1} and enthalpy changes ΔH^0 < 40–50 kJ·mol^{-1}, whereas chemisorption is characterized by stronger interactions, with ΔH^0 generally exceeding 80 kJ·mol^{-1} [201]. Most studies on ATZ adsorption report physisorption as the dominant mechanism [166,174,237]. This is corroborated by Chen et al. [166], de Suo et al. [201], and Hernandes et al. [214], who attributed ATZ uptake to weak interactions, such as van der Waals forces and hydrogen bonding, based on relatively low ΔH^0 values (e.g., 20 kJ·mol^{-1}, −27.96 kJ·mol^{-1}, and −15.72 kJ·mol^{-1}, respectively). Regarding ΔS^0, a negative value signifies a decrease in system randomness, often reflecting the immobilization and ordering of ATZ molecules at the solid–liquid interface [31,109]. Conversely, a positive ΔS^0 indicates increased disorder, typically associated with the release of hydrated water molecules from the adsorbent surface or adsorbate during adsorption, as observed by Dikshit and Bandyopadhyay [236] and others [220]. Notably, positive ΔS^0 values have also been linked to structural rearrangements in the adsorbent or displacement of bound solvent [196,223]. Since adsorption is inherently temperature–dependent, thermodynamic studies are essential to assess process spontane-

ity (via $\Delta G^0 < 0$), favorability, and underlying mechanisms. Collectively, the literature demonstrates significant potential for carbon-based materials in ATZ-contaminated water treatment, with thermodynamic analyses providing critical mechanistic insights. Nevertheless, several studies omit temperature-dependent experiments, precluding robust thermodynamic evaluation and leaving the nature of the adsorbate–adsorbent interaction (e.g., physisorption vs. chemisorption, role of solvation) inadequately resolved.

4.5. Mechanism for Atrazine Adsorption

The key lies in the chemical affinity and structural complementarity between the adsorbent and the atrazine molecule. High-performance adsorbents possess characteristics that maximize attractive forces and the space available for atrazine to bind. The main factors are: surface area and porosity, surface chemistry (functionalities), and electrostatic characteristics (surface charge). A high surface area (hundreds or thousands of m^2/g) provides more active sites for adsorption. Pore size is crucial: mesoporous pores (2–50 nm) are ideal for accommodating the atrazine molecule, which has dimensions in the range of 1.1 nm, facilitating diffusion and accommodation. The presence of specific functional groups on the adsorbent surface (such as carboxylic, hydroxyl, and amino groups, etc.) can form strong chemical bonds (e.g., hydrogen bonds) with the N and Cl atoms of atrazine. The adsorbent can have a positive or negative surface charge depending on the pH. Atrazine is a neutral molecule over a wide pH range, but in acidic media, the adsorbent can become positively charged and attract the molecule through dipole–dipole interactions or van der Waals forces. Each property of the adsorbent favors one or more specific adsorption mechanisms. Atrazine, being a molecule with a triazine ring, N and Cl atoms, and alkyl chains, can interact in various ways (Table 6). The pH of the medium is a critical factor that modulates many of these mechanisms, as it alters the surface charge of the adsorbent and the ionization state of atrazine (pKa = 1.7).

Regarding the trends emerging from the different datasets, analyzing the literature (Table 3), we can group the adsorbents and identify clear performance and development trends. Set 1 corresponds to carbonaceous adsorbents, which have an extremely high surface area (>1000 m^2/g) and developed porosity. The dominant mechanism is physisorption and pore-filling. It is the most efficient, but also the most expensive. Biochar, on the other hand, shows a main research trend focused on cost effectiveness. Its efficiency is highly variable, depending on the biomass of origin (sawdust, rice husk, sugarcane bagasse) and the pyrolysis temperature. As an emerging trend, pyrolysis at high temperature (>600 °C) produces biochars with a larger surface area and aromaticity (more hydrophobic), improving adsorption through π–π interactions (between the aromatic ring of biochar and the triazine ring of atrazine) and hydrophobic interactions. Modification of biochar with metals or amines to introduce new mechanisms (complexation, hydrogen bonding) is a burgeoning area. Group 2 includes clay and mineral adsorbents. Bentonite, montmorillonite, and zeolites generally exhibit moderate to low adsorption capacities for atrazine. As an emerging trend, modification with surfactants (e.g., CTAB) creates organophilic clays. The surfactant opens the space between the clay layers and creates hydrophobic sites where atrazine can be partitioned (partition mechanism), drastically increasing the adsorption capacity.

Set 3 includes "green" and low-cost adsorbents such as raw biomass, chitosan, and peat. These have low capacity but are attractive due to their sustainability. As an emerging trend, the focus is not on using them in pure form, but as precursors for the synthesis of more efficient compounds (e.g., chitosan hydrogels, biocomposites with magnetite) or in combined processes. High-tech and molecularly engineered adsorbents (set 4), such as molecularly imprinted polymers (MIPs), exhibit maximum specificity. They are synthesized to have "tailor-made" molecular cavities for atrazine. Their emerging trend is related to the

state of the art in selectivity, but the cost and complexity of synthesis still limit large-scale application. Ideal for sensors or final trace removal. Metal–organic frameworks (MOFs) exhibit exceptional performance due to their ultra-high porosity and diverse chemistry. As an emerging trend, research focuses on overcoming hydrolytic instability and high cost. Development of MOFs based on cheaper and more water-stable raw materials. Finally, the clearest trend that emerges from the analysis of all datasets is the transition from nonspecific adsorbents to "designed" or "modified" materials with multiple synergistic mechanisms. The ideal adsorbent of the future is not just one with a large surface area, but one that combines: An accessible porous structure (for high capacity). Specific functional groups (for strong affinity/chemisorption). Hydrophobic/aromatic characteristics (for π–π and hydrophobic interactions) and low cost and sustainability (using waste as raw material). Therefore, modified biochars and composites (e.g., biochar–iron nanoparticles, biochar–clay) represent the most promising frontier currently, as they seek to combine the efficiency of carbonaceous materials with the chemical functionality of other materials, at a viable cost.

Table 6. How physicochemical properties influence adsorption mechanisms.

Adsorbent Property	Adsorption Mechanism of Atrazine	Explanation
High surface area/pore volume	Physical adsorption (Physisorption)	Van der Waals forces. The greater the contact area, the stronger the physical adsorption. This is the primary mechanism in unmodified activated carbons.
Pores of appropriate size	Pore-filling/molecular sieving	The atrazine molecule (~1.1 nm) diffuses and is physically "trapped" in pores of equivalent or slightly larger size.
Oxygenated functional groups	Hydrogen bonding	The N atoms in the triazine ring of atrazine act as hydrogen acceptors. –OH and –COOH groups on the adsorbent surface donate H atoms, forming hydrogen bonds.
Hydrophobic surface	Hydrophobic interactions	The alkyl chain (isopropyl) of atrazine is hydrophobic. In an aqueous medium, it is "expelled" from the water and tends to adsorb onto hydrophobic surfaces, such as the graphitic carbon network of biochar.
Positive surface charge (at low pH)	Electrostatic interaction/charge complexation	At pH < pH_{pzc} (point of zero charge), the adsorbent surface becomes protonated (positive charge). It can attract the electronegative region of the atrazine's triazine ring.
Presence of metals or cations	Coordination complexation	Adsorbents like clays or modified magnetic compounds may have cations (Fe^{3+}, Cu^{2+}, etc.) that form complexes with the N atoms of atrazine.

Adsorption of organic compounds is mostly dependent on molecular properties of the molecules such as particle size and hydrophobicity, among others. Moreover, the functional groups of the adsorbents are also important in adsorbent/adsorbate interaction [249]. Consequently, the adsorption of atrazine (ATZ) cannot be reliably predicted unless specific variables such as the solution pH, adsorbents' point zero charge, adsorbents surface chemistry, and ATZ speciation properties [182]. In line with the review data presented in Table 6, the major adsorption mechanisms responsible for ATZ adsorption onto differ-

ent adsorbents include π–π electron donor–acceptor interactions, hydrogen bonding and pore-filling effect. Meanwhile, the pH of the solution is found to be much less important in regards to atrazine adsorption onto biochar adsorbent. As a result, the adsorption process is driven by hydrophobic interactions and π−π interactions between the heterocyclic rings of atrazine, rather than by electrostatic interactions [199]. The most plausible explanation is that ATZ exists predominantly in its neutral molecular form in aqueous solution, rather than as its conjugate acid, under the studied pH conditions. A comprehensive overview of the dominant adsorption mechanisms is provided in Table 7 and Figure 4, organized under the following subheadings.

Table 7. Dominant mechanisms for ATZ adsorption onto various adsorbents.

Adsorbent	Adsorption Mechanism	References
Biochar	π–π electron-donor-acceptor (EDA) interactions, hydrogen bond, pore-filling	[88]
Activated biochar	π–π EDA, π–H bond, H-bonding, hydrophobic interactions, pore-filling effect	[179]
Biochar	Hydrogen bonding, π–π or n–π interactions	[214]
Biochar	H-bonding, π–π EDA, and hydrophobic interactions, pore-filling effect	[23]
P-doped biochar	Hydrogen bonding, electrostatic interaction, and pore-filling effect	[201]
Activated carbon	π–π interactions, hydrogen bonding, hydrophobic interactions	[182]
Biochar	π–π EDA, pore-filling effect	[225]
N-doped biochar	π–π EDA interaction	[224]
Hydrochar	π–π EDA interaction, H-bond formation	[1]
Activated carbon	Hydrogen bonds, electrostatic interactions, π–π interactions	[218]
Activated biochar	H-bonding, π–π stacking, π–π electron interactions	[217]
Modified cellulose fiber	Hydrogen bonding	[165]
Activated zeolite-rich tuffs	Electrostatic interaction	[14]
Cyclodextrin modified polyacrylonitrile nanofiber membranes	Hydrophobic interactions, π–π bonding, hydrophobic interactions	[211]
Cu/Zn/Fe LDH	π–π stacking	[223]
rGO	H-bonding interaction, π–π stacking interaction,	[224]
Sulfonated polymeric microspheres	Hydrogen bonds, Bronsted acid–base interaction, π–π EDA interactions	[215]
Nanoporous carbons	Electrostatic interaction	[42]
Fe_3O_4/rGO nanocomposite	π–π interactions, Hydrophobic interaction	[189]
Metal−organic framework	Hydrophobic interactions and π−π interactions	[199]

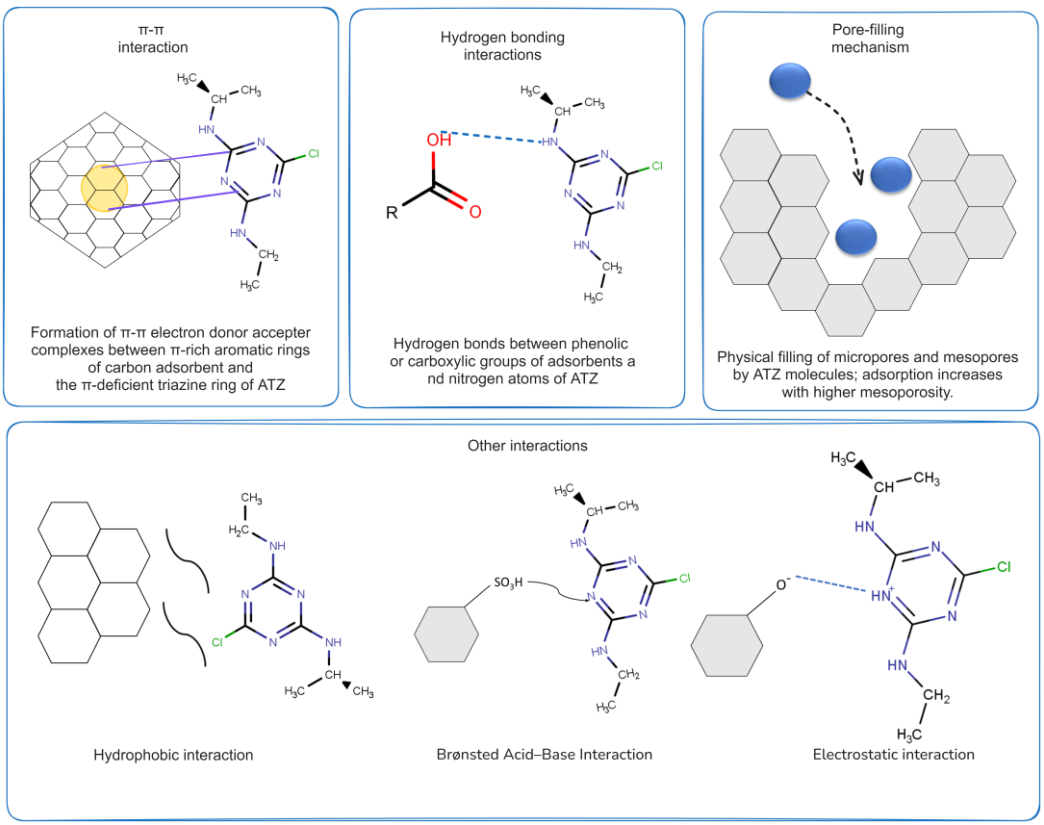

Figure 4. Adsorption mechanism and interactions of ATZ according to reported works.

π–π electron donor–acceptor (EDA) interaction: This mechanism is particularly prominent in carbon-based adsorbents rich in polar oxygen-containing functional groups (e.g., –OH, C=O, –COOH) and extended aromatic domains—such as activated carbon, biochar, and related materials [250]. During ATZ adsorption, the π-electron-rich aromatic systems of these adsorbents engage in π–π electron donor–acceptor (EDA) interactions with the electron-deficient triazine ring of ATZ. This π–deficiency arises from the strong electron–withdrawing effects of the ring nitrogen atoms and the chlorine substituent [182]. Experimental evidence supports this mechanism: Binh et al. [23] observed a new FTIR band corresponding to aromatic C=C stretching upon ATZ adsorption onto corncob-derived biochar (CBS), indicative of π–π coupling and the formation of an electron donor–acceptor complex between the electron-rich aromatic rings of CBS and the delocalized π–system of ATZ. Similarly, Cheng et al. [225] engineered an N-doped biochar with a high degree of graphitization and electron–deficient aromatic moieties, which function as π–acceptors, thereby enhancing π–π EDA interactions with ATZ, which acts as a π–donor in this context. Hernandes et al. [214] further elucidated the interplay between solution chemistry and adsorption mechanisms by analyzing ATZ speciation ($pK_a \approx 1.7$) across pH conditions. At pH < pK_a, ~61.3% of ATZ exists as a monocation (protonated at the alkylamino group), while the remainder remains neutral. Under acidic conditions, when the biochar surface is typically protonated (positively charged), conventional electrostatic repulsion would be expected; however, the study suggests that cation–π interactions, between the protonated ATZ species and the electron-rich aromatic rings of biochar, dominate over weak electrostatic effects. Complementing this, Jung et al. [180] investigated ATZ adsorption on N- and O-functionalized biochars and highlighted ATZ's amphoteric character, featuring both polar/charged groups and aromatic moieties, similar to many endocrine-disrupting compounds and pharmaceuticals. Their findings revealed that N-biochar exhibited higher surface polarity. At pH 3.5, partial protonation of ATZ reduced the fraction of the neutral

species, yet enhanced adsorption was observed, attributed to π–H bonding (a subset of hydrogen bonding involving aromatic C–H donors) between polar functional groups on the biochar and ATZ's aromatic rings.

Hydrogen bonding interaction: Another proposed mechanism for the adsorption of atrazine (ATZ) is through hydrogen bonding interactions. According to the review data (Table 6), this bonding interaction is particularly dominant with carbon-based adsorbents. Atrazine, acting as a hydrogen bond acceptor, often forms hydrogen bonds between the phenolic groups of carbon adsorbents and the nitrogen atoms of the atrazine ring [201]. Similarly, Binh, Nguyen, and Kajitvichyanukul [23] prepared biochar from corncob and identified a substantial presence of carbonyl, phenolic, carboxylic, and alcohol functional groups on the biochar adsorbent. The study reported that hydrogen bonds form between the hydrogen atoms of the carboxyl and phenolic groups of the biochar and the nitrogen atoms of the atrazine ring [88]. Additionally, the π-electrons of the nitrogen rings in atrazine also act as nucleophiles, facilitating hydrogen bonding with the biochar [23]. In the case of sulfonated polymeric microsphere adsorbents, Gong, Liu, Shen, Zhao, Wu, Zhang, Kang, Wu, Chen, and Xu [215] pointed out that the amino groups of the atrazine molecule could form hydrogen bonds with the oxygen atoms from the ester or sulfonic groups on the adsorbent's surface. The strong electronegativity of the oxygen atoms and the electron deficiency of the nitrogen atoms in the atrazine molecule, due to the triazine ring, further stabilize the hydrogen bonds formed [215].

Pore-filling mechanism: The pore-filling mechanism involves the successful occupation of an adsorbent's pores and void spaces by adsorbate molecules. This mechanism's success largely depends on the adsorbent's porosity, with a notable emphasis on the importance of the adsorbent's micro- and meso-porosity [88]. Also, Cao, Wang, Kang, Song, Guo, and Zhang [225] documented the occurrence of a pore-filling mechanism during ATZ adsorption onto a highly mesoporous biochar, as confirmed by SEM and BET surface area measurements. On the other hand, N-/O-doped biochar with larger micro- and macro-pore volumes exhibited limited pore-filling and sieving effects, highlighting the positive correlation between ATZ adsorption capacity and the pore properties of the adsorbent [179]. Additionally, Binh, Nguyen, and Kajitvichyanukul [23] observed that pore-filling adsorption enhanced ATZ adsorption onto corncob biochar.

Other adsorptive interactions: The Bronsted–Lowry's theory relating to proton transfer between chemical species also played out during ATZ adsorption. According to Gong, Liu, Shen, Zhao, Wu, Zhang, Kang, Wu, Chen, and Xu [215], the interaction between the triazine rings and the protons of the sulfonic groups (–SO_3H) on the sulfonated microspheres is attributed to Bronsted acid–base interactions. This is true because the nitrogen atoms on the triazine ring are protonated at low pH levels, allowing them to act as Bronsted bases, while the sulfonic groups on the adsorbent function as Bronsted acid sites. Also, Boruah, Sharma, Hussain, and Das [189] observed variations in the peak positions of the aliphatic and aromatic functional groups after ATZ adsorption onto the Fe_3O_4/rGO nanocomposite. These changes suggest electrostatic interactions between the ($=N^+-$) group of ATZ and the oxygen-containing functionalities of the Fe_3O_4/rGO nanocomposite. Additionally, it was reported that the hydrophobic edge and basal plane of reduced graphene oxide (rGO) formed strong hydrophobic interactions with the heterocyclic ATZ molecules [189].

4.6. Textural Properties and Adsorption Capacity

Adsorbent structural properties are fundamentally important to the efficiency of the adsorption process, influencing adsorption capacity, selectivity, kinetics, and overall effectiveness [231]. A critical aspect of adsorbent structural properties is surface area. The specific surface area represents the total area accessible for adsorption. Adsorbents

with greater surface areas possess more active sites, resulting in increased adsorption capacity [6,251]. Furthermore, porosity significantly contributes to contaminant removal through adsorptive processes. The porosity of an adsorbent refers to the presence of pores in its structure. Well-defined and controllable pores can increase the adsorption capacity because they provide additional sites for adsorbent molecules to bind. Porosity also affects adsorption kinetics, as it influences the diffusion of molecules into the adsorbent. It is important to highlight that very small pores can make it difficult for adsorbate molecules to penetrate the internal surface of adsorbent particles; therefore, it is essential to have a balance between surface area and pore size [252]. As illustrated in Table 3, an increase in adsorbent surface area correlates with enhanced ATZ adsorption capacity. For instance, coal-based activated carbon modified with sodium dodecylbenzene sulfonate exhibited a surface area of 990 m^2 g^{-1} and a high adsorption capacity of 222 mg g^{-1} [196]. It is important to note that numerous factors impact adsorption capacity, including pH, temperature, pollutant concentration, and the functional groups present on the adsorbent—as demonstrated by the case of graphene oxide, which exhibited an exceptional adsorption capacity of over 1000 mg g^{-1} despite having a surface area of only 250 m^2 g^{-1} [216].

4.7. Adsorption Analysis in Different Aqueous Matrices

Monitoring the water quality of reservoirs situated near agricultural areas is critical, as these systems often serve as sources of drinking water for livestock and support sensitive aquatic ecosystems [34]. From a treatment perspective, real-world wastewater and surface waters typically contain multiple pesticide residues, whose co-presence can significantly alter sorption behavior through competitive or synergistic effects [253]. Moreover, natural organic matter (NOM) in aquatic matrices is known to impede adsorption—either by blocking active sites on the adsorbent surface or by forming soluble complexes with target contaminants [254]. Table 8 compiles comparative data from studies employing real environmental samples for ATZ removal, highlighting the performance of various adsorbents across a range of initial concentrations and matrix conditions. Notably, Agdi et al. [158] evaluated diatomaceous earth for the simultaneous removal of ATZ and four organophosphate pesticides (chlorpyrifos, methidathion, parathion–methyl, and fenamiphos) from river water and wastewater (collected from a water treatment plant in Madrid, Spain). ATZ removal efficiency varied markedly with water type: 80% in treated wastewater, 55% in untreated wastewater, and 50% in river water. The lower efficiencies in river and untreated wastewater are attributed to their higher NOM content, which likely competes for adsorption sites or shields ATZ from interaction with the adsorbent surface.

Tang et al. [176] carried out a practical application on real samples with pure water, tap water, and river water (Xiangjiang, China) and found that pure water and tap water obtained almost identical adsorption capacities, while the adsorption capacity in river water was slightly greater than that in ultrapure water. It should be noted that the pH was not adjusted to simulate real conditions. Zhou et al. [228] simulated water treatment with natural water from the Yangtze River (China) enriched with 20 µg/L ATZ and reported that the removal capacity of the two adsorbents decreased due to the high proportion of dissolved organic matter. Even so, one of the adsorbents tested exhibited satisfactory removal capacity. In another study, Gong et al. [213] evaluated the adsorption mechanism on PADVB polyacrylate-divinylbenzene microspheres (PMs–03) and powdered activated carbon (PAC) to remove traces of organic micropollutants (OMPs) from reservoir water and deionized water, including ATZ. The samples were spiked with 5 µg/L of each OMP. PADVB microspheres obtained very similar removal efficiencies, both from deionized water and from reservoir water, and were superior to the removal efficiency of PAC. The ATZ removal percentages obtained from the use of PM–03 were greater than 90% for deionized

water, greater than 85% for reservoir water, greater than 80% for deionized water and approximately 60% for water reservoirs, both of which used PAC. Therefore, it appears that the complexity of the composition of natural surface water influenced the adsorption performance of PAC.

Table 8. Comparative data on concentration and percentage of atrazine removal in real samples.

Location (Country)	Concentration (mg L^{-1})	Removal (%)	Reference
Spain	10	>50	[158]
China	5×10^{10}	–	[176]
China	0.02	–	[228]
China	20	51.6	[209]
China	20	32.6	[209]
China	0.005	>85	[213]
Brazil	5	76.58	[214]
Brazil	5	71.29	[214]
Brazil	30	70	[248]
Brazil	10	>70	[33]
Brazil	4.7	85	[218]
China	1	>70	[10]
–	0.2	63.89	[220]
China	–	40.7	[20]
China	–	53.1	[20]
Brazil	15	>95	[35]

"–" stands for not given.

Cheng et al. [216] explored the use of three graphene-based materials—graphene oxide (GO), reduced graphene oxide (rGO), and graphene nanoplates (PNB)—to evaluate their effectiveness in removing ATZ from real samples. These adsorbents were evaluated by testing their ability to adsorb ATZ (at a concentration of 100 mg L^{-1}) in both enriched tap water and wastewater. The results demonstrated that all three adsorbents exhibited strong ATZ adsorption capacities, with GO showing the highest uptake (1078.24 mg g^{-1}), followed by rGO (1150.36 mg g^{-1}) and GNP (1011.66 mg g^{-1}) in the tap water environment. In wastewater, the removal capacities are slightly lower (GO = 1086.49 mg g^{-1}, rGO = 1142.84 mg g^{-1} and GNP = 975.52 mg g^{-1}) due to the complexity of the aqueous matrix. In the study by Hernandes et al. [253], samples from the Ijuí River and the Conceição River (Brazil) were contaminated with the herbicide ATZ, resulting in removal percentages of 76.58% and 71.29% for the Conceição and Ijuí Rivers, respectively. Lazarotto et al. [248] prepared samples collected from the Jacuí River (Brazil) with ATZ and achieved a removal of 70%. In a study by Salomón et al. [218], a sample from the Jacuí River (Brazil) was collected and showed an initial atrazine concentration of 4.7 mg L^{-1}. After adsorption, the remaining concentration was 0.70 mg L^{-1} (R = 85%). Netto et al. [33] collected water samples from three rivers (Brazil), and the samples achieved approximately 70% removal after 180 min. Lu et al. [10] investigated the use of a functionalized m-aminophenol as an adsorbent for removing four triazines—simazine, cyanazine, atrazine, and terbuthylazine—from environmental water samples collected in Baoding, China. Their experiments resulted in a 70% reduction in the concentration of all four triazines, irrespective of the water's pH level (acidic, alkaline) or salinity (high ionic strength). Yan S et al. [220] conducted

adsorption tests using N-doped hydrochar activated with KOH from surface water from agricultural land contaminated by ATZ and obtained a removal efficiency of 63.89%. To evaluate the possible application of the adsorbent, Tao et al. [20] used surface water samples from the Yangtze River (Wuhan, China), in addition to groundwater samples from the urban area of Huangshi (Hubei, China), obtaining 40.7% and 53.1% removal of ATZ in the Yangtze River and waters underground, respectively. Oliveira et al. [35] reported the use of graphitic porous carbon (GPC)-based material for the adsorption of ATZ in water samples collected from a reservoir (Bortolan) and a natural source of drinking water, with removal results > 95%. The results reported in this section do not allow us to conclude that the adsorbents exhibit good ATZ adsorption behavior in real aqueous matrices, confirming the possible applicability of some materials. Additionally, the quality of the water and the presence of diverse contaminants significantly affect the adsorption capacity of the materials used for removal—emphasizing the need to consider the complexity of real effluents, which often contain a mixture of various compounds.

5. Desorption Studies and Reuse

Desorption's main objective is the regeneration of adsorbents (Figure 5), thus constituting an important factor for real applications and the reduction of operational costs, as it recovers the adsorbate molecules leading to the reuse of the material [255,256]; furthermore, desorption studies also help in understanding the adsorption mechanism [246]. During the tests, cycles that reuse the saturated adsorbent occur, with the intention of investigating the efficiency of the desorption process [257]. Thus, as cycles and regeneration increase, the adsorption effect gradually decreases [224]. This is a critical consideration, directly impacting the cost–benefit ratio of the process [258]. Failure to implement regeneration can lead to the release of contaminants into the environment through the disposal or storage of used adsorbents [41]. Adsorbent regeneration and reuse are critical for sustainable ATZ remediation, offering substantial economic (e.g., reduced operational costs) and environmental (e.g., minimized waste generation) advantages [25,205,259,260]. In response, numerous studies have investigated desorption efficiency and cyclic reusability of diverse adsorbents for ATZ removal, key data from which are consolidated in Table 9. This section critically evaluates these regeneration strategies, focusing on desorption agents, retained capacity over cycles, and mechanistic implications for adsorbent stability.

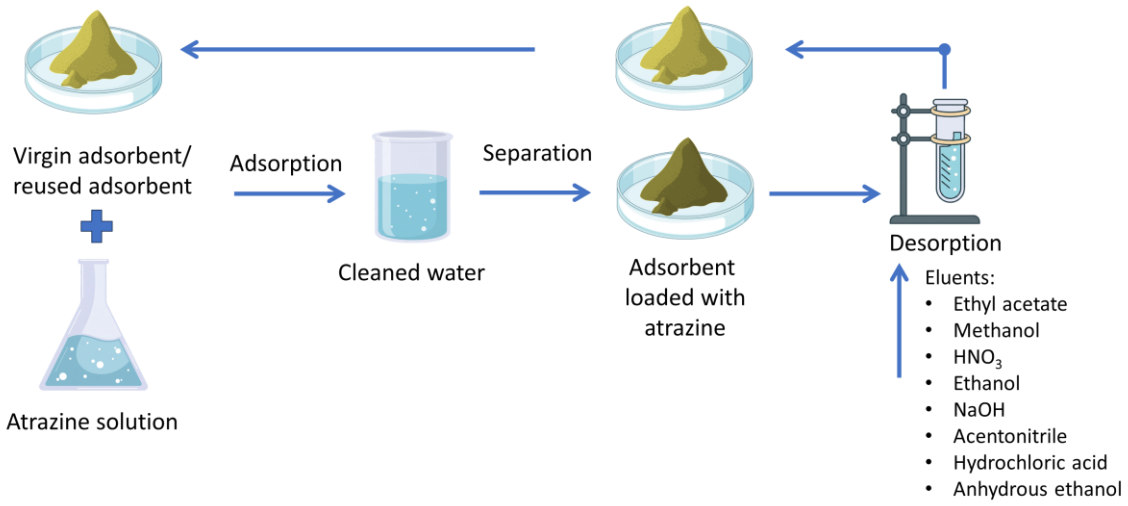

Figure 5. Regeneration of adsorbents and eluents used in desorption process for adsorption of atrazine.

Table 9. Summary of desorption and reuse of adsorbents with respective eluents used and capacities obtained.

Adsorbent	Eluent	Cycles Conducted (n)	Retention After n Cycles (%)	Reference
NZVI	–	4	15.8	[172]
NZVI/CTMA–Bent	–	4	57.3	[172]
Magnetic molecularly imprinted polymer (MSEP@MIP)	methanol	7	83.19	[184]
Biopolymer-stabilized silver nanoparticles	HNO_3	26	76	[183]
Iron nanocomposite material	hydrochloric acid	7	98	[31]
Wheat straw-derived biochar	methanol	3	70	[132]
Laser-induced graphitic material (LIG)	ethanol	4	90	[205]
Graphene oxide-supported nano zero-valent iron (GO/nZVI)	ethanol	4	62.2	[206]
β-cyclodextrin functionalized rice husk-based cellulose (β–CD@RH–C)	anhydrous ethanol	4	98.01	[109]
Thermally activated MCM– 41	ethanol	5	83	[210]
Graphene oxide nanosheets	NaOH	6	70	[32]
Modified carbon dots with amine supported onto cellulose sponge	NaOH	5	72	[208]
Cellulose doped with nitrogen	methanol	5	73	[224]
Cu–Zn–Fe layered double hydroxides (LDH)	NaOH	5	36	[223]
LDH dispersed on bamboo biochar (LDHBC)	NaOH	5	66	[223]
Surface oxidized pyrite (SOPy–90)	ethanol	4	79	[20]
Graphitic porous carbon (GPC)	acetonitrile	4	60.7	[35]

In alignment with these studies, Figure 6 presents the ATZ removal efficiency and adsorption capacity over successive regeneration cycles. Katsumata et al. [163] employed 100 mg of heat-treated diatomaceous earth and ethanol as the desorption eluent, achieving a high ATZ recovery of ~96%. Similarly, Singh [167] reported that ATZ exhibited the highest desorption extent among the herbicides investigated. In the present study, desorption from fly ash exposed to ATZ (10 mg L^{-1}) yielded only 9.07% ATZ recovery (3.0 μg g^{-1}) in the third cycle, consistent with the observed trend that lower initial herbicide concentrations led to reduced desorption. Recyclability assessments further highlight performance variations across adsorbents. For instance, NZVI/CTMA–Bent maintained higher ATZ removal efficiencies over four cycles (64.3%, 59.8%, 59.2%, and 57.3%) compared to bare NZVI (27.1%, 24.9%, 20.7%, and 15.8%) [172]. Tang et al. [176] regenerated magnetic multiwalled carbon nanotubes (MMWCNTs) using ethanol–water mixtures and identified 20% (v/v) ethanol as optimal for ATZ desorption. Although adsorption capacity generally declined with increasing cycle number—and was further diminished under acidic conditions—significant ATZ uptake persisted into the fourth cycle. Notably, granular activated carbon in this work achieved maximal removal (99.9% → 87.3%) during the third cycle. Long-term reusability was also examined in prior work: Zhou et al. [228], used 20 mL of methanol to regenerate magnetic microspheres (Q150) and activated carbon; while the latter lost all capacity after three cycles, Q150 retained ~50% of its initial adsorption capacity (53.55 mg g^{-1}) even after six reuse cycles. Likewise, Liu and Chen [184] demonstrated the robust regenerability of a magnetic molecularly imprinted polymer (MSEP@MIP) over seven cycles: using 0.02 g of adsorbent with 50 mL of ATZ solution (0.1 mg L^{-1}, pH 6.5, 3 h contact), they maintained a high removal efficiency of 83.19%, confirming the material's suitability for repeated application.

To test the reusability of functionalized nylon 6/polypyrrole core–shell nanofiber mats (PA6/PPy NFMs), Huang et al. [120] used methanol as an eluting agent, and the experimental desorption procedures were repeated six times to evaluate the material. The desorption results showed that the adsorption capacity remained almost unchanged after six cycles. In desorption studies by Pal et al. [183], the adsorbent (biopolymer-stabilized silver nanoparticles) used was treated with 0.05 N HNO3, and the desorption cycle was repeated 26 times with 76% removal in the last cycle, suggesting economic viability in the system. With the intention of regenerating and recycling the adsorbent, Ali, Alothman, and Al–Warthan [31] carried out tests with various acids, including hydrochloric, nitric and sulfuric acid; after the experiments, the maximum regeneration was obtained through the addition of hydrochloric acid. According to desorption studies of the materials, the regenerated compounds were subjected to seven cycles of ATZ adsorption, resulting in a removal efficiency ranging from 90–98%. Wang et al. [132] carried out recycling experiments on wheat straw-derived biochar (WS750) through washing with methanol, resulting in the sorption of 70% of WS750 to ATZ and 0.024 mmol g^{-1} in the third sorption. Using the microwave irradiation method for regeneration, ref. [197] found that biochar (RGO–BC) obtained a high adsorption capacity (above 81%) after the fourth cycle. Yang et al. [195] also used microwave irradiation to regenerate carbon sponges (S–PCSs), in which the material was recycled and reused five times, resulting in an ATZ concentration greater than 13 mg g^{-1}. Akpinar and Yazaydin [199] regenerated metal–organic framework materials (UiO–67) from washing with acetone followed by thermal activation, and the results did not show a significant decrease in adsorption capacity, suggesting that this material has potential for the removal of ATZ in water. At the end of the third cycle, UiO–67 lost less than 10% of its initial adsorption capacity. P-doped biochar from corn straw (CSWP) can be confirmed to be reusable through experiments by Suo et al. [201], showing potential for rapid and highly efficient removal of triazines. The chosen solvent was acetonitrile, in

which the material can be reused at least five times, with its adsorption capacity reduced by only 3.4% (R = 95%).

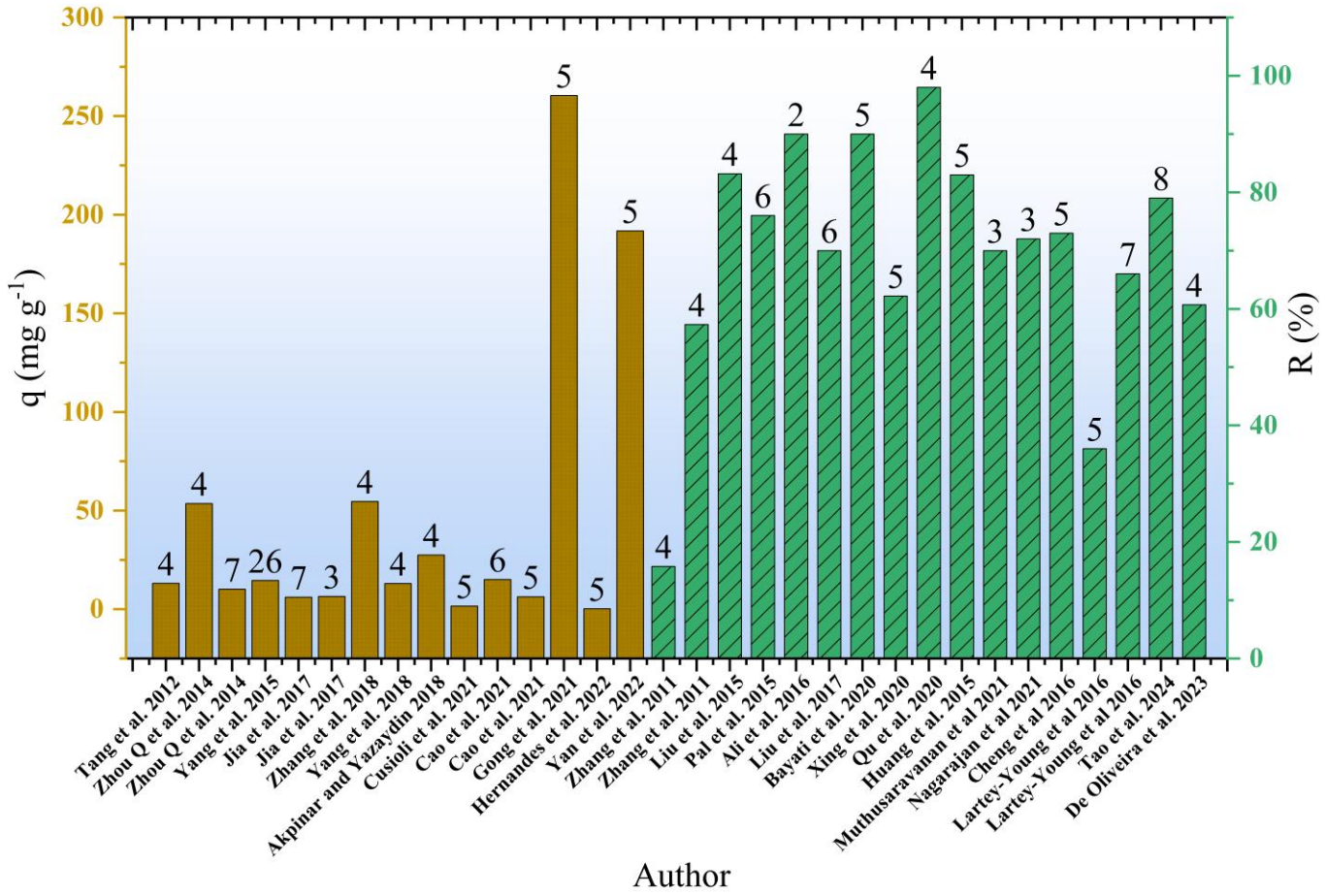

Figure 6. Adsorption capacity and percentage of removal according to author Tang et al. [176], Zhou Q et al. [228], Yang et al. [181], Jia et al. [193], Zhang et al. [197], Yang et al. [218], Akpinar and Yazaydin [199], Cusioli et al. [200], Cao et al. [209], Gong et al. [213], Hernandes et al. [214], Yan et al. [220], Zhang et al. [172], Liu et al. [184], Pal et al. [183], Ali et al. [31], Liu et al. [142], Bayati et al. [205], Xing et al. [206], Qu et al. [109], Huang et al. [210], Muthusaravanan et al. [32], Nagarajan et al. [208], Cheng et al. [216], Lartey-Young et al. [223], Tao et al. [20], De Oliveira et al. [35], with number of cycles on top of bars.

Bayati et al. [205] studied the regeneration and reuse of laser-induced graphene (LIG) using ethanol; after four cycles, the material retained its initial adsorption capacity, achieving 90% removal of the target contaminant. Sharma et al. [204] studied the reuse of nanohydrogel chitin-cl-polyl over six consecutive cycles, observing a decrease in efficiency from 71% in the first cycle to 50.8% in the sixth cycle. Ref. [206] tested graphene oxide-supported nano zero-valent iron (GO/nZVI) four times to evaluate the material's recyclability using ethanol. The removal efficiency decreased from 82.3% to 62.2% by the fourth test. In a study by Qu et al. [109], β-cyclodextrin functionalized rice husk-based cellulose (β–CD@RH–C) was used to test desorption with anhydrous ethanol, and the material exhibited an uptake above 98.01% after the fourth cycle. To study the reuse of unmodified biochar (LBC) and nano-MgO modified fallen leaf biochar (MgO–LBC), Cao et al. [209] added the biochar to a NaOH solution. The results indicated that the materials have potential for practical application, given their adsorption capacities of 71.11% and 76.25% of the initial values after five cycles. Muthusaravanan et al. [32] used 0.01 N NaOH as an eluent to recycle graphene oxide nanosheets for up to six cycles for ATZ removal. The modified carbon

dots with amine supported onto cellulose sponge, studied by Nagarajan et al. [208], also showed good efficiency for regeneration and reuse. The eluent used was 0.1 M NaOH, and the material was tested for up to five cycles, achieving 72% efficiency in the final cycle. Behrami et al. [6] evaluated the desorption of coal fly ash compounds from a power plant (Kosovo A) using hexane and dichloromethane as eluents, and the results indicated a concentration dependence. During three successive desorptions, approximately 8.9% of ATZ was desorbed. Cheng et al. [216] performed recycling experiments with cellulose doped with nitrogen. The eluent used was methanol, and after five cycles, 73% of the ATZ was removed. Lartey-Young and Ma [223] used Cu–Zn–Fe layered double hydroxides (LDHs) and LDHs dispersed on bamboo biochar (LDHBC) to evaluate the renegotiation and reuse of adsorbents after five cycles. NaOH solution at a concentration of 0.1 M was used as the eluent, and the results confirmed a reduction in efficiency that may be associated with the loss of chemical groups on the surface after each cycle. At the end of the fifth desorption cycle, the authors obtained removal efficiencies of 36% for LDH and 66% for LDHBC. Biochar from *C. fissilis* was used as an adsorbent for regeneration tests in studies by Hernandes et al. [214]. First, the adsorbent with ATZ was regenerated through heating for eight cycles, showing practically the same efficiency in the first three cycles.

In the work of Lu et al. [10], an ionic liquid-functionalized porous m-aminophenol formaldehyde polymer (IL-PMAF) was employed for the adsorption of four triazine herbicides, including ATZ. The adsorbent maintained 95% removal efficiency for ATZ over eight consecutive adsorption–regeneration cycles. In evaluating the surface oxidized pyrite (SOPy–90) adsorbent for real water treatment applications and good reusability, Tao et al. [20] used ethanol as the eluent, and in the fourth cycle, 79% removal of ATZ was obtained, proving the good reusability of the material. Oliveira et al. [35] employed graphitic porous carbon materials featuring magnetic domains for desorption studies, utilizing acetonitrile as the eluent. The results indicated that the material could be effectively recovered and reused for up to four cycles, thereby promoting sustainable practices. The decrease in efficiency throughout the cycles may be related to the loss of material throughout the desorption experiments, in addition to the treatment received by the material and the variety of adsorption mechanisms studied. In summary, as shown in Figure 3, the materials reported in the literature showed high percentages of removal. Even though three or more cycles were carried out, some adsorbents maintained satisfactory ATZ removal results, between 60 and 80%. Studies that obtained high removal capacities (83–98%) after four to seven cycles can also be cited. The excellent results cited can promote the reuse of many materials, saving costs for ATZ removal and thus promoting economic benefits.

As shown in Table 8, the works used different eluents for material regeneration studies. Among the eluents used in the reuse of adsorbents after ATZ removal are ethanol, ethyl acetate, methanol, HNO_3, hydrochloric acid, nitric and sulfuric acid, NaOH, acetone, a mixture of hexane and dichloromethane, dichloromethane and acetonitrile. Of the 36 studies reported and discussed, methanol, ethanol, and NaOH were the most commonly used in 23 studies. Greater use of ethanol and methanol was observed in 18 works. It is important to consider the selection of the eluent, recognizing that it must be non-toxic. Given that substantial volumes of residual effluent will be produced and require treatment prior to release into water sources, this factor is critical [245]. The works presented did not explain the reason for choosing the eluent, although satisfactory results were presented in its regeneration. Some studies have carried out tests with different eluents to determine the best eluent for the regeneration of the material. Romita et al. [11] carried out ATZ desorption experiments with ethanol and methanol, but defined the latter solvent as the most effective, in addition to highlighting that it is a highly biodegradable solvent, contributing to the circular economy. In this way, the benefits of using solvents are understood, given that they

are simple, effective, less time-consuming, environmentally friendly, and inexpensive [261]. Therefore, more studies should focus on methods such as microwave irradiation and heating to reduce energy consumption and increase the sustainability of the process by preventing the generation of secondary pollutants.

6. Column Adsorption Studies

Analyzing the effectiveness of fixed-bed columns involves examining breakthrough curves, graphical depictions illustrating the relationship between pollutant concentrations in the outflow and the operational timeline within the column [262]. These data must be investigated to calculate the design parameters and evaluate the most favorable operating conditions [263]. The breakthrough time is another important indicator that determines the operation and dynamic response of an adsorption column [264]. In the literature, several studies have investigated the efficiency of adsorbents for possible application in industrial projects. In the column (diameter: 2.4 cm and height: 13 cm) experiments of González-Pradas et al. [157], natural sepiolite showed reasonable results (46% efficiency) in ATZ removal. In a study by Alila and Boufi [165], three types of herbicides (alachlor, linuron, and atrazine) were removed from modified cellulose fibers. The results showed a maximum retention capacity, using a column of 3 cm in diameter and 10 cm in height, variation of 70 to 80%, with the advance time reaching 70, 50, and 30 min for flow rates of 10, 15, and 20 mL min^{-1}, respectively. Gupta et al. [170] used activated carbon from waste rubber tires to adsorbed atrazine in fixed bed experiments; the authors employed a glass column of 30 cm height and 1 cm of internal diameter. An adsorption capacity of 81.62 mg g^{-1} was determined, which is in agreement with the batch results (q = 104.90 mg g^{-1}), attributed to the different equilibrium time. In this study, a capacity of 81.62 mg g^{-1} was obtained. In the work of Zhou et al. [228], the adsorbents (Q150 and 1240AC) exhibited high ATZ adsorption capacity, with Q150 having greater performance in water treatment (600 mL, 14.3%) than 1240AC (column geometry not reported). Sivarajasekar et al. [265] used irradiated *Aegle marmelos* Correa fruit peel under the following optimal conditions: a bed height of 9.46 cm, an initial concentration of ATZ of 43.29 mg^{-1}, and a flow rate of 4.41 mL min^{-1}, ensuring an adsorption capacity of 12,303.3 mg g^{-1}. Levio-Raiman et al. [266] analyzed the performance of a column (diameter: 10 cm and height: 25 cm) filled with wheat straw, soil, and peat and reported that the amount of ATZ decreased as the pH increased from 4 to 8. Maximum pollutant removal occurred at a concentration of 5 mg/L (77.5%), demonstrating that ATZ removal was independent of the initial pollutant level. Operational studies revealed a stable removal rate sustained for 171 h before saturation was achieved after 490 h. Ultimately, the process achieved 98.65% ATZ removal with an adsorbed quantity of 95.32 mg g^{-1}. Sbizzaro et al. [22] evaluated the performance of biochars produced at 450 and 550 °C in fixed bed adsorption (diameter: not reported and height: 12 cm), where the total amount of ATZ adsorbed was greater in AC450 (1.90 mg g^{-1}) than in AC550 (1.61 mg g^{-1}). In a study by Nascimento et al. [217], column (diameter: not reported and height: 13.3 cm) behavior was reported using 2.2 g of corn straw fed in an upward flow with an efficiency of 72% and a rupture time of 520 min. Therefore, it is understood that fixed column tests are essential for evaluating the efficiency of contaminant removal, with a view to possible real applications in projects. However, the number of studies carrying out fixed bed tests to evaluate ATZ removal is still scarce, and therefore, more studies must be carried out to expand large-scale alternatives for ATZ herbicide treatment.

7. Knowledge Gap and Future Perspectives

Various adsorbents have been analyzed and used to remove ATZ present in water, and the preference for carbonaceous materials is evident; these materials are mainly derived

from plant residues. Due importance should also be given to inorganic waste, industrial waste, polymeric adsorbents, nanoadsorbents, and biosorbents. Materials with potential for modification include shells, starches, shavings, fibers, corks, and leaves. Several studies are investigating new methodologies and modification routes to improve textural properties and consequently increase removal. These processes increase the production costs of the adsorbent, which should be better analyzed by the scientific academy. This is because most of these materials do not break the cost application barrier. Considering that the business class attaches great importance to the cost of production, large-scale processes are carried out. Therefore, when applying these adsorbents on an environmental scale, researchers need to carry out cost and feasibility analyses. In addition, the disposal and final destination of solid materials must also be further investigated, with the aim of increasing sustainability and the real applicability of the process. An adsorbent from activated sewage sludge was proposed to be disposed of using the inertization process in a glass matrix; however, the literature also addresses the possibility of stabilization in a cementitious binder or polymeric resin [267]. The use of nanotechnology in adsorption is a reality; however, more studies that investigate the potential for the formation of secondary pollution and the fate and metabolic pathway of these materials in the environment must be conducted.

Complex solutions with more than one adsorbate increase the probability of competition in adsorbent pores; once ATZ is present in the environment, it coexists with metals, other herbicides, humic acid, and other chemical compounds. Therefore, competitive physical process studies must be conducted in greater numbers by the scientific community. These studies provide new answers and information regarding the hydrology of pollutants and, in this field, provide a framework for computational modeling. Studies applying phenomenological models (statistical physics studies) and density functional theory can corroborate new information regarding the interactions that occur between the adsorbate molecules and the chemical properties of the surface of the solid (adsorbent). In regard to real environmental conditions, there are challenges to overcome that go beyond the complexities of coexisting ions in soil or water. There is also the barrier of a lack of control over the parameters involved in the process; therefore, for successful remediation, adsorption can also be used in conjunction with other combined technologies, such as photo-Fenton, photocatalysis, photodegradation, and phytoremediation. In this sense, more studies with hybrid processes should be conducted by the scientific community. Often, combining technologies is the wisest approach. For example, using adsorption as a pretreatment to concentrate the pollutant, followed by an oxidative process to degrade the saturated adsorbent and the concentrated ATZ, offers a synergistic, efficient, and economically viable solution (Table 10).

Finally, the routes of entry of these contaminants into the environment are still uncertain since there are no numbers or controls by countries on the volume produced or the quantity applied to crops. This makes it unfeasible and difficult to monitor the presence of ATZ in different water compartments and even in fruits and vegetables. Here, it is recommended that legislation and government bodies present stricter and more uniform policies that are aligned between countries. These measures, together with advances in remediation technologies and detection sensors/biosensors, will provide a greater understanding of the areas with the greatest demand for decontamination, which are the main threats to animal, plant, and human life.

Table 10. Comparative table of technologies for ATZ removal.

Technology	Advantages	Disadvantages	Ideal Application Scenarios
Direct photodegradation	- Simple process using only light (usually UV). - Does not require the addition of catalysts or chemicals. - Does not generate sludge or additional solid waste.	- Slow and often incomplete degradation of ATZ. - May generate degradation by-products that are as toxic as or more toxic than the original compound. - Highly inefficient for effluents with high turbidity. - High energy consumption to generate high-intensity UV radiation.	- Pre-treatment or for studying degradation pathways in the laboratory. - Applicable only for very dilute and clear aqueous solutions. - Scenarios with very low efficiency requirements or as a complementary process within a treatment train.
Adsorption	- Simple and low-cost operation. - High efficiency in removing ATZ at low concentrations. - Wide variety of adsorbents (natural, waste-based, advanced). - Does not generate toxic degradation by-products. - Easy adaptation to continuous systems (fixed bed).	- Does not degrade the pollutant, only transfers it to another phase. - Generates a solid waste (spent adsorbent) that requires disposal or regeneration. - Efficiency is highly dependent on adsorbent properties and effluent chemistry. - Adsorption capacity can be reduced in the presence of natural organic matter or other contaminants.	- Treatment of waters with low to moderate concentrations of ATZ. - Final polishing of effluents after primary treatment. - Decentralized or small-scale systems. - When the goal is rapid and efficient removal without a focus on degradation.
Photo-fenton process [268]	- High degradation and mineralization rate of ATZ. - Efficient at degrading a wide range of recalcitrant pollutants. - Can utilize sunlight, reducing energy costs. - Highly reactive and non-selective oxidant (•OH radical).	- Operates at acidic pH (around 3), requiring pH adjustment and subsequent correction. - Generates iron sludge, requiring proper disposal. - The presence of anions (carbonate, chloride) can inhibit the reaction. - Moderate operational cost due to reagent consumption (H_2O_2, Fe^{2+}).	- Treatment of effluents with high organic load and high toxicity. - Applications where complete mineralization is required. - Locations with good sunlight availability to reduce lamp costs. - Robust treatment plants that can handle chemical and sludge management.

Table 10. *Cont.*

Technology	Advantages	Disadvantages	Ideal Application Scenarios
Photocatalysis	- Degrades ATZ into less toxic products or CO_2 and H_2O. - Uses solid catalysts (e.g., TiO_2), facilitating separation and reuse. - Can be activated by sunlight. - "Green" process that does not consume bulk chemicals.	- Efficiency limited by electron–hole pair recombination. - Cost associated with catalyst synthesis and immobilization. - Effluent turbidity can block light penetration. - Degradation rate is generally slower than photo-Fenton.	- Treatment of wastewater with low to moderate turbidity. - Applications where sludge generation is a major concern. - Advanced treatment systems seeking a more sustainable technology. - Combined with other technologies in hybrid systems.

Granular activated carbon (GAC) adsorption was shown to be an efficient method of reducing atrazine contamination in drinking water in a number of industrial-scale deployments between 2020 and 2025. By combining deep-well abstraction with GAC filtration, the Rottenburger Gruppe water utility, which serves about 38,000 residents in Lower Bavaria, Germany (2021), successfully addressed persistent atrazine and nitrate pollution, enabling a safe water supply despite historical agricultural inputs of prohibited herbicides and their metabolites [269]. Simultaneously, a new pesticide-treatment facility at Merpins (commissioned in September 2023) used continuous-renewal GAC filters to filter out atrazine and metolachlor metabolites from groundwater for 11,500 residents in the Grand Cognac region of France, continuously providing water that is below regulatory limits [270]. Using micro-grain activated carbon, a high-efficiency adsorbent that has been validated for the removal of trace pesticides, the same authority expanded the Jarnac facility in 2023 and opened Merpins in 2024, building on this success. They are currently building a third plant at Angeac-Charente, which is scheduled to open in December 2025, with a 240 m^3/h micro-grain GAC system [271]. In addition to these field applications, a 2024 Chinese pilot study [272] showed that combining intermittent ozone micro-nano bubble regeneration with GAC adsorption resulted in ~99.9% atrazine removal while maintaining carbon integrity and reducing bromate formation, providing a viable and affordable route for long-term full-scale implementation [272]. These cases collectively highlight GAC as a reliable, flexible atrazine remediation approach in actual water treatment systems, particularly in micro-grain or regenerable setups.

8. Conclusions

This comprehensive review consolidates the state of the art in the removal of the herbicide atrazine (ATZ) by adsorption, standing out for its mechanistic approach that transcends mere data compilation to offer fundamental guiding principles. The main contribution of this analysis lies in elucidating that the efficiency of the adsorption process is not solely a function of the adsorbent's surface area, but rather the result of a complex synergy between textural properties (porosity, surface area) and surface chemistry (functional groups, electrical charge). Operational parameters, especially the pH of the medium, were identified as critical for modulating the attractive forces (e.g., hydrogen bonding, π–π interactions, electrostatics) between the adsorbent surface and the ATZ molecule. The review clearly demonstrated that carbonaceous materials, such as activated carbons and biochars, often modified or functionalized, predominate in research due to their versatility and high adsorption capacity. However, the major breakthrough highlighted is the emerging trend

toward the development of "designed" adsorbents such as modified biochars, composites, and molecularly imprinted polymers that intentionally combine multiple adsorption mechanisms (physical and chemical) to maximize efficiency and selectivity. Furthermore, this review contributes significantly by synthesizing evidence on the applicability of materials in real aquatic matrices, a crucial test for translating laboratory research into practice. The reviewed desorption and reuse studies reinforce the potential economic viability of various adsorbents, while the still scarce, but promising, fixed-bed experiments point the way to pilot-scale and industrial-scale applications. In perspective, this analysis suggests that the future of treating ATZ-contaminated water via adsorption lies in the creation of sustainable, low-cost, and highly efficient materials designed to perform under real environmental conditions. Overcoming scaling-up challenges, cost–benefit analysis, and integration with other treatment technologies represent the next frontiers to be explored, guided by the mechanistic and critical principles consolidated in this review.

Author Contributions: Conceptualization, D.S.P.F. and Y.L.S., Methodology, Y.L.S., J.G. and D.G.P.A.; Validation, M.S.N. and C.O.A.; Formal analysis, Y.L.S. and J.G.; Investigation, Y.L.S. and D.G.P.A.; Resources, D.S.P.F. and J.O.I.; Data curation, Y.L.S. and J.G.; Writing—original draft preparation, Y.L.S. and J.G.; Writing—review and editing, D.S.P.F., C.O.A. and J.O.I.; Visualization, M.S.N.; Supervision, D.S.P.F. and J.O.I.; Project administration, D.S.P.F. All authors have read and agreed to the published version of the manuscript.

Funding: This work was carried out with the support of the Coordenação de Aperfeiçoamento de Pessoal de Nível Superior—CAPES.

Institutional Review Board Statement: Not applicable.

Informed Consent Statement: Not applicable.

Data Availability Statement: The data presented in this study are available on request from the corresponding author.

Acknowledgments: For the image preparation, Marvinsketch 21.18, Originlab 2018 SR1, Powerpoint 2021, and Obsidian 1.10.3 coupled with Excalidraw 1.5.0 were used.

Conflicts of Interest: The authors declare no conflicts of interest.

References

1. Phan, K.A.; Phihusut, D.; Tuntiwiwattanapun, N. Preparation of rice husk hydrochar as an atrazine adsorbent: Optimization, characterization, and adsorption mechanisms. *J. Environ. Chem. Eng.* **2022**, *10*, 107575. [CrossRef]
2. Aparecida Matias, C.; Vilela, P.B.; Becegato, V.A.; Paulino, A.T. Adsorption kinetic, isotherm and thermodynamic of 2, 4-dichlorophenoxyacetic acid herbicide in novel alternative natural adsorbents. *Water Air Soil Pollut.* **2019**, *230*, 276. [CrossRef]
3. González Blanco, S.; Müller, J.; Petrovic, M.; Barceló, D.; Knepper, T.P. Biodegradation studies of selected priority acidic pesticides and diclofenac in different bioreactors. *Envion. Pollut.* **2006**, *144*, 926–932. [CrossRef]
4. Navarra, W.; Sacco, O.; Daniel, C.; Venditto, V.; Vaiano, V.; Vignati, D.A.L.; Bojic, C.; Libralato, G.; Lofrano, G.; Carotenuto, M. Photocatalytic degradation of atrazine by an N-doped TiO_2/polymer composite: Catalytic efficiency and toxicity evaluation. *J. Environ. Chem. Eng.* **2022**, *10*, 108167. [CrossRef]
5. Chevrier, C.; Limon, G.; Monfort, C.; Rouget, F.; Garlantézec, R.; Petit, C.; Durand, G.; Cordier, S. Urinary biomarkers of prenatal atrazine exposure and adverse birth outcomes in the PELAGIE birth cohort. *Environ. Health Perspect.* **2011**, *119*, 1034–1041. [CrossRef] [PubMed]
6. Behrami, E.; Xhaxhiu, K.; Dragusha, B.; Reka, A.; Andoni, A.; Hamiti, X.; Drushku, S. The removal of atrazine and benalaxyl by the fly ash released from Kosovo a power plant. *Int. J. Anal. Chem.* **2022**, *2022*, 9945199. [CrossRef]
7. Martins, E.C.; Bohone, J.B.; Abate, G. Sorption and desorption of atrazine on soils: The effect of different soil fractions. *Geoderma* **2018**, *322*, 131–139. [CrossRef]
8. Taverna, M.E.; Busatto, C.A.; Lescano, M.R.; Nicolau, V.V.; Zalazar, C.S.; Meira, G.R.; Estenoz, D.A. Microparticles based on ionic and organosolv lignins for the controlled release of atrazine. *J. Hazard. Mater.* **2018**, *359*, 139–147. [CrossRef]

9. Jing, S.; Lan, M.X.; Wen, W.; Jing, Z.; Hao, Z.; Jun, W.Y. Adsorption characteristics of atrazine on different soils in the presence of Cd (II). *Adsorpt. Sci. Technol.* **2020**, *38*, 225–239. [CrossRef]
10. Lu, Y.; Yan, H.; Han, Y.; Li, P.; Shen, S. Hierarchical porous phenolic polymer for efficient adsorption of triazine herbicides: Novel preparation strategies and potential applications. *Sep. Purif. Technol.* **2022**, *286*, 120495. [CrossRef]
11. Romita, R.; Rizzi, V.; Semeraro, P.; Gubitosa, J.; Gabaldón, J.A.; Gorbe, M.I.F.; López, V.M.G.; Cosma, P.; Fini, P. Operational parameters affecting the atrazine removal from water by using cyclodextrin based polymers as efficient adsorbents for cleaner technologies. *Environ. Technol. Innov.* **2019**, *16*, 100454. [CrossRef]
12. Delwiche, K.B.; Lehmann, J.; Walter, M.T. Atrazine leaching from biochar-amended soils. *Chemosphere* **2014**, *95*, 346–352. [CrossRef]
13. Kica, M.; Ronka, S. The removal of atrazine from water using specific polymeric adsorbent. *Sep. Sci. Technol.* **2014**, *49*, 1634–1642. [CrossRef]
14. Salvestrini, S.; Sagliano, P.; Iovino, P.; Capasso, S.; Colella, C. Atrazine adsorption by acid-activated zeolite-rich tuffs. *Appl. Clay Sci.* **2010**, *49*, 330–335. [CrossRef]
15. Goli, A.; Alinezhad, H.; Ganji, M.D. Theoretical insights into the performance of graphene derivatives, h-BN and BNC heterostructures in the adsorption and elimination of atrazine: An all-electron DFT study. *Diam. Relat. Mater.* **2020**, *108*, 107967. [CrossRef]
16. Dhangar, K.; Kumar, M. Tricks and tracks in removal of emerging contaminants from the wastewater through hybrid treatment systems: A review. *Sci. Total Environ.* **2020**, *738*, 140320. [CrossRef] [PubMed]
17. An, X.; Wang, H.; Dong, C.; Jiang, P.; Wu, Z.; Yu, B. Core-shell P-laden biochar/ZnO/g-C3N4 composite for enhanced photocatalytic degradation of atrazine and improved P slow-release performance. *J. Colloid Interface Sci.* **2022**, *608*, 2539–2548. [CrossRef]
18. Zhu, J.; Fu, L.; Meng, Z.; Jin, C. Characteristics of an atrazine degrading bacterium and the construction of a microbial agent for effective atrazine degradation. *Water Environ. J.* **2021**, *35*, 7–17. [CrossRef]
19. Chan, K.H.; Chu, W. Model applications and mechanism study on the degradation of atrazine by Fenton's system. *J. Hazard. Mater.* **2005**, *118*, 227–237. [CrossRef] [PubMed]
20. Tao, M.; Zhang, J.; Lv, J.; Zhang, J.; Li, Y.; Liu, S.; Xiao, W.; Huang, Y.; Zheng, H. Highly efficient activation of sulfite by surface oxidized pyrite for atrazine degradation: Experimental and DFT study. *J. Environ. Chem. Eng.* **2023**, *11*, 109200. [CrossRef]
21. Ajala, O.J.; Nwosu, F.O.; Ahmed, R.K. Adsorption of atrazine from aqueous solution using unmodified and modified bentonite clays. *Appl. Water Sci.* **2018**, *8*, 214. [CrossRef]
22. Sbizzaro, M.; Sampaio, S.C.; dos Reis, R.R.; de Assis Beraldi, F.; Rosa, D.M.; de Freitas Maia, C.M.B.; do Nascimento, C.T.; da Silva, E.A.; Borba, C.E. Effect of production temperature in biochar properties from bamboo culm and its influences on atrazine adsorption from aqueous systems. *J. Mol. Liq.* **2021**, *343*, 117667. [CrossRef]
23. Binh, Q.A.; Nguyen, V.-H.; Kajitvichyanukul, P. Influence of pyrolysis conditions of modified corn cob bio-waste sorbents on adsorption mechanism of atrazine in contaminated water. *Environ. Technol. Innov.* **2022**, *26*, 102381. [CrossRef]
24. Luo, Z.; Yao, B.; Yang, X.; Wang, L.; Xu, Z.; Yan, X.; Tian, L.; Zhou, H.; Zhou, Y. Novel insights into the adsorption of organic contaminants by biochar: A review. *Chemosphere* **2022**, *287*, 132113. [CrossRef] [PubMed]
25. Gkika, D.A.; Mitropoulos, A.C.; Kyzas, G.Z. Why reuse spent adsorbents? The latest challenges and limitations. *Sci. Total Environ.* **2022**, *822*, 153612. [CrossRef]
26. Unuabonah, E.I.; Olu-Owolabi, B.I.; Fasuyi, E.I.; Adebowale, K.O. Modeling of fixed-bed column studies for the adsorption of cadmium onto novel polymer–clay composite adsorbent. *J. Hazard. Mater.* **2010**, *179*, 415–423. [CrossRef] [PubMed]
27. Lemić, J.; Kovačević, D.; Tomašević-Čanović, M.; Kovačević, D.; Stanić, T.; Pfend, R. Removal of atrazine, lindane and diazinone from water by organo-zeolites. *Water Res.* **2006**, *40*, 1079–1085. [CrossRef]
28. Yan, X.M.; Shi, B.Y.; Lu, J.J.; Feng, C.H.; Wang, D.S.; Tang, H.X. Adsorption and desorption of atrazine on carbon nanotubes. *J. Colloid Interface Sci.* **2008**, *321*, 30–38. [CrossRef]
29. Jain, S.; Yamgar, R.; Jayaram, R.V. Photolytic and photocatalytic degradation of atrazine in the presence of activated carbon. *Chem. Eng. J.* **2009**, *148*, 342–347. [CrossRef]
30. Liu, N.; Charrua, A.B.; Weng, C.-H.; Yuan, X.; Ding, F. Characterization of biochars derived from agriculture wastes and their adsorptive removal of atrazine from aqueous solution: A comparative study. *Bioresour. Technol.* **2015**, *198*, 55–62. [CrossRef]
31. Ali, I.; Alothman, Z.A.; Al-Warthan, A. Sorption, kinetics and thermodynamics studies of atrazine herbicide removal from water using iron nano-composite material. *Int. J. Environ. Sci. Technol.* **2016**, *13*, 733–742. [CrossRef]
32. Muthusaravanan, S.; Balasubramani, K.; Suresh, R.; Ganesh, R.S.; Sivarajasekar, N.; Arul, H.; Rambabu, K.; Bharath, G.; Sathishkumar, V.E.; Murthy, A.P. Adsorptive removal of noxious atrazine using graphene oxide nanosheets: Insights to process optimization, equilibrium, kinetics, and density functional theory calculations. *Environ. Res.* **2021**, *200*, 111428. [CrossRef]
33. Netto, M.S.; Georgin, J.; Franco, D.S.P.; Mallmann, E.S.; Foletto, E.L.; Godinho, M.; Pinto, D.; Dotto, G.L. Effective adsorptive removal of atrazine herbicide in river waters by a novel hydrochar derived from Prunus serrulata bark. *Environ. Sci. Pollut. Res.* **2022**, *29*, 3672–3685. [CrossRef] [PubMed]

34. Lazarotto, J.S.; da Boit Martinello, K.; Georgin, J.; Franco, D.S.P.; Netto, M.S.; Piccilli, D.G.A.; Silva, L.F.O.; Lima, E.C.; Dotto, G.L. Application of araçá fruit husks (*Psidium cattleianum*) in the preparation of activated carbon with $FeCl_3$ for atrazine herbicide adsorption. *Chem. Eng. Res. Des.* **2022**, *180*, 67–78. [CrossRef]
35. De Oliveira, C.; Renda, C.G.; Moreira, A.J.; Pereira, O.A.P.; Pereira, E.C.; Freschi, G.P.G.; Bertholdo, R. Evaluation of a graphitic porous carbon modified with iron oxides for atrazine environmental remediation in water by adsorption. *Environ. Res.* **2023**, *219*, 115054. [CrossRef]
36. Hassan, M.M.; Carr, C.M. Biomass-derived porous carbonaceous materials and their composites as adsorbents for cationic and anionic dyes: A review. *Chemosphere* **2021**, *265*, 129087. [CrossRef]
37. Jagadeesh, N.; Sundaram, B. Adsorption of pollutants from wastewater by biochar: A review. *J. Hazard. Mater. Adv.* **2023**, *9*, 100226. [CrossRef]
38. Jablonowski, N.D.; Schäffer, A.; Burauel, P. Still present after all these years: Persistence plus potential toxicity raise questions about the use of atrazine. *Environ. Sci. Pollut. Res.* **2011**, *18*, 328–331. [CrossRef] [PubMed]
39. Singh, R.P.; Banerjee, N. Exploring the influence of celebrity credibility on brand attitude, advertisement attitude and purchase intention. *Glob. Bus. Rev.* **2018**, *19*, 1622–1639. [CrossRef]
40. Singh, S.; Kumar, V.; Chauhan, A.; Datta, S.; Wani, A.B.; Singh, N.; Singh, J. Toxicity, degradation and analysis of the herbicide atrazine. *Environ. Chem. Lett.* **2018**, *16*, 211–237. [CrossRef]
41. Vakili, M.; Deng, S.; Cagnetta, G.; Wang, W.; Meng, P.; Liu, D.; Yu, G. Regeneration of chitosan-based adsorbents used in heavy metal adsorption: A review. *Sep. Purif. Technol.* **2019**, *224*, 373–387. [CrossRef]
42. Amézquita-Marroquín, C.P.; Torres-Lozada, P.; Giraldo, L.; Húmpola, P.D.; Rivero, E.; Poon, P.S.; Matos, J.; Moreno-Piraján, J.C. Sustainable production of nanoporous carbons: Kinetics and equilibrium studies in the removal of atrazine. *J. Colloid Interface Sci.* **2020**, *562*, 252–267. [CrossRef]
43. Galindo-Miranda, J.M.; Guízar-González, C.; Becerril-Bravo, E.J.; Moeller-Chávez, G.; León-Becerril, E.; Vallejo-Rodríguez, R. Occurrence of emerging contaminants in environmental surface waters and their analytical methodology–a review. *Water Supply* **2019**, *19*, 1871–1884. [CrossRef]
44. Başer, B.; Yousaf, B.; Yetis, U.; Abbas, Q.; Kwon, E.E.; Wang, S.; Bolan, N.S.; Rinklebe, J. Formation of nitrogen functionalities in biochar materials and their role in the mitigation of hazardous emerging organic pollutants from wastewater. *J. Hazard. Mater.* **2021**, *416*, 126131. [CrossRef] [PubMed]
45. Chan, C.Y.; Tao, S.; Dawson, R.; Wong, P.K. Treatment of atrazine by integrating photocatalytic and biological processes. *Environ. Pollut.* **2004**, *131*, 45–54. [CrossRef]
46. Dombek, T.; Davis, D.; Stine, J.; Klarup, D. Degradation of terbutylazine (2-chloro-4-ethylamino-6-terbutylamino-1,3,5-triazine), deisopropyl atrazine (2-amino-4-chloro-6-ethylamino-1,3,5-triazine), and chlorinated dimethoxy triazine (2-chloro-4, 6-dimethoxy-1, 3, 5-triazine) by zero valent iron and electrochemical reduction. *Environ. Pollut.* **2004**, *129*, 267–275. [CrossRef] [PubMed]
47. Sun, K.; Gao, B.; Zhang, Z.; Zhang, G.; Zhao, Y.; Xing, B. Sorption of atrazine and phenanthrene by organic matter fractions in soil and sediment. *Environ. Pollut.* **2010**, *158*, 3520–3526. [CrossRef]
48. Tan, G.; Sun, W.; Xu, Y.; Wang, H.; Xu, N. Sorption of mercury (II) and atrazine by biochar, modified biochars and biochar based activated carbon in aqueous solution. *Bioresour. Technol.* **2016**, *211*, 727–735. [CrossRef]
49. Singh, A.K.; Cameotra, S.S. Influence of microbial and synthetic surfactant on the biodegradation of atrazine. *Environ. Sci. Pollut. Res.* **2014**, *21*, 2088–2097. [CrossRef]
50. Jun Zhang, J.; Chen Lu, Y.; Jin Zhang, J.; Rong Tan, L.; Yang, H. Accumulation and toxicological response of atrazine in rice crops. *Ecotoxicol. Environ. Saf.* **2014**, *102*, 105–112. [CrossRef]
51. Visanji, Z.; Sadr, S.; Johns, M.; Savic, D.; Memon, F.A. Emerging pollutants in developing countries: Optimising sustainable treatment solutions. *EPiC* **2018**, *3*, 2204–2215. [CrossRef]
52. Callicott, K.; Hooper-Bùi, L. An investigation of environmental concentrations of atrazine, chlorothalonil, and fipronil in a Mississippi River-influenced marsh in southern Louisiana. *Microchem. J.* **2019**, *146*, 1241–1248. [CrossRef]
53. Grube, A.; Donaldson, D.; Kiely, T.; Wu, L. *Pesticides Industry Sales and Usage*; EPA: Washington, DC, USA, 2011.
54. Semren, T.Ž.; Žunec, S.; Pizent, A. Oxidative stress in triazine pesticide toxicity: A review of the main biomarker findings. *Arh. Za Hig. Rada I Toksikol.* **2018**, *69*, 109–125. [CrossRef]
55. Katsumata, H.; Kojima, H.; Kaneco, S.; Suzuki, T.; Ohta, K. Preconcentration of atrazine and simazine with multiwalled carbon nanotubes as solid-phase extraction disk. *Microchem. J.* **2010**, *96*, 348–351. [CrossRef]
56. Orlando, J.L.; McWayne, M.; Sanders, C.; Hladik, M. *Dissolved Pesticide Concentrations Entering the Sacramento-San Joaquin Delta from the Sacramento and San Joaquin Rivers, California, 2012–2013*; 2327-638X; US Geological Survey: Reston, VA, USA, 2014.
57. Hansen, A.M.; TreviÑO-Quintanilla, L.G.; MÁRquez-Pacheco, H.; Villada-Canela, M.; GonzÁLez-MÁRquez, L.C.; GuillÉN-GarcÉS, R.A.; HernÁNdez-Antonio, A. Atrazina: Un herbicida polémico. *Rev. Int. De Contam. Ambient.* **2013**, *29*, 65–84.
58. Montiel-León, J.M.; Duy, S.V.; Munoz, G.; Bouchard, M.F.; Amyot, M.; Sauvé, S. Quality survey and spatiotemporal variations of atrazine and desethylatrazine in drinking water in Quebec, Canada. *Sci. Total Environ.* **2019**, *671*, 578–585. [CrossRef]

59. Miltner, R.J.; Baker, D.B.; Speth, T.F.; Fronk, C.A. Treatment of seasonal pesticides in surface waters. *J. Am. Water Work. Assoc.* **1989**, *81*, 43–52. [CrossRef]
60. Triassi, M.; Montuori, P.; Provvisiero, D.P.; De Rosa, E.; Di Duca, F.; Sarnacchiaro, P.; Díez, S. Occurrence and spatial-temporal distribution of atrazine and its metabolites in the aquatic environment of the Volturno River estuary, southern Italy. *Sci. Total Environ.* **2022**, *803*, 149972. [CrossRef]
61. Le Coadou, L.; Le Ménach, K.; Labadie, P.; Dévier, M.-H.; Pardon, P.; Augagneur, S.; Budzinski, H. Quality survey of natural mineral water and spring water sold in France: Monitoring of hormones, pharmaceuticals, pesticides, perfluoroalkyl substances, phthalates, and alkylphenols at the ultra-trace level. *Sci. Total Environ.* **2017**, *603*, 651–662. [CrossRef] [PubMed]
62. Blahová, J.; Plhalová, L.; Hostovský, M.; Divišová, L.; Dobšíková, R.; Mikulíková, I.; Štěpánová, S.; Svobodová, Z. Oxidative stress responses in zebrafish *Danio rerio* after subchronic exposure to atrazine. *Food Chem. Toxicol.* **2013**, *61*, 82–85. [CrossRef]
63. Koroša, A.; Auersperger, P.; Mali, N. Determination of micro-organic contaminants in groundwater (Maribor, Slovenia). *Sci. Total Environ.* **2016**, *571*, 1419–1431. [CrossRef] [PubMed]
64. Chen, N.; Valdes, D.; Marlin, C.; Blanchoud, H.; Guerin, R.; Rouelle, M.; Ribstein, P. Water, nitrate and atrazine transfer through the unsaturated zone of the Chalk aquifer in northern France. *Sci. Total Environ.* **2019**, *652*, 927–938. [CrossRef]
65. Heijman, S.G.J.; Hopman, R. Activated carbon filtration in drinking water production: New developments and concepts. In *Studies in Surface Science and Catalysis*; Elsevier: Amsterdam, The Netherlands, 1999; Volume 120, pp. 723–743. [CrossRef]
66. Noppe, H.; Ghekiere, A.; Verslycke, T.; De Wulf, E.; Verheyden, K.; Monteyne, E.; Polfliet, K.; Van Caeter, P.; Janssen, C.R.; De Brabander, H.F. Distribution and ecotoxicity of chlorotriazines in the Scheldt Estuary (B-Nl). *Environ. Pollut.* **2007**, *147*, 668–676. [CrossRef] [PubMed]
67. Nödler, K.; Licha, T.; Voutsa, D. Twenty years later–atrazine concentrations in selected coastal waters of the Mediterranean and the Baltic Sea. *Mar. Pollut. Bull.* **2013**, *70*, 112–118. [CrossRef]
68. Vryzas, Z.; Papadakis, E.N.; Vassiliou, G.; Papadopoulou-Mourkidou, E. Occurrence of pesticides in transboundary aquifers of North-eastern Greece. *Sci. Total Environ.* **2012**, *441*, 41–48. [CrossRef]
69. Alonso, L.L.; Demetrio, P.M.; Etchegoyen, M.A.; Marino, D.J. Glyphosate and atrazine in rainfall and soils in agroproductive areas of the pampas region in Argentina. *Sci. Total Environ.* **2018**, *645*, 89–96. [CrossRef]
70. De Gerónimo, E.; Aparicio, V.C.; Bárbaro, S.; Portocarrero, R.; Jaime, S.; Costa, J.L. Presence of pesticides in surface water from four sub-basins in Argentina. *Chemosphere* **2014**, *107*, 423–431. [CrossRef] [PubMed]
71. Nogueira, E.N.; Dores, E.F.G.C.; Pinto, A.A.; Amorim, R.S.S.; Ribeiro, M.L.; Lourencetti, C. Currently used pesticides in water matrices in Central-Western Brazil. *J. Braz. Chem. Soc.* **2012**, *23*, 1476–1487. [CrossRef]
72. Azevedo, D.A.; Silva, T.R.; Knoppers, B.A.; Schulz-Bull, D. Triazines in the tropical lagoon system of Mundaú-Manguaba, NE-Brazil. *J. Braz. Chem. Soc.* **2010**, *21*, 1096–1105. [CrossRef]
73. Bortoluzzi, E.C.; Rheinheimer, D.S.; Gonçalves, C.S.; Pellegrini, J.B.R.; Maroneze, A.M.; Kurz, M.H.S.; Bacar, N.M.; Zanella, R. Investigation of the occurrence of pesticide residues in rural wells and surface water following application to tobacco. *Química Nova* **2007**, *30*, 1872–1876. [CrossRef]
74. Laabs, V.; Amelung, W.; Pinto, A.A.; Wantzen, M.; da Silva, C.J.; Zech, W. Pesticides in surface water, sediment, and rainfall of the northeastern Pantanal basin, Brazil. *J. Environ. Qual.* **2002**, *31*, 1636–1648. [CrossRef]
75. Gwenzi, W.; Chaukura, N.; Mukome, F.N.D.; Machado, S.; Nyamasoka, B. Biochar production and applications in sub-Saharan Africa: Opportunities, constraints, risks and uncertainties. *J. Environ. Manag.* **2015**, *150*, 250–261. [CrossRef]
76. Aparecido dos Santos, E.; da Cruz, C.; Carraschi, S.P.; Marques Silva, J.R.; Grossi Botelho, R.; Velini, E.D.; Pitelli, R.A. Atrazine levels in the Jaboticabal water stream (São Paulo State, Brazil) and its toxicological effects on the pacu fish Piaractus mesopotamicus. *Arh. Hig. Rada I Toksikol.* **2015**, *66*, 73–81. [CrossRef]
77. Sousa, A.S.; Duaví, W.C.; Cavalcante, R.M.; Milhome, M.A.L.; do Nascimento, R.F. Estimated levels of environmental contamination and health risk assessment for herbicides and insecticides in surface water of Ceará, Brazil. *Bull. Environ. Contam. Toxicol.* **2016**, *96*, 90–95. [CrossRef]
78. Riquinho, D.L.; Souto, L.H.D.; Carlotto, F.D.; Pinto, V.L. Mortality rate and water contamination by atrazine in Rio Grande do Sul State: Na ecological study. *Int. J. Dev. Res.* **2020**, *10*, 38235–38240.
79. Gfrerer, M.; Wenzl, T.; Quan, X.; Platzer, B.; Lankmayr, E. Occurrence of triazines in surface and drinking water of Liaoning Province in Eastern China. *J. Biochem. Biophys. Methods* **2002**, *53*, 217–228. [CrossRef]
80. Ghosh, P.K.; Philip, L. Environmental significance of atrazine in aqueous systems and its removal by biological processes: An overview. *Glob. NEST J.* **2006**, *8*, 159–178. [CrossRef]
81. Mishra, R.K.; Kumar, D.J.P.; Narula, A.; Chistie, S.M.; Naik, S.U. Production and beneficial impact of biochar for environmental application: A review on types of feedstocks, chemical compositions, operating parameters, techno-economic study, and life cycle assessment. *Fuel* **2023**, *343*, 127968. [CrossRef]
82. Yoon, Y.; Ryu, J.; Oh, J.; Choi, B.-G.; Snyder, S.A. Occurrence of endocrine disrupting compounds, pharmaceuticals, and personal care products in the Han River (Seoul, South Korea). *Sci. Total Environ.* **2010**, *408*, 636–643. [CrossRef] [PubMed]

83. Almasi, H.; Takdastan, A.; Jaafarzadeh, N.; Babaei, A.A.; Birgani, Y.T.; Cheraghian, B.; Saki, A.; Jorfi, S. Spatial distribution, ecological and health risk assessment and source identification of atrazine in Shadegan international wetland, Iran. *Mar. Pollut. Bull.* **2020**, *160*, 111569. [CrossRef] [PubMed]
84. Rimayi, C.; Odusanya, D.; Weiss, J.M.; de Boer, J.; Chimuka, L. Seasonal variation of chloro-s-triazines in the Hartbeespoort Dam catchment, South Africa. *Sci. Total Environ.* **2018**, *613*, 472–482. [CrossRef] [PubMed]
85. Lewis, S.E.; Brodie, J.E.; Bainbridge, Z.T.; Rohde, K.W.; Davis, A.M.; Masters, B.L.; Maughan, M.; Devlin, M.J.; Mueller, J.F.; Schaffelke, B. Herbicides: A new threat to the Great Barrier Reef. *Environ. Pollut.* **2009**, *157*, 2470–2484. [CrossRef]
86. Köck-Schulmeyer, M.; Ginebreda, A.; Postigo, C.; Garrido, T.; Fraile, J.; de Alda, M.L.; Barceló, D. Four-year advanced monitoring program of polar pesticides in groundwater of Catalonia (NE-Spain). *Sci. Total Environ.* **2014**, *470*, 1087–1098. [CrossRef]
87. Bethsass, J.; Colangelo, A. European Union bans atrazine, while the United States negotiates continued use. *Int. J. Occup. Environ. Health* **2006**, *12*, 260–267. [CrossRef]
88. Shirmardi, M.; Alavi, N.; Lima, E.C.; Takdastan, A.; Mahvi, A.H.; Babaei, A.A. Removal of atrazine as an organic micro-pollutant from aqueous solutions: A comparative study. *Process Saf. Environ. Prot.* **2016**, *103*, 23–35. [CrossRef]
89. Caquet, T.; Roucaute, M.; Mazzella, N.; Delmas, F.; Madigou, C.; Farcy, E.; Burgeot, T.; Allenou, J.P.; Gabellec, R. Risk assessment of herbicides and booster biocides along estuarine continuums in the Bay of Vilaine area (Brittany, France). *Environ. Sci. Pollut. Res.* **2013**, *20*, 651–666. [CrossRef] [PubMed]
90. Masiá, A.; Campo, J.; Navarro-Ortega, A.; Barceló, D.; Picó, Y. Pesticide monitoring in the basin of Llobregat River (Catalonia, Spain) and comparison with historical data. *Sci. Total Environ.* **2015**, *503*, 58–68. [CrossRef] [PubMed]
91. Literathy, P.; Laszlo, F.; Csanyi, B. Approaches for sediment associated pollutant monitoring in the river Danube. *Water Sci. Technol.* **1994**, *30*, 157. [CrossRef]
92. Caldas, S.S.; Arias, J.L.O.; Rombaldi, C.; Mello, L.L.; Cerqueira, M.B.R.; Martins, A.F.; Primel, E.G. Occurrence of pesticides and PPCPs in surface and drinking water in southern Brazil: Data on 4-year monitoring. *J. Braz. Chem. Soc.* **2019**, *30*, 71–80. [CrossRef]
93. Kookana, R.; Holz, G.; Barnes, C.; Bubb, K.; Fremlin, R.; Boardman, B. Impact of climatic and soil conditions on environmental fate of atrazine used under plantation forestry in Australia. *J. Environ. Manag.* **2010**, *91*, 2649–2656. [CrossRef]
94. Solomon, R.D.J.; Kumar, A.; Satheeja Santhi, V. Atrazine biodegradation efficiency, metabolite detection, and trzD gene expression by enrichment bacterial cultures from agricultural soil. *J. Zhejiang Univ. Sci. B* **2013**, *14*, 1162–1172. [CrossRef] [PubMed]
95. Mishra, S.; Kumar, P.; Mehrotra, I.; Kumar, M. Prevalence of organic micropollutants in the Yamuna River, Delhi, India: Seasonal variations and governing factors. *Sci. Total Environ.* **2023**, *858*, 159684. [CrossRef]
96. Qu, M.; Li, H.; Li, N.; Liu, G.; Zhao, J.; Hua, Y.; Zhu, D. Distribution of atrazine and its phytoremediation by submerged macrophytes in lake sediments. *Chemosphere* **2017**, *168*, 1515–1522. [CrossRef]
97. Nasseri, S.; Dehghani, M.; Amin, S.; Naddafi, K.; Zamanian, Z. Fate of atrazine in the agricultural soil of corn fields in Fars province of Iran. *J. Environ. Health Sci. Eng.* **2009**, *6*, 223–232.
98. Zeljezic, D.; Garaj-Vrhovac, V.; Perkovic, P. Evaluation of DNA damage induced by atrazine and atrazine-based herbicide in human lymphocytes in vitro using a comet and DNA diffusion assay. *Toxicol. Vitr.* **2006**, *20*, 923–935. [CrossRef]
99. Alam, J.B.; Dikshit, A.K.; Bandyopadhyay, M. Efficacy of adsorbents for 2, 4-D and atrazine removal from water environment. *Glob. Nest Int. J* **2000**, *2*, 139–148. [CrossRef]
100. Boyd, R.A. Herbicides and herbicide degradates in shallow groundwater and the Cedar River near a municipal well field, Cedar Rapids, Iowa. *Sci. Total Environ.* **2000**, *248*, 241–253. [CrossRef]
101. Lakudzala, D.D. Atrazine and metolachlor contamination in surface and ground water in the Zomba/Bvumbwe region in Malawi. *Int. Lett. Chem. Phys. Astron.* **2013**, *1*, 33–45. [CrossRef]
102. Vargha, M.; Takáts, Z.; Márialigeti, K. Degradation of atrazine in a laboratory scale model system with Danube river sediment. *Water Res.* **2005**, *39*, 1560–1568. [CrossRef] [PubMed]
103. Huber, W. Ecotoxicological relevance of atrazine in aquatic systems. *Environ. Toxicol. Chem. Int. J.* **1993**, *12*, 1865–1881. [CrossRef]
104. Lima, D.L.D.; Silva, C.P.; Schneider, R.J.; Esteves, V.I. Development of an ELISA procedure to study sorption of atrazine onto a sewage sludge-amended luvisol soil. *Talanta* **2011**, *85*, 1494–1499. [CrossRef]
105. Lasserre, J.-P.; Fack, F.; Serchi, T.; Revets, D.; Planchon, S.; Renaut, J.; Hoffmann, L.; Gutleb, A.C.; Muller, C.P.; Bohn, T. Atrazine and PCB 153 and their effects on the proteome of subcellular fractions of human MCF-7 cells. *Biochim. Et Biophys. Acta (BBA)-Proteins Proteom.* **2012**, *1824*, 833–841. [CrossRef]
106. Kurk, F.; Eagan, P. The value of adding design-for-the-environment to pollution prevention assistance options. *J. Clean. Prod.* **2008**, *16*, 722–726. [CrossRef]
107. Gammon, D.W.; Aldous, C.N.; Carr, W.C., Jr.; Sanborn, J.R.; Pfeifer, K.F. A risk assessment of atrazine use in California: Human health and ecological aspects. *Pest Manag. Sci. Former. Pestic. Sci.* **2005**, *61*, 331–355. [CrossRef]
108. Wirbisky, S.E.; Weber, G.J.; Sepúlveda, M.S.; Lin, T.-L.; Jannasch, A.S.; Freeman, J.L. An embryonic atrazine exposure results in reproductive dysfunction in adult zebrafish and morphological alterations in their offspring. *Sci. Rep.* **2016**, *6*, 21337. [CrossRef] [PubMed]

109. Qu, J.; Yuan, Y.; Meng, Q.; Zhang, G.; Deng, F.; Wang, L.; Tao, Y.; Jiang, Z.; Zhang, Y. Simultaneously enhanced removal and stepwise recovery of atrazine and Pb (II) from water using β–cyclodextrin functionalized cellulose: Characterization, adsorptive performance and mechanism exploration. *J. Hazard. Mater.* **2020**, *400*, 123142. [CrossRef]
110. Kettles, M.K.; Browning, S.R.; Prince, T.S.; Horstman, S.W. Triazine herbicide exposure and breast cancer incidence: An ecologic study of Kentucky counties. *Environ. Health Perspect.* **1997**, *105*, 1222–1227. [CrossRef]
111. Rhoades, M.G.; Meza, J.L.; Beseler, C.L.; Shea, P.J.; Kahle, A.; Vose, J.M.; Eskridge, K.M.; Spalding, R.F. Atrazine and nitrate in public drinking water supplies and non-Hodgkin lymphoma in Nebraska, USA. *Environ. Health Insights* **2013**, *7*, EHI-S10629. [CrossRef] [PubMed]
112. Liu, H.; Chen, W.; Liu, C.; Liu, Y.U.; Dong, C. Magnetic mesoporous clay adsorbent: Preparation, characterization and adsorption capacity for atrazine. *Microporous Mesoporous Mater.* **2014**, *194*, 72–78. [CrossRef]
113. Siripattanakul, S.; Wirojanagud, W.; McEvoy, J.; Limpiyakorn, T.; Khan, E. Atrazine degradation by stable mixed cultures enriched from agricultural soil and their characterization. *J. Appl. Microbiol.* **2009**, *106*, 986–992. [CrossRef]
114. Tesfamichael, A.A.; Kaluarachchi, J.J. A methodology to assess the risk of an existing pesticide and potential future pesticides for regulatory decision-making. *Environ. Sci. Policy* **2006**, *9*, 275–290. [CrossRef]
115. Lin, Z.; Roede, J.R.; He, C.; Jones, D.P.; Filipov, N.M. Short-term oral atrazine exposure alters the plasma metabolome of male C57BL/6 mice and disrupts α-linolenate, tryptophan, tyrosine and other major metabolic pathways. *Toxicology* **2014**, *326*, 130–141. [CrossRef]
116. Hayes, T.B.; Collins, A.; Lee, M.; Mendoza, M.; Noriega, N.; Stuart, A.A.; Vonk, A. Hermaphroditic, demasculinized frogs after exposure to the herbicide atrazine at low ecologically relevant doses. *Proc. Natl. Acad. Sci. USA* **2002**, *99*, 5476–5480. [CrossRef]
117. Hayes, T.; Haston, K.; Tsui, M.; Hoang, A.; Haeffele, C.; Vonk, A. Atrazine-induced hermaphroditism at 0.1 ppb in American leopard frogs (*Rana pipiens*): Laboratory and field evidence. *Environ. Health Perspect.* **2003**, *111*, 568–575. [CrossRef] [PubMed]
118. Cook, L.E.; Chen, Y.; Renfree, M.B.; Pask, A.J. Long-term maternal exposure to atrazine in the drinking water reduces penis length in the tammar wallaby Macropus eugenii. *Reprod. Fertil. Dev.* **2020**, *32*, 1099–1107. [CrossRef]
119. Muir, K.; Rattanamongkolgul, S.; Smallman-Raynor, M.; Thomas, M.; Downer, S.; Jenkinson, C. Breast cancer incidence and its possible spatial association with pesticide application in two counties of England. *Public Health* **2004**, *118*, 513–520. [CrossRef] [PubMed]
120. Huang, P.; Yang, J.; Ning, J.; Wang, M.; Song, Q. Atrazine triggers DNA damage response and induces DNA double-strand breaks in MCF-10A cells. *Int. J. Mol. Sci.* **2015**, *16*, 14353–14368. [CrossRef]
121. Zhao, F.; Li, K.; Zhao, L.; Liu, J.; Suo, Q.; Zhao, J.; Wang, H.; Zhao, S. Effect of Nrf2 on rat ovarian tissues against atrazine-induced anti-oxidative response. *Int. J. Clin. Exp. Pathol.* **2014**, *7*, 2780. [PubMed]
122. Lim, S.; Ahn, S.Y.; Song, I.C.; Chung, M.H.; Jang, H.C.; Park, K.S.; Lee, K.-U.; Pak, Y.K.; Lee, H.K. Chronic exposure to the herbicide, atrazine, causes mitochondrial dysfunction and insulin resistance. *PLoS ONE* **2009**, *4*, e5186. [CrossRef]
123. Kiesecker, J.M. Synergism between trematode infection and pesticide exposure: A link to amphibian limb deformities in nature? *Proc. Natl. Acad. Sci. USA* **2002**, *99*, 9900–9904. [CrossRef]
124. Sai, L.; Dong, Z.; Li, L.; Guo, Q.; Jia, Q.; Xie, L.; Bo, C.; Liu, Y.; Qu, B.; Li, X. Gene expression profiles in testis of developing male Xenopus laevis damaged by chronic exposure of atrazine. *Chemosphere* **2016**, *159*, 145–152. [CrossRef]
125. Huang, M.; Zhao, Q.; Yin, J.; Cao, S.; Chen, H.; Duan, R. The toxic effects of chronic atrazine exposure on the intestinal microbiota, metabolism and transcriptome of Pelophylax nigromaculatus larvae. *J. Hazard. Mater.* **2022**, *440*, 129817. [CrossRef]
126. Xia, J.; Qin, L.; Du, Z.-H.; Lin, J.; Li, X.-N.; Li, J.-L. Performance of a novel atrazine-induced cerebellar toxicity in quail (*Coturnix C. coturnix*): Activating PXR/CAR pathway responses and disrupting cytochrome P450 homeostasis. *Chemosphere* **2017**, *171*, 259–264. [CrossRef]
127. Podda, M.V.; Deriu, F.; Solinas, A.; Demontis, M.P.; Varoni, M.V.; Spissu, A.; Anania, V.; Tolu, E. Effect of atrazine administration on spontaneous and evoked cerebellar activity in the rat. *Pharmacol. Res.* **1997**, *36*, 199–202. [CrossRef]
128. Urseler, N.; Bachetti, R.; Biolé, F.; Morgante, V.; Morgante, C. Atrazine pollution in groundwater and raw bovine milk: Water quality, bioaccumulation and human risk assessment. *Sci. Total Environ.* **2022**, *852*, 158498. [CrossRef] [PubMed]
129. Ostiguy, N.; Drummond, F.A.; Aronstein, K.; Eitzer, B.; Ellis, J.D.; Spivak, M.; Sheppard, W.S. Honey bee exposure to pesticides: A four-year nationwide study. *Insects* **2019**, *10*, 13. [CrossRef] [PubMed]
130. Fellows, C.J.; Anderson, T.D.; Swale, D.R. Acute toxicity of atrazine, alachlor, and chlorpyrifos mixtures to honey bees. *Pestic. Biochem. Physiol.* **2022**, *188*, 105271. [CrossRef] [PubMed]
131. dos Santos Araújo, R.; Bernardes, R.C.; Martins, G.F. A mixture containing the herbicides Mesotrione and Atrazine imposes toxicological risks on workers of Partamona helleri. *Sci. Total Environ.* **2021**, *763*, 142980. [CrossRef]
132. Wang, P.; Yin, Y.; Guo, Y.; Wang, C. Preponderant adsorption for chlorpyrifos over atrazine by wheat straw-derived biochar: Experimental and theoretical studies. *RSC Adv.* **2016**, *6*, 10615–10624. [CrossRef]
133. Shenoy, K. Environmentally realistic exposure to the herbicide atrazine alters some sexually selected traits in male guppies. *PLoS ONE* **2012**, *7*, e30611. [CrossRef]

134. Cavas, T. In vivo genotoxicity evaluation of atrazine and atrazine–based herbicide on fish Carassius auratus using the micronucleus test and the comet assay. *Food Chem. Toxicol.* **2011**, *49*, 1431–1435. [CrossRef] [PubMed]
135. Araujo, C.V.M.; Silva, D.C.V.R.; Gomes, L.E.T.; Acayaba, R.D.; Montagner, C.C.; Moreira-Santos, M.; Ribeiro, R.; Pompeo, M.L.M. Habitat fragmentation caused by contaminants: Atrazine as a chemical barrier isolating fish populations. *Chemosphere* **2018**, *193*, 24–31. [CrossRef] [PubMed]
136. Nwani, C.D.; Lakra, W.S.; Nagpure, N.S.; Kumar, R.; Kushwaha, B.; Srivastava, S.K. Toxicity of the herbicide atrazine: Effects on lipid peroxidation and activities of antioxidant enzymes in the freshwater fish *Channa punctatus* (Bloch). *Int. J. Environ. Res. Public Health* **2010**, *7*, 3298–3312. [CrossRef]
137. Xu, T.; Liu, Q.; Chen, D.; Liu, Y. Atrazine exposure induces necroptosis through the P450/ROS pathway and causes inflammation in the gill of common carp (*Cyprinus carpio* L.). *Fish Shellfish Immunol.* **2022**, *131*, 809–816. [CrossRef]
138. Chen, D.; Zhang, Z.; Yao, H.; Cao, Y.; Xing, H.; Xu, S. Pro-and anti-inflammatory cytokine expression in immune organs of the common carp exposed to atrazine and chlorpyrifos. *Pestic. Biochem. Physiol.* **2014**, *114*, 8–15. [CrossRef]
139. Papoulias, D.M.; Tillitt, D.E.; Talykina, M.G.; Whyte, J.J.; Richter, C.A. Atrazine reduces reproduction in Japanese medaka (*Oryzias latipes*). *Aquat. Toxicol.* **2014**, *154*, 230–239. [CrossRef]
140. Salaberria, I.; Hansen, B.H.; Asensio, V.; Olsvik, P.A.; Andersen, R.A.; Jenssen, B.M. Effects of atrazine on hepatic metabolism and endocrine homeostasis in rainbow trout (*Oncorhynchus mykiss*). *Toxicol. Appl. Pharmacol.* **2009**, *234*, 98–106. [CrossRef]
141. Shelley, L.K.; Ross, P.S.; Miller, K.M.; Kaukinen, K.H.; Kennedy, C.J. Toxicity of atrazine and nonylphenol in juvenile rainbow trout (*Oncorhynchus mykiss*): Effects on general health, disease susceptibility and gene expression. *Aquat. Toxicol.* **2012**, *124*, 217–226. [CrossRef] [PubMed]
142. Liu, Z.; Fu, Z.; Jin, Y. Immunotoxic effects of atrazine and its main metabolites at environmental relevant concentrations on larval zebrafish (*Danio rerio*). *Chemosphere* **2017**, *166*, 212–220. [CrossRef]
143. Liu, Z.; Wang, Y.; Zhu, Z.; Yang, E.; Feng, X.; Fu, Z.; Jin, Y. Atrazine and its main metabolites alter the locomotor activity of larval zebrafish (*Danio rerio*). *Chemosphere* **2016**, *148*, 163–170. [CrossRef]
144. Bordin, E.R.; Yamamoto, F.Y.; Mannes, Y.; Munhoz, R.C.; Muelbert, J.R.E.; de Freitas, A.M.; Cestari, M.M.; Ramsdorf, W.A. Sublethal effects of the herbicides atrazine and glyphosate at environmentally relevant concentrations on South American catfish (Rhamdia quelen) embryos. *Environ. Toxicol. Pharmacol.* **2023**, *98*, 104057. [CrossRef]
145. Van Der Kraak, G.; Matsumoto, J.; Kim, M.; Hosmer, A.J. Atrazine and its degradates have little effect on the corticosteroid stress response in the zebrafish. *Comp. Biochem. Physiol. Part C Toxicol. Pharmacol.* **2015**, *170*, 1–7. [CrossRef]
146. Juhel, G.; Bayen, S.; Goh, C.; Lee, W.K.; Kelly, B.C. Use of a suite of biomarkers to assess the effects of carbamazepine, bisphenol A, atrazine, and their mixtures on green mussels, Perna viridis. *Environ. Toxicol. Chem.* **2017**, *36*, 429–441. [CrossRef]
147. Mac Loughlin, C.; Canosa, I.S.; Silveyra, G.R.; Greco, L.S.L.; Rodríguez, E.M. Effects of atrazine on growth and sex differentiation, in juveniles of the freshwater crayfish *Cherax quadricarinatus*. *Ecotoxicol. Environ. Saf.* **2016**, *131*, 96–103. [CrossRef]
148. Rabban, C.; Contreras, K.; Goolsby, D.; Hamdan, R.; Fedraw, C.; Bosah, A.; Muskovac, M.; Evans, K.; Belanger, R. Quantitation of atrazine and its metabolites for toxicological studies in the keystone species Faxonius virilis. *J. Biol. Chem.* **2023**, *299*, 103722. [CrossRef]
149. Russart, K.L.G.; Rhen, T. Atrazine alters expression of reproductive and stress genes in the developing hypothalamus of the snapping turtle, *Chelydra serpentina*. *Toxicology* **2016**, *366*, 1–9. [CrossRef]
150. Kabra, A.N.; Ji, M.-K.; Choi, J.; Kim, J.R.; Govindwar, S.P.; Jeon, B.-H. Toxicity of atrazine and its bioaccumulation and biodegradation in a green microalga, Chlamydomonas mexicana. *Environ. Sci. Pollut. Res.* **2014**, *21*, 12270–12278. [CrossRef]
151. Wang, J.; Guo, X. Adsorption kinetic models: Physical meanings, applications, and solving methods. *J. Hazard. Mater.* **2020**, *390*, 122156. [CrossRef] [PubMed]
152. Ali, I.; Asim, M.; Khan, T.A. Low cost adsorbents for the removal of organic pollutants from wastewater. *J. Environ. Manag.* **2012**, *113*, 170–183. [CrossRef] [PubMed]
153. Bonilla-Petriciolet, A.; Mendoza-Castillo, D.I.; Reynel-Ávila, H.E. *Adsorption Processes for Water Treatment and Purification*; Springer: Berlin/Heidelberg, Germany, 2017; Volume 256. [CrossRef]
154. Al-Ghouti, M.A.; Al-Absi, R.S. Mechanistic understanding of the adsorption and thermodynamic aspects of cationic methylene blue dye onto cellulosic olive stones biomass from wastewater. *Sci. Rep.* **2020**, *10*, 15928. [CrossRef] [PubMed]
155. Al-Ghouti, M.A.; Da'ana, D.A. Guidelines for the use and interpretation of adsorption isotherm models: A review. *J. Hazard. Mater.* **2020**, *393*, 122383. [CrossRef] [PubMed]
156. Ayawei, N.; Ebelegi, A.N.; Wankasi, D. Modelling and interpretation of adsorption isotherms. *J. Chem.* **2017**, *2017*, 3039817. [CrossRef]
157. González-Pradas, E.; Villafranca-Sánchez, M.; Socías-Viciana, M.; Fernández-Pérez, M.; Ureña-Amate, M.D. Preliminary studies in removing atrazine, isoproturon and imidacloprid from water by natural sepiolite. *J. Chem. Technol. Biotechnol.* **1999**, *74*, 417–422. [CrossRef]

158. Agdi, K.; Bouaid, A.; Esteban, A.M.; Hernando, P.F.; Azmani, A.; Camara, C. Removal of atrazine and four organophosphorus pesticides from environmental waters by diatomaceous earth–remediation method. *J. Environ. Monit.* **2000**, *2*, 420–423. [CrossRef]
159. Gonzalez-Pradas, E.; Socıas-Viciana, M.; Saifi, M.; Urena-Amate, M.D.; Flores-Cespedes, F.; Fernández-Pérez, M.; Villafranca-Sanchez, M. Adsorption of atrazine from aqueous solution on heat treated kerolites. *Chemosphere* **2003**, *51*, 85–93. [CrossRef]
160. Abate, G.; Masini, J.C. Sorption of atrazine, propazine, deethylatrazine, deisopropylatrazine and hydroxyatrazine onto organovermiculite. *J. Braz. Chem. Soc.* **2005**, *16*, 936–943. [CrossRef]
161. Ureña-Amate, M.D.; Socías-Viciana, M.; González-Pradas, E.; Saifi, M. Effects of ionic strength and temperature on adsorption of atrazine by a heat treated kerolite. *Chemosphere* **2005**, *59*, 69–74. [CrossRef]
162. Chingombe, P.; Saha, B.; Wakeman, R.J. Sorption of atrazine on conventional and surface modified activated carbons. *J. Colloid Interface Sci.* **2006**, *302*, 408–416. [CrossRef] [PubMed]
163. Katsumata, H.; Kaneco, S.; Suzuki, T.; Ohta, K. Determination of atrazine and simazine in water samples by high-performance liquid chromatography after preconcentration with heat-treated diatomaceous earth. *Anal. Chim. Acta* **2006**, *577*, 214–219. [CrossRef]
164. Cao, X.; Ma, L.; Gao, B.; Harris, W. Dairy-manure derived biochar effectively sorbs lead and atrazine. *Environ. Sci. Technol.* **2009**, *43*, 3285–3291. [CrossRef]
165. Alila, S.; Boufi, S. Removal of organic pollutants from water by modified cellulose fibres. *Ind. Crops Prod.* **2009**, *30*, 93–104. [CrossRef]
166. Chen, G.-C.; Shan, X.-Q.; Zhou, Y.-Q.; Shen, X.-e.; Huang, H.-L.; Khan, S.U. Adsorption kinetics, isotherms and thermodynamics of atrazine on surface oxidized multiwalled carbon nanotubes. *J. Hazard. Mater.* **2009**, *169*, 912–918. [CrossRef] [PubMed]
167. Singh, N. Adsorption of herbicides on coal fly ash from aqueous solutions. *J. Hazard. Mater.* **2009**, *168*, 233–237. [CrossRef]
168. Castro, C.S.; Guerreiro, M.C.; Gonçalves, M.; Oliveira, L.C.A.; Anastácio, A.S. Activated carbon/iron oxide composites for the removal of atrazine from aqueous medium. *J. Hazard. Mater.* **2009**, *164*, 609–614. [CrossRef] [PubMed]
169. Zheng, W.; Guo, M.; Chow, T.; Bennett, D.N.; Rajagopalan, N. Sorption properties of greenwaste biochar for two triazine pesticides. *J. Hazard. Mater.* **2010**, *181*, 121–126. [CrossRef]
170. Gupta, V.K.; Gupta, B.; Rastogi, A.; Agarwal, S.; Nayak, A. Pesticides removal from waste water by activated carbon prepared from waste rubber tire. *Water Res.* **2011**, *45*, 4047–4055. [CrossRef]
171. Rambabu, N.; Guzman, C.A.; Soltan, J.; Himabindu, V. Adsorption characteristics of atrazine on granulated activated carbon and carbon nanotubes. *Chem. Eng. Technol.* **2012**, *35*, 272–280. [CrossRef]
172. Zhang, Y.; Li, Y.; Zheng, X. Removal of atrazine by nanoscale zero valent iron supported on organobentonite. *Sci. Total Environ.* **2011**, *409*, 625–630. [CrossRef]
173. Chen, Z.; Wen, Q.; Lian, J.; Ren, N. Preparation and characterization of a lipoid adsorption material and its atrazine removal performance. *J. Environ. Sci.* **2011**, *23*, 1293–1298. [CrossRef] [PubMed]
174. Jamil, T.S.; Gad-Allah, T.A.; Ibrahim, H.S.; Saleh, T.S. Adsorption and isothermal models of atrazine by zeolite prepared from Egyptian kaolin. *Solid State Sci.* **2011**, *13*, 198–203. [CrossRef]
175. Chaparadza, A.; Hossenlopp, J.M. Adsorption kinetics, isotherms and thermodynamics of atrazine removal using a banana peel based sorbent. *Water Sci. Technol.* **2012**, *65*, 940–947. [CrossRef]
176. Tang, W.-W.; Zeng, G.-M.; Gong, J.-L.; Liu, Y.; Wang, X.-Y.; Liu, Y.-Y.; Liu, Z.-F.; Chen, L.; Zhang, X.-R.; Tu, D.-Z. Simultaneous adsorption of atrazine and Cu (II) from wastewater by magnetic multi-walled carbon nanotube. *Chem. Eng. J.* **2012**, *211*, 470–478. [CrossRef]
177. Li, L.; Rowbotham, J.S.; Greenwell, H.C.; Dyer, P.W. *An Introduction to Pyrolysis and Catalytic Pyrolysis: Versatile Techniques for Biomass Conversion*; Elsevier: Amsterdam, The Netherlands, 2013. [CrossRef]
178. Zhao, X.; Ouyang, W.; Hao, F.; Lin, C.; Wang, F.; Han, S.; Geng, X. Properties comparison of biochars from corn straw with different pretreatment and sorption behaviour of atrazine. *Bioresour. Technol.* **2013**, *147*, 338–344. [CrossRef]
179. Jung, C.; Park, J.; Lim, K.H.; Park, S.; Heo, J.; Her, N.; Oh, J.; Yun, S.; Yoon, Y. Adsorption of selected endocrine disrupting compounds and pharmaceuticals on activated biochars. *J. Hazard. Mater.* **2013**, *263*, 702–710. [CrossRef]
180. Nam, S.-W.; Choi, D.-J.; Kim, S.-K.; Her, N.; Zoh, K.-D. Adsorption characteristics of selected hydrophilic and hydrophobic micropollutants in water using activated carbon. *J. Hazard. Mater.* **2014**, *270*, 144–152. [CrossRef] [PubMed]
181. Yang, B.-Y.; Cao, Y.; Qi, F.-F.; Li, X.-Q.; Xu, Q. Atrazine adsorption removal with nylon6/polypyrrole core-shell nanofibers mat: Possible mechanism and characteristics. *Nanoscale Res. Lett.* **2015**, *10*, 207. [CrossRef] [PubMed]
182. Lladó, J.; Lao-Luque, C.; Ruiz, B.; Fuente, E.; Solé-Sardans, M.; Dorado, A.D. Role of activated carbon properties in atrazine and paracetamol adsorption equilibrium and kinetics. *Process Saf. Environ. Prot.* **2015**, *95*, 51–59. [CrossRef]
183. Pal, J.; Deb, M.K.; Sircar, J.K.; Agnihotri, P.K. Microwave green synthesis of biopolymer-stabilized silver nanoparticles and their adsorption behavior for atrazine. *Appl. Water Sci.* **2015**, *5*, 181–190. [CrossRef]
184. Liu, H.; Chen, W. Magnetic mesoporous imprinted adsorbent based on Fe_3O_4-modified sepiolite for organic micropollutant removal from aqueous solution. *Rsc Adv.* **2015**, *5*, 27034–27042. [CrossRef]

185. Grundgeiger, E.; Lim, Y.H.; Frost, R.L.; Ayoko, G.A.; Xi, Y. Application of organo-beidellites for the adsorption of atrazine. *Appl. Clay Sci.* **2015**, *105*, 252–258. [CrossRef]
186. Coldebella, P.F.; Fagundes-Klen, M.R.; Nishi, L.; Valverde, K.C.; Cavalcanti, E.B.; Andreo dos Santos, O.A.; Bergamasco, R. Potential effect of chemical and thermal treatment on the kinetics, equilibrium, and thermodynamic studies for atrazine biosorption by the Moringa oleifera pods. *Can. J. Chem. Eng.* **2017**, *95*, 961–973. [CrossRef]
187. Engel, M.; Chefetz, B. Adsorption and desorption of dissolved organic matter by carbon nanotubes: Effects of solution chemistry. *Environ. Pollut.* **2016**, *213*, 90–98. [CrossRef]
188. Saha, A.; Bhaduri, D.; Pipariya, A.; Kumar Ghosh, R. Linear and nonlinear sorption modelling for adsorption of atrazine onto activated peanut husk. *Environ. Prog. Sustain. Energy* **2017**, *36*, 348–358. [CrossRef]
189. Boruah, P.K.; Sharma, B.; Hussain, N.; Das, M.R. Magnetically recoverable Fe3O4/graphene nanocomposite towards efficient removal of triazine pesticides from aqueous solution: Investigation of the adsorption phenomenon and specific ion effect. *Chemosphere* **2017**, *168*, 1058–1067. [CrossRef]
190. Toledo-Jaldin, H.P.; Blanco-Flores, A.; Sánchez-Mendieta, V.; Martín-Hernández, O. Influence of the chain length of surfactant in the modification of zeolites and clays. Removal of atrazine from water solutions. *Environ. Technol.* **2018**, *39*, 2679–2690. [CrossRef] [PubMed]
191. Wei, X.; Wu, Z.; Du, C.; Wu, Z.; Ye, B.-C.; Cravotto, G. Enhanced adsorption of atrazine on a coal-based activated carbon modified with sodium dodecyl benzene sulfonate under microwave heating. *J. Taiwan Inst. Chem. Eng.* **2017**, *77*, 257–262. [CrossRef]
192. Alahabadi, A.; Moussavi, G. Preparation, characterization and atrazine adsorption potential of mesoporous carbonate-induced activated biochar (CAB) from Calligonum Comosum biomass: Parametric experiments and kinetics, equilibrium and thermodynamic modeling. *J. Mol. Liq.* **2017**, *242*, 40–52. [CrossRef]
193. Jia, D.; Li, A.; Li, C.; Liu, G.; Li, Y. Removal atrazine using two anion-exchange resins supported nanohydrous metal-oxide particle. *Chin. J. Chem. Eng.* **2017**, *25*, 180–186. [CrossRef]
194. Chen, D.; Chen, C.; Shen, W.; Quan, H.; Chen, S.; Xie, S.; Luo, X.; Guo, L. MOF-derived magnetic porous carbon-based sorbent: Synthesis, characterization, and adsorption behavior of organic micropollutants. *Adv. Powder Technol.* **2017**, *28*, 1769–1779. [CrossRef]
195. Yang, F.; Zhang, S.; Sun, L.; Zhang, Y. Facile synthesis of highly porous "carbon sponge" with adsorption and co-adsorption behavior of lead ions and atrazine. *Environ. Sci. Pollut. Res.* **2018**, *25*, 18705–18716. [CrossRef]
196. Wei, X.; Wu, Z.; Wu, Z.; Ye, B.-C. Adsorption behaviors of atrazine and Cr(III) onto different activated carbons in single and co-solute systems. *Powder Technol.* **2018**, *329*, 207–216. [CrossRef]
197. Zhang, Y.; Cao, B.; Zhao, L.; Sun, L.; Gao, Y.; Li, J.; Yang, F. Biochar-supported reduced graphene oxide composite for adsorption and coadsorption of atrazine and lead ions. *Appl. Surf. Sci.* **2018**, *427*, 147–155. [CrossRef]
198. Liu, Y.; Ma, S.; Chen, J. A novel pyro-hydrochar via sequential carbonization of biomass waste: Preparation, characterization and adsorption capacity. *J. Clean. Prod.* **2018**, *176*, 187–195. [CrossRef]
199. Akpinar, I.; Yazaydin, A.O. Adsorption of atrazine from water in metal–organic framework materials. *J. Chem. Eng. Data* **2018**, *63*, 2368–2375. [CrossRef]
200. Cusioli, L.F.; Bezerra, C.d.O.; Quesada, H.B.; Alves Baptista, A.T.; Nishi, L.; Vieira, M.F.; Bergamasco, R. Modified *Moringa oleifera* Lam. Seed husks as low-cost biosorbent for atrazine removal. *Environ. Technol.* **2021**, *42*, 1092–1103. [CrossRef]
201. Suo, F.; You, X.; Ma, Y.; Li, Y. Rapid removal of triazine pesticides by P doped biochar and the adsorption mechanism. *Chemosphere* **2019**, *235*, 918–925. [CrossRef] [PubMed]
202. Gao, Y.; Jiang, Z.; Li, J.; Xie, W.; Jiang, Q.; Bi, M.; Zhang, Y. A comparison of the characteristics and atrazine adsorption capacity of co-pyrolysed and mixed biochars generated from corn straw and sawdust. *Environ. Res.* **2019**, *172*, 561–568. [CrossRef] [PubMed]
203. N'Diaye, A.D.; Boudokhane, C.; Kankou, M.; Dhaouadi, H. Potential of rice husk ash in atrazine removal. *Chem. Ecol.* **2019**, *35*, 678–692. [CrossRef]
204. Sharma, G.; Thakur, B.; Kumar, A.; Sharma, S.; Naushad, M.; Stadler, F.J. Atrazine removal using chitin-cl-poly (acrylamide-co-itaconic acid) nanohydrogel: Isotherms and pH responsive nature. *Carbohydr. Polym.* **2020**, *241*, 116258. [CrossRef]
205. Bayati, M.; Numaan, M.; Kadhem, A.; Salahshoor, Z.; Qasim, S.; Deng, H.; Lin, J.; Yan, Z.; Lin, C.-H.; de Cortalezzi, M.F. Adsorption of atrazine by laser induced graphitic material: An efficient, scalable and green alternative for pollution abatement. *J. Environ. Chem. Eng.* **2020**, *8*, 104407. [CrossRef]
206. Xing, R.; He, J.; Hao, P.; Zhou, W. Graphene oxide-supported nanoscale zero-valent iron composites for the removal of atrazine from aqueous solution. *Colloids Surf. A Physicochem. Eng. Asp.* **2020**, *589*, 124466. [CrossRef]
207. Fruehwirth, M.; Sbizzaro, M.; Rosa, D.M.; Sampaio, S.C.; Reis, R.R.d. Adsorption of atrazine by biochars produced from byproducts of the wood industry. *Eng. Agrícola* **2020**, *40*, 769–776. [CrossRef]
208. Nagarajan, D.; Varada, O.M.; Venkatanarasimhan, S. Carbon dots coated on amine functionalized cellulose sponge for the adsorption of the toxic herbicide atrazine. *Mater. Today Proc.* **2021**, *47*, 790–799. [CrossRef]

209. Cao, Y.; Jiang, S.; Zhang, Y.; Xu, J.; Qiu, L.; Wang, L. Investigation into adsorption characteristics and mechanism of atrazine on nano-MgO modified fallen leaf biochar. *J. Environ. Chem. Eng.* **2021**, *9*, 105727. [CrossRef]
210. Goyal, N.; Bulasara, V.K.; Li, G.; Liu, L. Rapid uptake of atrazine from aqueous phase by thermally activated MCM-41. *Sci. Total Environ.* **2021**, *753*, 142091. [CrossRef]
211. Chabalala, M.B.; Al-Abri, M.Z.; Mamba, B.B.; Nxumalo, E.N. Mechanistic aspects for the enhanced adsorption of bromophenol blue and atrazine over cyclodextrin modified polyacrylonitrile nanofiber membranes. *Chem. Eng. Res. Des.* **2021**, *169*, 19–32. [CrossRef]
212. Allam, E.A.; Ali, A.S.M.; Elsharkawy, R.M.; Mahmoud, M.E. Framework of nano metal oxides N-NiO@ N-Fe3O4@ N-ZnO for adsorptive removal of atrazine and bisphenol-A from wastewater: Kinetic and adsorption studies. *Environ. Nanotechnol. Monit. Manag.* **2021**, *16*, 100481. [CrossRef]
213. Gong, Y.; Chen, Z.; Bi, L.; Kang, J.; Zhang, X.; Zhao, S.; Wu, Y.; Tong, Y.; Shen, J. Adsorption property and mechanism of polyacrylate-divinylbenzene microspheres for removal of trace organic micropollutants from water. *Sci. Total Environ.* **2021**, *781*, 146635. [CrossRef] [PubMed]
214. Hernandes, P.T.; Franco, D.S.P.; Georgin, J.; Salau, N.P.G.; Dotto, G.L. Adsorption of atrazine and 2, 4-D pesticides on alternative biochars from cedar bark sawdust (*Cedrella fissilis*). *Environ. Sci. Pollut. Res.* **2022**, *29*, 22566–22575. [CrossRef]
215. Gong, Y.; Liu, Y.; Shen, J.; Zhao, S.; Wu, H.; Zhang, H.; Kang, J.; Wu, Y.; Chen, C.; Xu, X. Simultaneous removal of atrazine and heavy metal ions using sulfonated polymeric microspheres through an adsorptive filtration process: Insights into the synergistic and competitive adsorption. *J. Clean. Prod.* **2022**, *358*, 132046. [CrossRef]
216. Cheng, C.; Shi, X.; Yin, G.; Peng, F.; Hou, W.; Zhang, W.; Lin, X.; Li, J.; Wang, X. Atrazine adsorption by graphene-based materials: Interaction mechanism and application in real samples. *Environ. Technol. Innov.* **2022**, *28*, 102823. [CrossRef]
217. do Nascimento, C.T.; Vieira, M.G.A.; Scheufele, F.B.; Palú, F.; da Silva, E.A.; Borba, C.E. Adsorption of atrazine from aqueous systems on chemically activated biochar produced from corn straw. *J. Environ. Chem. Eng.* **2022**, *10*, 107039. [CrossRef]
218. Salomón, Y.L.; Georgin, J.; Franco, D.S.P.; Netto, M.S.; Piccilli, D.G.A.; Foletto, E.L.; Pinto, D.; Oliveira, M.L.S.; Dotto, G.L. Adsorption of atrazine herbicide from water by diospyros kaki fruit waste activated carbon. *J. Mol. Liq.* **2022**, *347*, 117990. [CrossRef]
219. Vieira, Y.; Silveira, J.P.; Dotto, G.L.; Knani, S.; Vieillard, J.; Georgin, J.; Franco, D.S.P.; Lima, E.C. Mechanistic insights and steric interpretations through statistical physics modelling and density functional theory calculations for the adsorption of the pesticides atrazine and diuron by Hovenia dulcis biochar. *J. Mol. Liq.* **2022**, *367*, 120418. [CrossRef]
220. Yan, S.; Qu, J.; Bi, F.; Wei, S.; Wang, S.; Jiang, Z.; Wang, L.; Yu, H.; Zhang, Y. One-pot synthesis of porous N-doped hydrochar for atrazine removal from aqueous phase: Co-activation and adsorption mechanisms. *Bioresour. Technol.* **2022**, *364*, 128056. [CrossRef]
221. Zhang, Z.; Zhou, C.; Yang, J.; Yan, B.; Liu, J.; Wang, S.; Li, Q.; Zhou, M. Preparation and Characterization of Apricot Kernel Shell Biochar and Its Adsorption Mechanism for Atrazine. *Sustainability* **2022**, *14*, 4082. [CrossRef]
222. Wang, Y.; Liu, C.; Wang, F.; Sun, Q. Behavior and mechanism of atrazine adsorption on pristine and aged microplastics in the aquatic environment: Kinetic and thermodynamic studies. *Chemosphere* **2022**, *292*, 133425. [CrossRef] [PubMed]
223. Lartey-Young, G.; Ma, L. Optimization, equilibrium, adsorption behaviour of Cu/Zn/Fe LDH and LDHBC composites towards atrazine reclamation in an aqueous environment. *Chemosphere* **2022**, *293*, 133526. [CrossRef]
224. Cheng, Y.; Wang, B.; Shen, J.; Yan, P.; Kang, J.; Wang, W.; Bi, L.; Zhu, X.; Li, Y.; Wang, S. Preparation of novel N-doped biochar and its high adsorption capacity for atrazine based on π–π electron donor-acceptor interaction. *J. Hazard. Mater.* **2022**, *432*, 128757. [CrossRef]
225. Cao, Y.; Wang, L.; Kang, X.; Song, J.; Guo, H.; Zhang, Q. Insight into atrazine removal by fallen leaf biochar prepared at different pyrolysis temperatures: Batch experiments, column adsorption and DFT calculations. *Environ. Pollut.* **2023**, *317*, 120832. [CrossRef] [PubMed]
226. Lazorko-Connon, S.; Achari, G. Atrazine: Its occurrence and treatment in water. *Environ. Rev.* **2009**, *17*, 199–214. [CrossRef]
227. Gupta, S.S.; Bhattacharyya, K.G. Kinetics of adsorption of metal ions on inorganic materials: A review. *Adv. Colloid Interface Sci.* **2011**, *162*, 39–58. [CrossRef]
228. Zhou, Q.; Wang, W.; Shuang, C.; Wang, M.; Ma, Y.; Li, A. Reusable magnetic microspheres for efficient removal of atrazine in aqueous media. *Chem. Eng. J.* **2014**, *253*, 190–197. [CrossRef]
229. Qiu, H.; Lv, L.; Pan, B.-c.; Zhang, Q.-j.; Zhang, W.-m.; Zhang, Q.-x. Critical review in adsorption kinetic models. *J. Zhejiang Univ. Sci. A* **2009**, *10*, 716–724. [CrossRef]
230. Azizian, S. Kinetic models of sorption: A theoretical analysis. *J. Colloid Interface Sci.* **2004**, *276*, 47–52. [CrossRef]
231. Ruthven, D.M. *Principles of Adsorption and Adsorption Processes*; John Wiley & Sons: Hoboken, NJ, USA, 1984.
232. Largitte, L.; Pasquier, R. A review of the kinetics adsorption models and their application to the adsorption of lead by an activated carbon. *Chem. Eng. Res. Des.* **2016**, *109*, 495–504. [CrossRef]
233. Ocampo-Pérez, R.; Rivera-Utrilla, J.; Gómez-Pacheco, C.; Sánchez-Polo, M.; López-Peñalver, J.J. Kinetic study of tetracycline adsorption on sludge-derived adsorbents in aqueous phase. *Chem. Eng. J.* **2012**, *213*, 88–96. [CrossRef]

234. Ho, Y.S.; McKay, G. A comparison of chemisorption kinetic models applied to pollutant removal on various sorbents. *Process Saf. Environ. Prot.* **1998**, *76*, 332–340. [CrossRef]
235. Ayranci, E.; Hoda, N. Studies on removal of metribuzin, bromacil, 2, 4-D and atrazine from water by adsorption on high area carbon cloth. *J. Hazard. Mater.* **2004**, *112*, 163–168. [CrossRef]
236. Alam, J.B.; Dikshit, A.K.; Bandyopadhayay, M. Evaluation of thermodynamic properties of sorption of 2, 4-D and atrazine by tire rubber granules. *Sep. Purif. Technol.* **2005**, *42*, 85–90. [CrossRef]
237. Kovaios, I.D.; Paraskeva, C.A.; Koutsoukos, P.G. Adsorption of atrazine from aqueous electrolyte solutions on humic acid and silica. *J. Colloid Interface Sci.* **2011**, *356*, 277–285. [CrossRef]
238. Zhang, W.; Zheng, J.; Zheng, P.; Qiu, R. Atrazine immobilization on sludge derived biochar and the interactive influence of coexisting Pb(II) or Cr(VI) ions. *Chemosphere* **2015**, *134*, 438–445. [CrossRef]
239. Vieira, W.T.; Bispo, M.D.; de Melo Farias, S.; de Almeida, A.d.S.V.; da Silva, T.L.; Vieira, M.G.A.; Soletti, J.I.; Balliano, T.L. Activated carbon from macauba endocarp (*Acrocomia aculeate*) for removal of atrazine: Experimental and theoretical investigation using descriptors based on DFT. *J. Environ. Chem. Eng.* **2021**, *9*, 105155. [CrossRef]
240. Piccin, J.S.; Cadaval, T.R.S.A.; De Pinto, L.A.A.; Dotto, G.L. Adsorption isotherms in liquid phase: Experimental, modeling, and interpretations. In *Adsorption Processes for Water Treatment and Purification*; Springer International Publishing: Cham, Switzerland, 2017; pp. 19–51. [CrossRef]
241. Lima, E.C.; Hosseini-Bandegharaei, A.; Moreno-Piraján, J.C.; Anastopoulos, I. A critical review of the estimation of the thermodynamic parameters on adsorption equilibria. Wrong use of equilibrium constant in the Van't Hoof equation for calculation of thermodynamic parameters of adsorption. *J. Mol. Liq.* **2019**, *273*, 425–434. [CrossRef]
242. El-Khaiary, M.I. Least-squares regression of adsorption equilibrium data: Comparing the options. *J. Hazard. Mater.* **2008**, *158*, 73–87. [CrossRef]
243. Kalra, A.; Hadi, P.; Mackey, H.R.; Al Ansari, T.; McKay, G. Sorption of heavy metal ions onto e-waste-derived ion-exchange material–selecting the optimum isotherm. *Desalination Water Treat.* **2018**, *126*, 196–207. [CrossRef]
244. Vasiliu, S.; Bunia, I.; Racovita, S.; Neagu, V. Adsorption of cefotaxime sodium salt on polymer coated ion exchange resin microparticles: Kinetics, equilibrium and thermodynamic studies. *Carbohydr. Polym.* **2011**, *85*, 376–387. [CrossRef]
245. Georgin, J.; Franco, D.S.P.; Ramos, C.G.; Piccilli, D.G.A.; Lima, E.C.; Sher, F. A review of the antibiotic ofloxacin: Current status of ecotoxicology and scientific advances in its removal from aqueous systems by adsorption technology. *Chem. Eng. Res. Des.* **2023**, *193*, 99–120. [CrossRef]
246. Rápó, E.; Tonk, S. Factors affecting synthetic dye adsorption; desorption studies: A review of results from the last five years (2017–2021). *Molecules* **2021**, *26*, 5419. [CrossRef]
247. Horsfall Jnr, M.; Spiff, A.I. Effects of temperature on the sorption of Pb^{2+} and Cd^{2+} from aqueous solution by Caladium bicolor (Wild Cocoyam) biomass. *Electron. J. Biotechnol.* **2005**, *8*, 43–50. [CrossRef]
248. Lazarotto, J.S.; Schnorr, C.; Georgin, J.; Franco, D.S.P.; Netto, M.S.; Piccilli, D.G.A.; Silva, L.F.O.; Rhoden, C.R.B.; Dotto, G.L. Microporous activated carbon from the fruits of the invasive species Hovenia dulcis to remove the herbicide atrazine from waters. *J. Mol. Liq.* **2022**, *364*, 120014. [CrossRef]
249. Petrovic, B.; Gorbounov, M.; Soltani, S.M. Impact of surface functional groups and their introduction methods on the mechanisms of CO2 adsorption on porous carbonaceous adsorbents. *Carbon Capture Sci. Technol.* **2022**, *3*, 100045. [CrossRef]
250. Aniagor, C.O.; Elshkankery, M.; Fletcher, A.J.; Morsy, O.M.; Abdel-Halim, E.S.; Hashem, A. Equilibrium and kinetic modelling of aqueous cadmium ion and activated carbon adsorption system. *Water Conserv. Sci. Eng.* **2021**, *6*, 95–104. [CrossRef]
251. Lizzio, A.A.; DeBarr, J.A. Effect of surface area and chemisorbed oxygen on the SO2 adsorption capacity of activated char. *Fuel* **1996**, *75*, 1515–1522. [CrossRef]
252. Stavropoulos, G.G.; Samaras, P.; Sakellaropoulos, G.P. Effect of activated carbons modification on porosity, surface structure and phenol adsorption. *J. Hazard. Mater.* **2008**, *151*, 414–421. [CrossRef] [PubMed]
253. Hernandes, P.T.; Franco, D.S.P.; Georgin, J.; Salau, N.P.G.; Dotto, G.L. Investigation of biochar from Cedrella fissilis applied to the adsorption of atrazine herbicide from an aqueous medium. *J. Environ. Chem. Eng.* **2022**, *10*, 107408. [CrossRef]
254. Humbert, H.; Gallard, H.; Suty, H.; Croué, J.-P. Natural organic matter (NOM) and pesticides removal using a combination of ion exchange resin and powdered activated carbon (PAC). *Water Res.* **2008**, *42*, 1635–1643. [CrossRef]
255. Park, H.N.; Choi, H.A.; Won, S.W. Fibrous polyethylenimine/polyvinyl chloride crosslinked adsorbent for the recovery of Pt (IV) from acidic solution: Adsorption, desorption and reuse performances. *J. Clean. Prod.* **2018**, *176*, 360–369. [CrossRef]
256. Zanella, O.; Tessaro, I.C.; Féris, L.A. Desorption- and Decomposition-Based Techniques for the Regeneration of Activated Carbon. *Chem. Eng. Technol.* **2014**, *37*, 1447–1459. [CrossRef]
257. Patel, H. Review on solvent desorption study from exhausted adsorbent. *J. Saudi Chem. Soc.* **2021**, *25*, 101302. [CrossRef]
258. Iwuozor, K.O.; Emenike, E.C.; Gbadamosi, F.A.; Ighalo, J.O.; Umenweke, G.C.; Iwuchukwu, F.U.; Nwakire, C.O.; Igwegbe, C.A. Adsorption of organophosphate pesticides from aqueous solution: A review of recent advances. *Int. J. Environ. Sci. Technol.* **2023**, *20*, 5845–5894. [CrossRef]

259. Kyzas, G.Z.; Lazaridis, N.K.; Kostoglou, M. Adsorption/desorption of a dye by a chitosan derivative: Experiments and phenomenological modeling. *Chem. Eng. J.* **2014**, *248*, 327–336. [CrossRef]
260. Mondal, P.; George, S. A review on adsorbents used for defluoridation of drinking water. *Rev. Environ. Sci. Bio/Technol.* **2015**, *14*, 195–210. [CrossRef]
261. Patel, H. Elution profile of cationic and anionic adsorbate from exhausted adsorbent using solvent desorption. *Sci. Rep.* **2022**, *12*, 1665. [CrossRef] [PubMed]
262. Patel, H. Fixed-bed column adsorption study: A comprehensive review. *Appl. Water Sci.* **2019**, *9*, 45. [CrossRef]
263. Mondal, S.; Aikat, K.; Halder, G. Ranitidine hydrochloride sorption onto superheated steam activated biochar derived from mung bean husk in fixed bed column. *J. Environ. Chem. Eng.* **2016**, *4*, 488–497. [CrossRef]
264. Chen, J.H.; Xing, H.T.; Guo, H.X.; Li, G.P.; Weng, W.; Hu, S.R. Preparation, characterization and adsorption properties of a novel 3-aminopropyltriethoxysilane functionalized sodium alginate porous membrane adsorbent for Cr (III) ions. *J. Hazard. Mater.* **2013**, *248*, 285–294. [CrossRef]
265. Sivarajasekar, N.; Balasubramani, K.; Mohanraj, N.; Maran, J.P.; Sivamani, S.; Koya, P.A.; Karthik, V. Fixed-bed adsorption of atrazine onto microwave irradiated Aegle marmelos Correa fruit shell: Statistical optimization, process design and breakthrough modeling. *J. Mol. Liq.* **2017**, *241*, 823–830. [CrossRef]
266. Levio-Raiman, M.; Schalchli, H.; Briceño, G.; Bornhardt, C.; Tortella, G.; Rubilar, O.; Diez, M.C. Performance of an optimized fixed-bed column packed with an organic biomixture to remove atrazine from aqueous solution. *Environ. Technol. Innov.* **2021**, *21*, 101263. [CrossRef]
267. Eletta, O.A.A.; Adeniyi, A.G.; Ighalo, J.O.; Onifade, D.V.; Ayandele, F.O. Valorisation of Cocoa (Theobroma cacao) pod husk as precursors for the production of adsorbents for water treatment. *Environ. Technol. Rev.* **2020**, *9*, 20–36. [CrossRef]
268. Xiao, C.; Li, S.; Yi, F.; Zhang, B.; Chen, D.; Zhang, Y.; Chen, H.; Huang, Y. Enhancement of photo-Fenton catalytic activity with the assistance of oxalic acid on the kaolin–FeOOH system for the degradation of organic dyes. *RSC Adv.* **2020**, *10*, 18704–18714. [CrossRef] [PubMed]
269. Rundschau24. Nitrate, Pestizide und Atrazine Gefährden Trinkwasser. Available online: https://www.rundschau24.de/landkreis-nb-by/bayern/55052-nitrate-pestizide-und-atrazine-gefaehrden-trinkwasser (accessed on 7 November 2025).
270. Grand-Cognac. Inauguration de la Station de Traitement des Pesticides de Mer-Pins. Available online: https://www.grand-cognac.fr/les-actualites/inauguration-de-la-station-de-traitement-des-pesticides-de-merpins (accessed on 7 November 2025).
271. Grand-Cognac. Pose de la 1ère Pierre de l'usine de Traitement des Pesticides d'Angeac-Charente. Available online: https://www.grand-cognac.fr/les-actualites/pose-de-la-1ere-pierre-de-lusine-de-traitement-des-pesticides-dangeac-charente (accessed on 7 November 2025).
272. Liu, S.; Chen, Z.; Shen, Y.; Chen, H.; Li, Z.; Cai, L.; Yang, H.; Zhu, C.; Shen, J.; Kang, J. Simultaneous regeneration of activated carbon and removal of adsorbed atrazine by ozonation process: From laboratory scale to pilot studies. *Water Res.* **2024**, *251*, 121113. [CrossRef] [PubMed]

Disclaimer/Publisher's Note: The statements, opinions and data contained in all publications are solely those of the individual author(s) and contributor(s) and not of MDPI and/or the editor(s). MDPI and/or the editor(s) disclaim responsibility for any injury to people or property resulting from any ideas, methods, instructions or products referred to in the content.